The Dynamics of Ecological Invasions and Epidemics

Isla Cruickshank B.Sc. M.Sc.

Submitted for

Degree of Doctor of Philosophy,

Department of Statistics and Modelling Science
University of Strathclyde

September 1998

Acknowledgements

Abstract

The systems of interest in this study are the spread of epidemics and invasions from a small propagule introduced into an arena that was initially devoid of the given species or stage of illness.

In reaction-diffusion models, populations are continuous. Populations at low densities have the same growth functions as populations at high densities. In nature, such low densities would signify extinction of a population or of a disease.

This property can be removed from reaction-diffusion models by small changes in the formulation so that small populations become extinct. This can be achieved by the use of a threshold density or an Allee effect, so there is negative growth at low densities. Both these alterations were made to the Fisher model, a predator-prey model and a two stage and a three stage epidemic model.

A semi-numerical method, termed the Shooting method, was developed to predict the shapes and velocities of these wave fronts. This was found to correctly predict the velocity, the peak density of the invading stage or species and the width of the wave front.

It was found that in oscillatory cases of the multi species models, a high threshold can remove the wave train or wake which would normally follow the wave front, so the wave becomes a soliton. The next step is to investigate probable causes of persistence behind the initial wavefront. To do this, discrete time and space versions of the models were formulated so that experiments investigating persistence can be carried out in a two dimensional arena with less computational effort. The formulations were chosen so that at reasonable time and space steps the discrete models show no behaviour different to that of the reaction diffusion model, and so that the Shooting method could also be used to make predictions about these wavefronts.

Three mechanisms of persistence are investigated; environmental heterogeneity, long range dispersal and self organised patterns.

iii

Contents

Chapter 1

Introduction

1.1 Modelling Spatial Processes

1.1.1 Ecological Applications

The modelling of spatial processes is of interest in an ecological sense as a way of representing the spatial spread of many species and of diseases, spreading from a small propagule of a new species or of a stage of an illness not already in the spatial arena of interest.

The spread of a species can be thought of in 2 different ways. The species may be exotic to that region, such as a species introduced into an area for exploitation for man. An example of this is the introduction of the musk rat into Bohemia at the start of this century for sporting purposes . The spread of the muskrat has been modelled by van den Bosch et al. (1992). The species may be re-released into an area in which it has gone extinct. Californian sea otters were hunted to near extinction in the 1900s. A small population was discovered in 1914 (Bryant 1915), and due to protection laws the population has increased in number and spatial range (Peterson and Odemar 1969). Lubina and Levin (1988) have used the data collected concerning this range expansion to parameterise an invasion model.

The spread of epidemics is also an interesting and important area of study. Eco-

logical epidemics are important in human health terms, as in rabies epidemics (Murray 1987) and economically, such as the spread of bovine tuberculosis by badgers (White and Harris 1995b) (White and Harris 1995a). The importance of modelling in the field of epidemiology is as a method of assessing disease control strategies. White and Harris (1995b) and White and Harris (1995a) both vaccination regimes and culling are investigated as control strategies for bovine tuberculosis in badgers by using model simulations.

1.1.2   Modelling Approaches

There are a number of approaches to ecological modelling. There are random effects in ecological systems due to variation in the environment and in individuals. Such randomness is taken into account in stochastic models. In stochastic models, the population is treated as integer individuals. At a given time, these individuals are attributed a probability of being in a given state. A stochastic simulation results in a realization of the model. Realizations are different due to random effects. Deterministic models do not include random effects, and so only provide information about the trend in the system. In a deterministic model, the state of the system at any future time can be predicted by the state of the system at the present time. Populations are treated as continuous, real densities. Frequently the mean of many stochastic realisations is very similar to the trend predicted by the deterministic model (Renshaw 1991), so in this thesis it is assumed that deterministic models provide adequate means for representing ecological systems.

There are also many approaches to modelling spatial processes. Assuming that the system is homogeneously mixed over its extent allows the model to be described by ordinary differential equations or difference equations, the mean field approach. The spatial component is important if mixing is not homogeneous (Levin 1974), as in the case of an epidemic starting from a point innoculum. Space can be split into one or more colonies, with transfer rates or probabilities between them, the meta-population approach. Reaction-diffusion models

assume that individuals within a population move in a random manner. If this random motion results in a macroscopic regular motion of the whole population, the motion can be described as a diffusion process (Skellam 1951). In reaction-diffusion models, partial differential equations are used to model the growth and behaviour of the population density. Discrete space and time analogues of the continuous reaction-diffusion models can be formulated. These discrete models use update rules to predict the outcome of continuous time models after a finite time increment.

Reaction-diffusion models are used in this thesis as the species which are modelled are thought to move in any direction and any distance i.e. diffusively (Skellam 1951).

Interestingly enough, in deterministic reaction-diffusion models, the population density is a continuous variable; individuals are not considered as discrete entities. This makes it impossible for the population density to ever reach zero. Normally, in reaction-diffusion models, low density populations have exactly the same dynamics as high density populations. Mollison (1991) showed that the 3 stage rabies model, a rabid population of 1 individual per quintillion square kilometres was large enough to re-infect susceptible populations and keep the epidemic going. At very low densities, stochastic effects become much more important, so the deterministic assumptions fail (Rand and Wilson 1991). So reaction-diffusion models need to be modified so that regrowth does not occur from low densities. Allee (1938) described population decline in low density populations associated with a lack of reproductive opportunity. An Allee effect in the growth function can be used to remove the low density populations from the dynamics of a model (Lewis and Karieva 1993) (Kot et al. 1996). A threshold formulation where any population of less than the threshold density dies out can be used (Kessler and Levine 1998) (Brunet and Derrida 1997). In the case of their models a cutoff was used, where all populations of less than a given density instantaneously become extinct. This formulation does not work in a continuous model.

1.2 Invasion Models

In (1937), Fisher formulated a reaction-diffusion model for describing the spread of an advantageous gene. The population described by the model grows logistically and disperses diffusively. He also devised a calculation for the velocity of the wave front (see chapter 2 for details). If an Allee effect or a threshold is added to the growth function of the Fisher model, the velocity of the wave front decreases and the wave front shortens (Brunet and Derrida 1997). Brunet and Derrida (1997) touched upon another important concept, that these models cannot be predicted with Fisher's calculation as it assumes that low density populations grow in the same way as high density populations. Brunet and Derrida (1997) approximated a calculation for the velocity of the Fisher wave with their cutoff. This threshold formulation will not work for continuous time models. Lewis and Karieva (1993) calculated the velocity of a wave front of a system with Allee dynamics, created by a cubic term in the growth function. The cubic term in the growth function cannot easily be attributed to a biological mechanism and the calculation cannot be modified to fit the growth functions with Allee effects formulated in this thesis. A more general calculation for the velocity of a wave with no regrowth from low densities is needed. In Chapter 2, a semi-numerical method for predicting the wave shape and the velocity of the Fisher wave with no regrowth from low densities is devised (Cruickshank et al. 1998). The accuracy of this new method, termed the Shooting method, is tested against three formulations of the Fisher model with no regrowth from low population densities, one being the addition of a threshold and the other two different Allee effect formulations.

The methods of removing regrowth from low population densities are then applied to a 2 component system, a predator-prey model, formulated by Rosenzweig (1971) from principles developed by Rosenzweig and MacArthur (1963). This predator-prey model is unstable at high carrying capacities (Rosenzweig 1971) (Gilpin 1972). The model is made spatially explicit by having diffusively dispersing predators and immobile prey (Gurney et al. 1998) (Cruickshank et al. 1998)

4

(Gurney and Veitch 1998). The velocity of the predator wave front has been calculated for a predator-prey model Dunbar (1983); Dunbar (1984). In chapter 3, the reaction-diffusion, predator-prey model is modified to remove regrowth from low densities of predators, by use of a threshold (Gurney et al. 1998) and an Allee effect (Cruickshank et al. 1998). Two methods of predicting the wave characteristics of the models are considered, the method devised by (Gurney et al. 1998) for the threshold formulation and the Shooting method (Cruickshank et al. 1998), are compared and tested.

1.3   Epidemic Models

The epidemic models considered in this thesis were both developed to model the rabies epidemic in European foxes. Rabies is currently sweeping through Europe, having appeared in Poland in the late 1930s (Anderson et al. 1981) (Murray 1987). Control mechanisms for the epidemic can be investigated by the use of mathematical models.

A non-spatial model was formulated by Anderson et al. (1981). This model has two staged of infection; susceptible and infective. Källén et al. (1985) formulated a reaction-diffusion model for the rabies epidemic. This model assumes that adult susceptibles remain within the same territory after recruitment to the adult population, so the susceptibles are considered immobile. Infectives either contract the paralytic form of the disease and die without reinfecting or run in a random manner, infecting any susceptible contacted, described by the model as diffusion. The velocity of the wave front can be calculated from Dunbar's work on a two component model. The velocity this model predicts for a rabies epidemic is always much higher than the velocity of the epidemic front travelling through Europe.

The two stage epidemic model ignores an important factor in the course of the rabies infection. Once infected, there is an incubation period when the fox is asymptomatic and not infective. Murray et al. (1986) added this third stage of infection to Källén et al.'s model. The incubating foxes are assumed to be

immobile, as the susceptibles are. Murray et al. (1986) and Murray (1989) describe a calculation for the velocity of the wave front in this 3 stage epidemic system.

Mollison (1991)'s description of an atto-fox is based on the dynamics of rabies models. To reduce the impact of the low density populations on the rabies models, the infectivity of low density population is reduced, both by use of a threshold and by a more continuous formulation (Cruickshank et al. 1998) are used. The Shooting method is altered to make predictions about the velocity and shape of the wave front in the epidemic systems with these formulations.

In chapter 6 there is a case study of the European fox rabies epidemic. Suitable threshold densities are calculated, based on the likelihood of a fox being infected at the given density (Cruickshank et al. 1998). van den Bosch et al. (1992)'s idea that fox territory size depends on population density is also investigated. This has implications for the diffusion rate and the threshold density of the system.

1.4   Discrete Models

When the dynamics of the predator-prey model are unstable, and the first trough behind the wave front dips to a density near the threshold density, the invasion of predators dies out behind the wave front forming a soliton wave (Gurney et al. 1998) (Cruickshank et al. 1998). The epidemic models with regrowth from low densities have complicated wakes behind the epidemic wave front (Mollison 1991). If the trough behind the initial wave front falls to a density near that of the threshold, the epidemic dies out behind the wave front forming a soliton wave. This raises the question of persistence of the epidemic or invasion behind the wave front in these systems.

Mechanisms which may allow the establishment of an invading predator or the epidemic to reach an endemic state within the system are reviewed in chapter 10 and investigated in the following 3 chapters. The continuous models, which have been used up to this point of the thesis, are very computationally intensive.

Some of the mechanisms considered are only realizable in 2 dimensions (Gurney et al. 1998) (Hassell et al. 1994), and 2 dimensional simulations of reaction-diffusion models take long times to run to completion. As 4 mechanisms are to be investigated, in 3 different systems, it is essential that simulations run quickly.

Discrete time and space analogues of the continuous invasion (Gurney et al. 1998) and epidemic models (Gurney and Nisbet 1998) are formulated in chapters 7 and 8. Discrete simulations are more computationally efficient and have much shorter run times than continuous simulations. It is important that the discrete models do not demonstrate dynamics unseen in the continuous models and that as the time and space steps increase the solutions of the discrete models diverge slowly from those of the continuous models.

van den Bosch et al. (1990) extended the work of Fisher Kolmogorov et al. to calculate the velocity for integrodifference equations to a general invasion so that advective dispersal may be taken into account. Again, this velocity calculation is founded on the exponential shape of the toe of the wave front. Kot, Lewis, and van den Dreissche (1996) considered the velocity of a discrete model with an Allee effect. The calculation of the velocity was developed for a piecewise continuous analogue of an Allee effect and, although the calculation successfully predict the velocity of the wave front of the model it was developed for, it does not extend well to other models, as shown in chapter 7. The Shooting method can, however, be used to predict the velocity and shape of the wavefronts of all the discrete systems as long as the space and time steps are small, as demonstrated by chapters 7 and 8.

The discrete time and space models are then extended to 2 spatial dimensions in chapter 9. Circular waves are generated (Gurney et al. 1998) where the wave spreads out in all directions at the same rate (Skellam 1951). Spiral waves are known to form in chemical systems in excitable media (Winfree 1972) (Keener and Tyson 1986) (Kessler and Levine 1989). Models of these systems can be understood in terms of their geometry and the kinetics of the excitable medium (Keener and Tyson 1986). The models formulated in this thesis describe systems

with excitable media; there is reduced predation or infection below a threshold density. Spiral waves can be generated in the 2 dimensional arenas when the wave front is a soliton wave (Gurney et al. 1998). The circular waves are similar enough in cross section to the the waves generated in the 1 dimensional model, so the Shooting method is used to make predictions about the velocity and shape of the wave front. Spiral waves are not as easy to make predictions about, and the Shooting method can only be used to predict the scale of the velocity and the shape of the wave front as opposed to predicting exact values for these quantities.

Part I

Reaction-Diffusion Models of Invasions and Epidemics

Chapter 2

Single Species Continuous Models

Reaction-diffusion models permit populations at very low densities to exist and grow, a situation which is biologically unrealistic. If the growth of these small populations is removed from these models, this situation is improved. In this chapter three formulations which create this effect are examined. The Fisher model (Fisher 1937) is adapted so that there is no reproduction under a threshold. This is implemented both by a critical threshold for reproduction and an Allee Effect (Allee 1938) growth term. A method for analysing the wave front properties of invasions of organisms with no growth at low densities is then developed.

2.1 Introduction

2.1.1 The Logistic Model

The logistic model describes the density dependent growth of a single population, N, at time T. To achieve logistic growth, the birth process, $B(N)$, must decrease and the death process, $D(N)$, must increase as N increases (Renshaw 1991), so

$$B(N) = (a_1 - b_1 N)N \quad \text{and} \quad D(N) = (a_2 + b_2 N)N , \qquad (2.1.1)$$

where a_1, a_2, b_1 and b_2 are positive constants. The logistic equation is therefore

$$\frac{dN}{dT} = B(N) - D(N) = N\left[(a_1 - a_2) - (b_1 + b_2)N\right] \ . \tag{2.1.2}$$

In a biological context this equation is usually rewritten in the form

$$\frac{dN}{dT} = RN\left(1 - \frac{N}{K}\right) \tag{2.1.3}$$

where $R \equiv (a_1 - a_2)$ is the intrinsic rate of natural increase for growth and $K \equiv (a_1 - a_2)/(b_1 + b_2)$ is the density of the carrying capacity of the environment, so

$$\frac{dN}{dT} \to 0 \quad \text{as} \quad N \to K \quad \text{or} \quad N \to 0 \tag{2.1.4}$$

and

$$N \to K \quad \text{as} \quad t \to \infty \ . \tag{2.1.5}$$

2.1.2   The Fisher Model

Now a logistically growing population which disperses in one dimension is considered, the Fisher model. It was originally intended to describe the invasion of an advantageous gene into a gene pool, but now it is commonly used to describe an invasion wave of an exotic or re-invading species (Skellam 1951). The population disperses diffusively, representing the spread of organisms with low intelligence or no tropisms. The population at time T and position X, $N(X,T)$ diffuses with diffusion coefficient Ψ. The Fisher model is

$$\frac{\partial N}{\partial T} = RN\left(1 - \frac{N}{K}\right) + \Psi\frac{\partial^2 N}{\partial X^2} \tag{2.1.6}$$

To simplify the algebra and increase the speed of computations, the equations are reduced to a dimensionless or scaled form (Nisbet and Gurney 1982). This process may also lead to biological insight into controlling groups of parameters. The scaling process involves multiplying or dividing the model by one or more parameters, producing dimensionless variables and parameter groups. In this case there are 6 quantities: the population, the carrying capacity, space, the diffusion coefficient, the per capita intrinsic growth rate and time. The carrying capacity,

11

K, has the dimension of the population. Therefore K can be used as the scale of N, so the scale of population, N_0, is $N_0 \equiv K$. This scaling produces the dimensionless variable $n \equiv N/N_0$. The per capita intrinsic growth rate, R, has the dimension of one over time. Therefore, $1/R$ can be used as the scale of time, so $T_0 \equiv R^{-1}$. This scaling produces the dimensionless variable $t \equiv T/T_0$. The diffusion coefficient has the dimension of the diffusion length, so $X_0 \equiv \sqrt{\Psi/R}$ can be used as the scale of space. This results in the dimensionless variable $x \equiv X\sqrt{R/\Psi}$. This choice of scaling produces the dimensionless model

$$\frac{\partial n}{\partial t} = n(1-n) + \frac{\partial^2 n}{\partial x^2}. \tag{2.1.7}$$

One method used to predict the velocity and the shape of the wave front of this model was suggested by Fisher (1937) and Kolmogorov et al. (1937) and later extensively ratified by Hadeler and Rothe (1975) and Mollison (1977). To see the relationship between front velocity and model parameters the leading edge of the front where $n << 1$ was investigated. In this case the n^2 term can be ignored in comparison with the n term. This linearises equation (2.1.7) to

$$\frac{\partial n}{\partial t} = n + \frac{\partial^2 n}{\partial x^2}. \tag{2.1.8}$$

A solution is sought in the form $n(x) = Ae^{-\lambda(x-vt)}$, where v is the velocity of the wave front, λ is the exponential lapse rate of the front, $\lambda > 0$ and $A > 0$ and is arbitrary. Substituting this form of solution for $n(x)$ into the linear equation gives the relationship between the velocity of the wave front, v, and λ,

$$v = \frac{1}{\lambda} + \lambda. \tag{2.1.9}$$

This suggests that any value of v is possible with λ chosen to suit, as long as v is larger than a minimum velocity, v_0, which occurs when $\lambda = 1$. For the scaled Fisher model,

$$v_0 = 2. \tag{2.1.10}$$

v_0 is the velocity of the wave front as long as the initial condition of the population has compact support (Fisher 1937) (Kolmogorov et al. 1937).

The derivation of this velocity calculation exploits the fact that the population grows in the same way at low densities as at high densities. If the model is changed so that there is no in-situ regrowth of non-biological populations, another method will have to be found to predict the velocity of the invasion wave front.

2.2 Invasions of Populations with no Reproduction at Low Densities

A situation is considered in the Fisher model that when a population falls beneath a threshold density, n_P, there is no reproduction. This removes the problem of regrowth from low densities from this reaction-diffusion model.

A method to calculate the velocity of a single component reaction-diffusion model with an Allee effect in the growth function has been devised by Lewis and Karieva (1993). Their growth function is given by a cubic. No obvious biological mechanism produces such a growth function, so in this chapter Allee effects are achieved by more biologically realistic mechanisms. Their velocity calculation is specific to the cubic growth function, so is not applicable to the formulations of the Fisher model with no regrowth as described below. A new method of analysing the properties of an invasion wave of with these growth functions is devised.

2.2.1 General Case

A generalisation of the Fisher model is considered, where $g(n)$ is the scaled local net population growth function, giving

$$\frac{\partial n}{\partial t} = g(n) + \frac{\partial^2 n}{\partial x^2} \; . \tag{2.2.1}$$

In this section the scaled carrying capacity is referred to as k, so in the scaled Fisher model, since the carrying capacity is 1, $k = 1$. The restrictions on $g(n)$ are that

$$g(0) = g(n_P) = g(k) = 0 \; , \tag{2.2.2}$$

$$g(n) < 0 \quad \text{if} \quad 0 < n < n_P \quad \text{or} \quad n > k \tag{2.2.3}$$

and

$$g(n) > 0 \quad \text{if} \quad n_P < n < k \ . \tag{2.2.4}$$

These restrictions cause the velocity of the wave to decrease from that of the original Fisher model, so $v < v_0$ (Brunet and Derrida 1997).

It is assumed that a travelling wave solution exists and that the wave is moving from right to left in a 1 dimensional arena. The model is transformed into a moving frame of reference which moves from right to left with velocity $-v_R$. This allows n to depend only on one parameter z, where $z \equiv x + v_R t$. Equation (2.2.1) can then be written as a second order ODE,

$$\frac{d^2 n}{dz^2} - v_R \frac{dn}{dz} + g(n) = 0 \ . \tag{2.2.5}$$

If $\phi \equiv dn/dz$, the transformed model can be rewritten as a pair of first order ODEs, where

$$\frac{dn}{dz} = \phi \quad \text{and} \quad \frac{d\phi}{dz} = v_R \phi - g(n) \ . \tag{2.2.6}$$

The solution sought requires $n \to 0$ as $z \to -\infty$. $z = 0$ is placed at a point where $n = n_0 << n_P$ so that for $z \leq 0$, equations (2.2.6) can be approximated by

$$\frac{dn}{dz} = \phi \quad \text{and} \quad \frac{d\phi}{dz} = v_R \phi - g'(0)n \quad \text{where} \quad g'(0) \equiv \left[\frac{dg}{dn}\right]_{n=0} . \tag{2.2.7}$$

Equation (2.2.7) has the solution $n = n_0 e^{\lambda z}$, where $n \to 0$ as $z \to -\infty$, provided that $\lambda > 0$. Since $g'(0) < 0$,

$$\lambda = \frac{1}{2}\left(v_R + \sqrt{v_R^2 - 4g'(0)}\right) , \tag{2.2.8}$$

so for $z \geq 0$, equations (2.2.6) are solved with the initial conditions

$$n(0) = n_0 \quad \text{and} \quad \phi(0) = \lambda n_0 \ . \tag{2.2.9}$$

An inspection of equations (2.2.6) shows that for n to increase with z, $\phi > 0$ and for ϕ to increase with z,

$$\phi > \frac{g(n)}{v_R}. \tag{2.2.10}$$
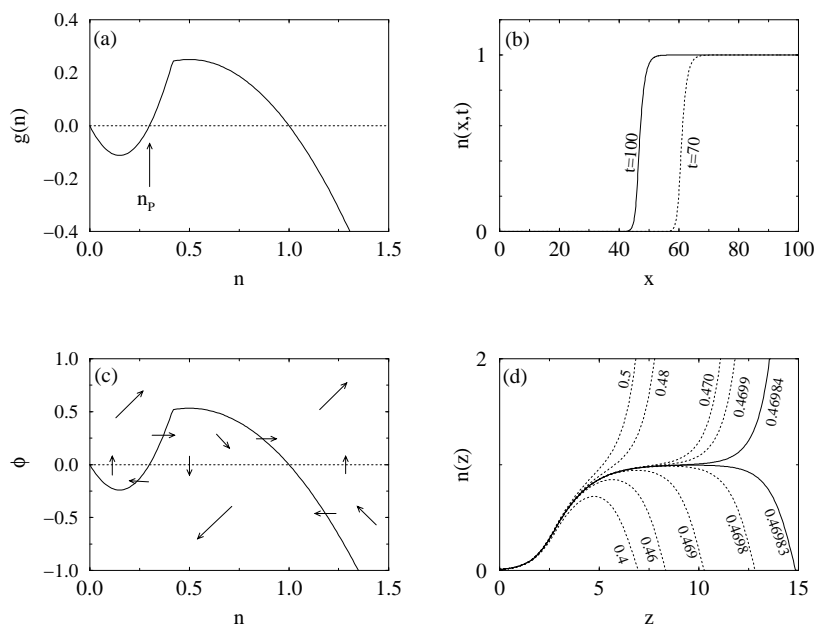
Figure 2.1: *Generic behaviour of growth with an Allee effect, with the specific equation for $g(n)$ given by equation (2.2.40) with $a = 1.5$ and $n_P = 0.3$. (a) net growth function. (b) typical invasion front generated from a simulation of the model described by equation (2.2.40) with $\Delta x = 1$, the time step varying between $\Delta t = 0.001 \rightarrow 0.1$ and a numerical integration tolerance of 0.0001. (c) phase plane analysis with $v_R = 0.47$: solid line shows separatrix implied by inequality (2.2.10). (d) group of solutions for $z > 0$ in a moving frame of reference with v_R for each run marked.*

These conditions can lead to an understanding of the characteristics of the resulting solutions in the phase plane. These equations are solved using an adaptive

step RK4 numerical integration algorithm. Δz varies between 1×10^{-5} and 1×10^{-3} and the integration tolerance is 1×10^{-5}. The implications of the characteristics of the solutions are illustrated in figure 2.1(c).

If n_0 is kept constant and λ increases from zero, the initial condition moves in a vertical line in the positive quadrant at $n = n_0$. Above $\phi = 0$, n increases, so the movement is from left to right. Below $\phi = 0$, n decreases, so the movement is from right to left. When the $\phi = 0$ line is crossed the trajectories must move vertically. The bold line in the figure depicts the curve obtained for $\phi = g(n)/v_R$. Above this line, ϕ increases so the movement is from bottom to top, and below the line g decreases, so the movement is from top to bottom. Trajectories must move horizontally while crossing this curve as $d\phi/dz = 0$.

The initial conditions for a set of trajectories, given in equation(2.2.35), with varying λ would lie on a vertical line which would cross the x axis at $n = n(0)$ and increasing as a function of v_R. If the initial conditions lie above the bold curve then the trajectory initially moves towards the top right. There are 4 possibilities for the direction of movement of the trajectories:

1. The trajectory misses the curve and $n \to \infty$ monotonically.

2. The trajectory intersects the bold line twice while $\phi > 0$ and re-enters the region where $v\phi > g(n)$ and $n \to \infty$ monotonically.

3. The trajectory hits the point $(k, 0)$, where it stops as this is a steady state.

4. The trajectory intersects the bold line while $\phi > 0$ but curves down into the region where $\phi < 0$, intersects the bold line again, then falls back below n_P. Eventually, perhaps after some oscillations, it falls into the region where $n < 0$.

The first 2 possibilities correspond to v_R being greater than the wave front velocity, v. The third possibility corresponds to $v_R = v$ and the fourth possibility corresponds to $v_R < v$. So there is only one trajectory that leads to the $(k, 0)$

16

steady state. This has been proved by Cruickshank et al. (1998) (see Appendix A).

If there is only one trajectory which leads to $(k, 0)$, if n_P is held constant, and v_R is varied, a bisection search can be used to find where $v_R = v$, the velocity of the wave. A bracket which is known to contain v is chosen; in the case of the modified Fisher models, this bracket is chosen to be $(0 \rightarrow 2)$. The centre point is used as v_R and equation (2.2.6) is solved with the initial conditions described by equation (2.2.9), and Δz and integration tolerance as used previously. When $n > 2$ or $n < 0$ then $\frac{d\phi}{dz} = 0$ or $\frac{dn}{dz} = 0$, so the simulation terminates either at $n > 2$ or $n < 0$. This end result can be used as the criterion for the bisection search. If $n > 2$ then the mid-point of the bracket becomes the new high end of the bracketing pair. If $n < 0$ then the centre of the bracket becomes the low end of the bracketing pair. Figure 2.1 (d) shows that when close to v, the trajectories of the upper and lower bounds of v_R run together until k is nearly attained, then the trajectories diverge. Therefore the criterion for the completion of the search is that the upper and lower bounds have identical trajectories to the asymptote of the wave, where $n \approx k$, $\phi \approx 0$ and $d\phi/dz \approx 0$.

This method of calculating the velocity of an invading wave in an excitable medium has been coined the Shooting method.

The models dependent on time and space are numerically simulated to provide observed results with which to compare the Shooting method.

$$\rho(x) = \frac{\partial^2 n}{\partial x^2} \tag{2.2.11}$$

is substituted by the finite difference representation

$$\rho(x) = \frac{n(x + \Delta x) - 2n(x) + n(x - \Delta x)}{\Delta x^2} , \tag{2.2.12}$$

where Δx is the space step. The model is then solved by a RK4 numerical integration method with an adaptive time step, Δt.

In all simulations of models to which the Shooting method is applied in this thesis, quadratic interpolation is used to find the width of wave fronts to a higher

17

accuracy than the space step length. The exact times of the passage of the wave at various positions of the arena, needed for the observed velocity calculations, are also obtained at higher accuracy than the time step length by quadratic interpolation.

2.2.2 Invasions with Thresholds

One method to stop reproduction at low population densities is to use a threshold. The Fisher model is modified so that if a population falls below a density N_P, the individuals in the population stop reproducing, so that when

$$\frac{\partial N}{\partial T} = G(N) + \Psi \frac{\partial^2 N}{\partial X^2} \tag{2.2.13}$$

where

$$G(N) = \begin{cases} -DN & N < N_P \\ RN(1 - N/K) & \text{otherwise} \end{cases} \tag{2.2.14}$$

and D is the per capita mortality rate.

This is scaled in the same way as the original Fisher model, so $T_0 = R^{-1}$ and $T_0 = K$. N_P has the dimension of population, so the dimensionless threshold $n_P \equiv N_P/N_0$. D has the dimension of time, so the dimensionless per capita mortality rate is $d \equiv D/T_0$. The model then becomes

$$\frac{\partial n}{\partial t} = g(n) + \frac{\partial^2 n}{\partial x^2} \tag{2.2.15}$$

where

$$g(n) = \begin{cases} -dn & n < n_P \\ n(1 - n) & \text{otherwise} \end{cases} . \tag{2.2.16}$$

Brunet and Derrida (1997) devised an approximate calculation for the velocity of the wave front of a Fisher model with a small cutoff. The cutoff in this case is imposed by setting all population below the cutoff density to zero. The calculation is based on the fact that in their formulation there is a relationship between the size of the cutoff and the reduction in velocity from v_0, so

$$v \simeq v_0 - \frac{\pi^2}{(\ln n_P)^2} . \tag{2.2.17}$$

18

d	n_P	Observed v	Predicted v
0.1	1×10^{-5}	1.923	1.926
0.1	1×10^{-3}	1.802	1.793
0.1	1×10^{-2}	1.639	1.535
0.1	1×10^{-1}	1.220	0.1385

Table 2.1: *Comparisons between wave velocities calculated from equation (2.2.17) and those observed from simulations of the continuous Fisher model with a threshold. In the simulations, $d = 0.1$, $\Delta x = 1$, the time step varying between $\Delta t = 0.001..0.1$ and a numerical integration tolerance of 0.0001.*

Equation (2.2.17) is used to calculate the velocity of the wave front in the Fisher model with a threshold. This calculation only works for small thresholds (Brunet and Derrida 1997), as is clearly demonstrated in table 2.1. Because of the form of the cutoff used by Brunet and Derrida, the per capita mortality rate below the threshold is not taken into account in the calculation. Their model can only be simulated in discrete time due to the "setting to zero" nature of their cutoff. Therefore this calculation cannot be used to predict the velocity of wave fronts generated by the continuous time Fisher model with a threshold.

The Shooting method can be used to calculate the velocity in this model.As in the general case, the wave is originally travelling from left to right in a 1 dimensional arena. The model is transformed into a moving frame of reference with velocity $-v_R$, with the n dependent only on $z \equiv x + v_R t$, with the wave travelling from right to left.

Within the moving frame of reference, $z = 0$ is set where $n(0) = n_0 = n_P$ so that the dynamics of the model where $z \leq 0$ are then described by

$$\frac{d^2 n}{dz^2} - v_R \frac{dn}{dz} - dn = 0. \tag{2.2.18}$$

With $z \leq 0$, a solution is sought in the form $n(z) = n_P e^{\lambda z}$, so the exponential lapse rate, λ, must be the solution of

$$\lambda^2 - v_R \lambda - d = 0. \tag{2.2.19}$$

As $\lambda > 0$,

$$\lambda = \frac{1}{2} \left(v_R + \sqrt{v_R^2 + 4d} \right). \tag{2.2.20}$$

19
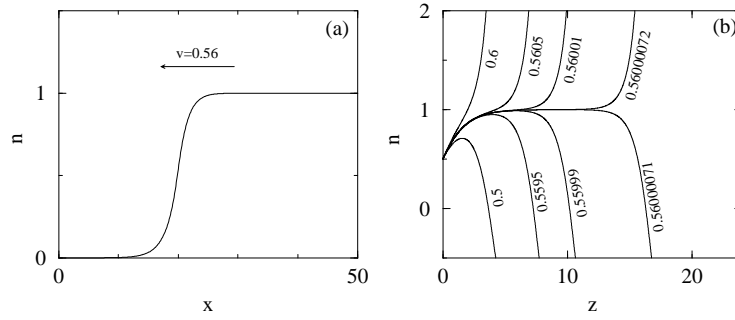
Figure 2.2: *(a)Fisher wave with a threshold travelling from left to right with velocity v = 0.56, Δx = 0.5, the time step varying between Δt = 0.001 $\rightarrow$ 0.1 and a numerical integration tolerance of 0.0001. (b)Trajectories of simulations in a moving frame of reference with d = 0.00001 and n_P = 0.5. The velocity of the frame of reference, v_R, is as marked. When $v_R \approx$ 0.56, the trajectories run concurrently until the (1,0) point is nearly reached, then diverge.*

This implies that any value of v_R is possible if λ is chosen appropriately. The solution is required (by conservation theory) to be continuous in slope and value

at $z = 0$, so the slope of the solution is related to n_P and v by

$$n'(0) = \lambda n_P. \qquad (2.2.21)$$

For $z > 0$, n is the solution of the coupled first order equivalent of the transformed model,

$$\frac{dn}{dz} = \phi \quad \text{and} \quad \frac{d\phi}{dz} = v\phi - n(1-n) \,, \qquad (2.2.22)$$

subject to the initial conditions

$$n(0) = n_P \quad \text{and} \quad \phi(0) = n_P \lambda \,. \qquad (2.2.23)$$

The Shooting method then uses the bisection search algorithm described in subsection 2.2.1, where equation (2.2.22) is solved with the initial conditions described in equation (2.2.23).

A series of numerical simulations of the Fisher wave with a threshold were carried out to check the accuracy of the Shooting method's predictions.

d	n_P	Predicted Values		Observed Values	
		v	w_f	v	w_f
0.1	1×10^{-5}	1.921	8.5	1.923	8.5
0.1	1×10^{-3}	1.803	8.0	1.802	8.1
0.1	1×10^{-2}	1.638	7.3	1.639	7.3
0.1	1×10^{-1}	1.223	5.7	1.220	5.7
0.1	2×10^{-1}	0.9777	4.4	0.9780	5.0
0.1	4×10^{-1}	0.6078	2.9	0.6051	5.0
0.1	5×10^{-1}	0.4417	2.3	0.4386	5.0
1	1×10^{-5}	1.913	8.5	1.914	8.5
1	1×10^{-3}	1.773	7.9	1.778	7.9
1	1×10^{-2}	1.575	7.1	1.579	7.1
1	1×10^{-1}	1.042	5.1	1.039	5.1
1	2×10^{-1}	0.7016	3.7	0.6969	4.2
1	4×10^{-1}	0.1231	2.1	0.1018	3.5

Table 2.2: *Comparisons between wave properties predicted by the Shooting method and those observed from simulations of the continuous Fisher model with a threshold. $\Delta x = 1$, the time step varying between $\Delta t = 0.001..0.1$ and an integration tolerance of 0.0001. v is the wave front velocity and w_f is the width of the wavefront measured from $n = 0.1$ to $n = 0.9$.*

The width of the wave front can also be estimated from this analysis. Figure 2.2 (b) shows that at the end of the bisection search the trajectories of the upper and lower brackets of v_R are identical until $n \approx 1$. Until this divergence occurs, the trajectories are following the trajectory of $v_R = v$ (Brunet and Derrida 1997) (Kessler and Levine 1998).The width of this region of the solution in the z transformed model is the same as the width of the wavefront.

Table 2.2 shows that when the threshold is high the observed velocities and widths of the fronts of the simulations are not exactly predicted by the Shooting method. The cause of this is believed to be the presence of the discontinuity in the growth function which renders the numerical simulation of the untransformed model inaccurate. The simulations involve numerical integration with variable time steps. It is possible for these steps to overshoot the exact time when the population in a given space increment increases or decreases across the threshold. At low thresholds this effect is reduced due to the low impact of small thresholds on the properties of the wave front.

2.2.3 Spreading Populations with a Continuous Allee Growth Function

A growth function with an Allee effect is negative at high and low population densities and positive for intermediate population densities, as typified by figure 2.1(a), where there is negative growth where the population n is larger than the carrying capacity, 1, and where $n < n_P$, the threshold value.

One way of achieving such a growth function is to use a model with the *per capita* birth rate function showing a Michaelis–Menten type dependency on population density, with N_h as the half saturation coefficient and F is the maximum reproductive rate, while the *per capita* death rate, $D(N)$, is linearly dependent on population density, so

$$D(N) = N(D_1 - D_2 N) .$$ (2.2.24)

This results in the equation for population growth,

$$G(N) = \left[\frac{FN}{N + N_h} - D_1 - D_2 N\right] N .$$

(2.2.25)

It is now assumed that the population, N, disperses diffusively, with the diffusion coefficient, Ψ, so the spatial model is,

$$\frac{\partial N}{\partial T} = G(N) + \Psi \frac{\partial^2 N}{\partial X^2}.$$

(2.2.26)

In equation (2.2.26) B, D_1 and D_2 have the dimension of time, T. The scale of time, T_0, is chosen as $T_0 \equiv 1/(F - D_1)$. The half saturation constant, N_h, has the dimension of population, N. The scale of population, N_0, is chosen to be $N_0 \equiv (F - D_1)/D_2$. The diffusion coefficient, Ψ, has the dimensions of space, X, and time. $X_0 \equiv \sqrt{\Psi T_0}$ is taken to be the natural scale of space. Then the model is scaled, producing the scaled variables, $t \equiv T/T_0$, $n \equiv N/N_0$ and $x \equiv X/X_0$, and the parameter groups, $n_h \equiv N_h/N_0$ and $\delta \equiv D_1/(F - D_1)$, transforming the model into

$$\frac{\partial n}{\partial t} = g(n) + \frac{\partial^2 n}{\partial x^2} ,$$

(2.2.27)

which is the same as equation (2.2.1), where

$$g(n) = \left[(1 + \delta)\frac{n}{n + n_h} - \delta - n\right] n .$$

(2.2.28)

This has the exterior steady state,

$$n = 0 ,$$

(2.2.29)

and an interior steady state, n^*.

$$n^* = \frac{1}{2}\left[(1 - n_h) + \sqrt{(1 - n_h)^2 - 4\delta n_h}\right] .$$

(2.2.30)

n^* is the carrying capacity of the system and is equivalent to k in equations (2.2.2) and (2.2.4), The system can only exist if

$$n_h < 1 \quad \text{and} \quad \delta < \frac{1 + n_h^2}{2n_h} - \frac{1}{2} .$$

(2.2.31)

The steady state, n^*, is always locally stable, as is the steady state where but $n = 0$.

This model has negative growth when $n < n_P$, with

$$n_P = \frac{1}{2}\left[(1 - n_h) - \sqrt{(1 - n_h)^2 - 4\delta n_h}\right] . \tag{2.2.32}$$

The model is transformed into a moving frame of reference with velocity $-v_R$, moving from left to right, as in the Fisher model with a threshold. This gives the second order ODE,

$$\frac{d^2 n}{dz^2} - v\frac{dn}{dz} + \left[(1 + \delta)\frac{n}{n + n_h} - \delta - n\right]n = 0. \tag{2.2.33}$$

If $dn/dz = \phi$, this can be rewritten as a coupled first order ODE,

$$\frac{dn}{dz} = \phi \quad \text{and} \quad \frac{d\phi}{dz} = v\phi - \left[(1 + \delta)\frac{n}{n + n_h} - \delta - n\right]n . \tag{2.2.34}$$

For $z > 0$, n is the solution of equation (2.2.34) subject to

$$n(0) << n_P \quad \text{and} \quad \phi(0) = \frac{n(0)}{2}\left(v_R + \sqrt{v_R^2 + 4\delta}\right) \tag{2.2.35}$$

The Shooting method is then used to predict the velocity and width of the resulting wave front, solving equation (2.2.34) with the initial conditions $n_0 = min(0.001, n_P/100)$ and ϕ as described in equation (2.2.35) in the bisection search algorithm described in 2.2.1.

A series of simulations of the Fisher wave with an Allee effect were carried out to check the accuracy of the shooting method's predictions.

The width of the wave front between 10% and 90% of n^* can be estimated from this analysis in the same manner as in the threshold formulation.

Table 2.3 shows that the Shooting method correctly predicts the wave front velocities and widths of the simulations to up to 4 decimal places. The excellent comparison of the wave front widths and velocities of the simulations and those predicted by the Shooting method holds throughout this set of runs, supporting the argument in the previous section that the disagreement between the simulations and the Shooting method predictions is caused by numerical inaccuracies in the simulations of the Fisher model with a threshold and not by an inaccuracy in the Shooting method.

24

d	n_h	Predicted Values		Observed Values	
		v	w_f	v	w_f
0.1	1×10^{-5}	1.900	8.4	1.899	8.5
0.1	1×10^{-4}	1.844	8.2	1.844	8.2
0.1	1×10^{-2}	1.515	7.1	1.515	7.3
0.1	5×10^{-2}	1.211	6.6	1.211	6.6
0.1	1×10^{-1}	1.101	6.7	1.101	6.7
0.1	1.3×10^{-1}	0.9170	6.9	0.9171	6.9
0.1	1.4×10^{-1}	0.8888	6.9	0.8887	6.9
1	1×10^{-5}	1.885	8.4	1.885	8.3
1	1×10^{-4}	1.814	8.1	1.814	8.0
1	1×10^{-2}	1.361	6.6	1.362	6.7
1	5×10^{-2}	0.8709	6.0	0.8709	6.1
1	1×10^{-1}	0.4615	6.1	0.4614	6.3
1	1.3×10^{-1}	0.2115	6.3	0.2115	6.4
1	1.4×10^{-1}	0.1172	6.5	0.1172	6.4

Table 2.3: *Comparisons between calculated wave properties and those measured from numerical simulations of the Fisher model with a continuous growth function with an Allee effect. $\Delta x = 1$, the time step varies between $\Delta t = 0.001..0.1$ and a numerical integration tolerance of 0.0001. v is the wavefront velocity and w_f is the width of the wavefront measured from $n = 0.1$ to $n = 0.9$.*

As n_h is increased, the width of the wave front initially decreases with velocity, which is expected, as demonstrated in figure 2.4. However, when the velocity starts to decrease very rapidly, the wave front width increases again. Figure 2.3 shows that decreasing n_h has the effect of decreasing n^* and the rate of growth, and increasing n_P. Decreasing the rate of growth has the effect of making the front less steep. At large n_h this is the effect which governs the width of the front. There are no similar dynamics in the original Fisher model. This formulation is not a good approximation of the Fisher model with regrowth from low densities removed. Another Allee model, which has the dynamics of the Fisher model at high densities should be sought.
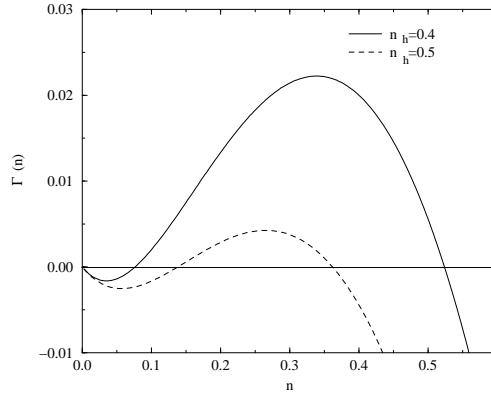
Figure 2.3: *Shape of the continuous Allee growth function with $\delta = 0.1$.*

2.2.4 Spreading Populations with an Allee Growth Function which is Continuous in Value but not Slope

A Fisher wave with an Allee effect is sought with growth dynamics similar to those of the Fisher model at high densities but with no regrowth from low population densities. The formulation should also minimise errors in numerical simulations due to discontinuities in the growth function. One compromise that could be considered is a growth function with an Allee effect which is continuous in value, but not in slope. This example of a Fisher wave with an Allee effect considers a population, N, with a linearly density dependent per capita death rate M, and a per capita fecundity rate B which is a constant, B_0, at high densities but increases linearly with slope B_1 at low densities, giving

$$M = M_0 + M_1 N \tag{2.2.36}$$

and

$$B = \begin{cases} B_0 & N \geq (B_0/B_1) \\ B_1 N & \text{otherwise} \end{cases} . \tag{2.2.37}$$

If $R \equiv B_0 - M_0$ and $K = R/M_1$ then these assumptions imply that the unscaled net growth function $G(N)$ is

$$G(N) = \begin{cases} RN(1 - N/K) & N \geq (B_0/B_1) \\ -M_0 N + (B_1 - M_1)N^2 & \text{otherwise} \end{cases} . \tag{2.2.38}$$

Adopting the same scaling for time and space as in the thresholded version of the model, and defining the parameter groups $a \equiv M_0/(B_0 - M_0)$ and $n_P \equiv aM_1/(B_1 - M_1)$, the scaled equivalent is

$$\frac{\partial n}{\partial t} = g(n) + \frac{\partial^2 n}{\partial x^2} , \tag{2.2.39}$$

which is the same as the general model. In this formulation,

$$g(n) = \begin{cases} an[(n/n_P) - 1] & n < n_c \\ n(1 - n) & \text{otherwise} \end{cases} \tag{2.2.40}$$

where

$$n_c \equiv \frac{1 + a}{1 + (a/n_P)} . \tag{2.2.41}$$

n_P represents the scaled threshold value and $-a$ is the slope of the growth function at $n = 0$.

As in the previous examples, this model is transformed into a moving frame of reference moving with velocity, v_R. The model is then rewritten as a coupled ODE. $z = 0$ is placed where $n = n_0 << n_P$, so that $g(n_0) \approx -a$.

The initial population for equation (2.2.6) is chosen to be $n_0 = \min(0.001, n_P/100)$ and equation (2.2.8) is used to relate λ to v_R. A bisection search is then conducted in exactly the same manner and using the same criteria as in the previous example.

Table 2.4 shows that there is a good agreement between predicted velocities, widths and peak heights of the wavefront and those measured from simulations in this model. The small difference arises from the discontinuity in the slope of the growth function. This discontinuity creates an error in the numerical simulations.

a	n_P	Predicted Values		Observed Values	
		v	w_f	v	w_f
1.5	2×10^{-4}	1.844	8.20	1.844	8.20
1.5	5×10^{-2}	1.264	5.89	1.264	5.89
1.5	3×10^{-1}	0.4699	3.84	0.4696	3.80
15	2×10^{-4}	1.809	8.05	1.803	8.05
15	2×10^{-2}	1.288	5.97	1.287	5.97
15	1×10^{-1}	0.6699	3.99	0.6690	3.99
150	1×10^{-4}	1.782	7.94	1.781	7.94
150	6×10^{-3}	1.288	5.98	1.288	5.98
150	4×10^{-2}	0.5389	3.66	0.5374	3.66

Table 2.4: *Comparisons between calculated wave properties and those observed from numerical simulations of the Fisher model with an Allee effect which is continuous in slope only.* $\Delta x = 0.1$, *the time step varies between* $\Delta t = 0.00001..0.001$ *and the numerical integration tolerance is* 0.00001. v *is the wave front velocity and* w_f *is the width of the wavefront, measured from* $n = 0.1$ *to* $n = 0.9$.

The dynamics of high density populations are still those of the Fisher model, so this model can be compared with the original Fisher model, whilst low density populations become extinct.

2.3 Discussion

The Fisher model was altered so that populations with very low densities did not reproduce, ensuring that biologically unrealistic populations did not contribute to the dynamics of the model. This alteration reduces the velocity of wave front of the Fisher model (Brunet and Derrida 1997). As $n_P \to 0$, $v \to v_0$, as shown by figure 2.4.

Three formulations of the Fisher model with no or reduced population growth at low densities were considered. The threshold formulation was discontinuous in slope and value. Above the threshold the dynamics were exactly that of the Fisher model. The first example of an Allee effect was completely continuous but did not have the same dynamics as the system described by the Fisher model. The second example of an Allee effect was discontinuous in slope but not in value. Above a critical density, n_c, the dynamics of the model were the same as

the original Fisher model.

Brunet and Derrida (1997)'s calculation for the velocity of a Fisher wave with a cutoff cannot be applied to the system with a threshold formulated in this chapter. The calculation can predict the velocity of the wave front at low thresholds, but does not work for high thresholds. The model formulation the calculation was developed for is very different from this formulation and the below threshold per capita mortality rate is not included in the calculation.

A semi-numerical method of predicting the velocity and the width of the wave front was developed. This was termed the Shooting method. The models were transformed into a moving frame of reference and a bisection search was used to seek the frame of reference velocity so that it was equal to the velocity of the wave, therefore predicting the velocity of the wave. Although the frame of reference velocity equal to the wave velocity cannot be found, the Shooting method can predict the wave velocity to within 1% of the observed values.

The Shooting method was then used to predict the velocities and wave front widths of the three model formulations described above. It was able to do this for the completely continuous formulation to 4 decimal places. In the threshold formulation, the discontinuity in the growth function could not be correctly solved by the numerical continuous time simulations used as comparisons for the Shooting predictions. This discrepancy between the predictions and the continuous time and space simulation velocities and front widths increased with the threshold density. In the Allee formulation with the discontinuity in slope, this also occurred, but to a lesser extent as the density was continuous.

Figure 2.4 shows that the predictions can be used to further our understanding of the dynamics of the wave fronts. The velocities are near $v_0 \equiv 2$ when the threshold is very small. The Fisher wave can have a negative velocity at high thresholds, which corresponds to the wave retreating. The wave front widths only are affected by the threshold when the the thresholds are very high and the continuous Allee effect model wave front gets wider at high thresholds, showing that the dynamics of this model are very different to those of the other 2 formulations.

Although the Shooting method predictions are best for the continuous Allee formulation model, the dynamics of the model are very different from those of the original Fisher model, demonstrated by figure 2.4. This model with a continuous growth function was used to show that the inaccuracy of the Shooting method is due to errors in the numerical simulations rather than errors in the method. This formulation will not be applied to other models looked at in later chapters.

The Fisher model was used in this chapter as a simple model to be used to develop a method for predicting the velocity and shape of a wavefront in a reaction-diffusion model where there was no growth from low densities. Now more complex models should be treated in the same manner.
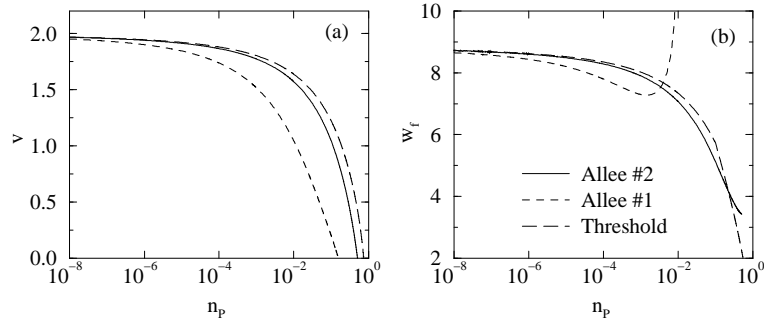
Figure 2.4: *Wave characteristics as predicted by the Shooting method. (a) the velocity of the 3 Fisher model formulations. (b) the width of the wave front of the 3 formulations. In the threshold formulation, $d = 0.1$. In the continuous Allee formulation(#1), $\delta = 0.1$ and in the discontinuous Allee formulation(#2) $a = 1.5$.*

Chapter 3

The Predator-Prey Model

Regrowth from unbiologically low population densities has been removed from a single species reaction-diffusion model. A method, coined the Shooting method, has been developed, so characteristics of invasion waves in this model can be predicted. To assess whether the same treatment works for a more complex model, now a two species predator-prey model is considered. The prey are immobile and the predators disperse. The growth rate of the predator population is reduced at low densities, by both addition to the model of a threshold density below which the population decreases, and use of an Allee effect. The biological correctness of these formulations is assessed. Then the Shooting method is adapted from the previous chapter and applied to these models, and the accuracy of the predictions made about the characteristics of the resultant wave fronts is determined.

3.1 Introduction

3.1.1 The Paradox of Enrichment

The predator-prey model to be considered was formulated by Rosenzweig (1971) from ideas discussed by Rosenzweig and MacArthur (1963). In this model there is one predator species, $C(T)$, and one prey species, $F(T)$, at time T. The prey grow logistically with intrinsic growth rate, R, to their carrying capacity, K. The predators have a Holling type II functional response with half saturation at H,

so the term for the uptake of prey by predators, $U(F)$, is

$$U(F) = \frac{U_m F}{F + H} \ .$$ (3.1.1)

The prey dynamics are described by

$$\frac{\partial F}{\partial T} = RF \left(1 - \frac{F}{K}\right) - U(F)C \ .$$ (3.1.2)

The predators die with the per capita mortality rate D. Ingested prey are converted to predator offspring with efficiency ε. This results in the equation for predator dynamics,

$$\frac{\partial C}{\partial T} = \varepsilon U(F)C - DC \ .$$ (3.1.3)

The model has exterior steady states at $(K, 0)$, where there are no predators present and the prey are at carrying capacity and $(0, 0)$, where there are neither predators nor prey present, and an interior steady state when

$$F^* = \frac{DH}{\varepsilon U_m - D}, \quad C^* = r \left(\frac{F^* + H}{U_m}\right) \left(1 - \frac{F^*}{K}\right)$$ (3.1.4)

The interior steady state can only exist if

$$K > \frac{DH}{\varepsilon U_m - D}.$$ (3.1.5)

If prey are present and this inequality is not fulfilled, the system will eventually reach the $((K, 0)$ steady state. For a locally stable interior stable state to exist,

$$\frac{K}{H} < \left[\frac{\varepsilon U_m + D}{\varepsilon U_m - D}\right].$$ (3.1.6)

If this condition is satisfied then the system reaches the interior steady state after a series of damped oscillations. If this condition is not satisfied then the predator and prey populations display stable limit cycles. This behaviour was termed the "Paradox of Enrichment" by Rosenzweig (1971). By enriching the environment for the prey species, the system becomes unstable and limit cycles result. The troughs of the limit cycles reaching very low densities would mean catastrophe for a real population.

3.1.2 Invasions of Predators in the Predator-Prey Model

It is then assumed that the predators disperse in a one dimensional arena with diffusion coefficient Φ, and that the prey are immobile. This gives a prey species $F(X, T)$ and a predator species $C(X, T)$ at time T and at position X. These assumptions result in the model

$$\frac{\partial F}{\partial T} = RF\left(1 - \frac{F}{K}\right) - U(F)C \tag{3.1.7}$$

and

$$\frac{\partial C}{\partial T} = \varepsilon U(F)C - DC + \Psi \frac{\partial^2 C}{\partial X^2} . \tag{3.1.8}$$

As in the single species model in the previous chapter, the model is then scaled. It is important that both equations in the model have the same scales of space and time. The scale of time is chosen to be $1/R$, so $T_0 = R^{-1}$, the scale of population is chosen to be H, so $F_0 = H$, and the scale of space is chosen to be $\sqrt{\Psi/R}$, so $X_0 = \sqrt{\Psi/R}$. This gives the dimensionless variables $t \equiv T/T_0$, $f \equiv F/F_0$, $c \equiv C/F_0$ and $x \equiv X\sqrt{R/\Psi}$, and the parameter groups $u_m \equiv U_m/T_0$, $d = D/T_0$ and $k \equiv K/F_0$. This produces the dimensionless uptake term

$$u(f) = \frac{u_m f}{f + 1} , \tag{3.1.9}$$

and the dimensionless model

$$\frac{\partial f}{\partial t} = f\left(1 - \frac{f}{k}\right) - u(f)c \tag{3.1.10}$$

and

$$\frac{\partial c}{\partial t} = \varepsilon u(f)c - dc + \frac{\partial^2 c}{\partial x^2} . \tag{3.1.11}$$

Assuming spatial homogeneity, the exterior steady states are $(0, 0)$ and $(k, 0)$ and the scaled interior steady state is

$$f^* = \frac{d}{\varepsilon u_m - d} , \quad c^* = \left(\frac{f^* + 1}{u_m}\right)\left(1 - \frac{f^*}{k}\right) , \tag{3.1.12}$$

which is equivalent to the steady state of the scaled version of the steady state of the non-spatial unscaled model. The scaled criterion for both populations to be real and positive is

$$k > \frac{d}{\varepsilon u_m - d} \tag{3.1.13}$$

34

and for the scaled system to be able to achieve the internal steady state and non-oscillatory,

$$k < \left[\frac{\varepsilon u_m + d}{\varepsilon u_m - d}\right]. \tag{3.1.14}$$

If this condition is satisfied and a travelling wave solution exists, a complicated wake structure follows a peak at the wave front which eventually reaches the (f, c) steady state, else a series of regular oscillations follow the wave front.

Dunbar (1983) has already developed a method to predict the velocity and exponential lapse rate of the front of the predator-prey model. To do this the wave is transformed to a moving frame of reference, where it is dependent only on $z \equiv x + v_R t$ with frame of reference velocity, $-v_R$. Equations (3.1.10) and (3.1.11) then become

$$\frac{d^2 c}{dz} + v_R \frac{dc}{dz} + (\varepsilon u(f) - d) c = 0, \tag{3.1.15}$$

$$v_R \frac{df}{dz} + f \left(1 - \frac{f}{k}\right) - u(f)c = 0. \tag{3.1.16}$$

If the leading edge of the front is close to the $(k, 0)$ steady state, then the equations decouple, with predator dynamics being described by

$$\frac{d^2 c}{dz} + v_R \frac{dc}{dz} + (\varepsilon u(k) - d) c = 0. \tag{3.1.17}$$

A solution is sought in form $c(z) = c_0 e^{-\lambda z}$, which must be non-negative as $z \to \infty$, so that the exponential increase rate, λ, is real. Such a solution is possible if λ is related to the velocity, v_R, by

$$v_R = \lambda + \frac{\varepsilon u(k) - d}{\lambda}. \tag{3.1.18}$$

There are an infinite number of solutions for v_R, if λ chosen correspondingly. The solution excited depends in the initial conditions. If $\varepsilon u(k) - d > 0$, there is minimum velocity, $v_0 = 2\sqrt{\varepsilon u(k) - d}$, which occurs when $\lambda = \sqrt{\varepsilon u(k) - d}$. Compact initial conditions excite the minimum velocity solution (Dunbar 1983)(Dunbar 1984). Therefore the velocity and the exponential lapse rate can be calculated for this system.

3.2 Increased Mortality of Predators at Densities beneath a Threshold

If the system displays limit cycles, the troughs may dip to very low densities. The dynamics following behind the first trough can be entirely dependent on regrowth from a very low density in a reaction-diffusion model. To stop this happening, the growth function of the predator population is altered so that at low densities there is negative growth. If reproduction is sexual, a low population density may lead to asexual reproduction, self fertilisation or inbreeding, reducing the genetic variability of the population and chromosomal breakage, leading to a reduction in fitness of the population. To model this, under a threshold density, C_P, the predators have an increased mortality rate, D_B, which is less than the above threshold rate, D_0. These values are scaled in the same way as the original predator-prey model, so the scaled threshold is $c_P = C_P/F_0$, the scaled mortality rate above the threshold is $d_0 = D_0/F_0$ and the scaled mortality rate below the the threshold is $d_B = D_B/F_0$. So in equations (3.1.10) and (3.1.11), d becomes,

$$d = \begin{cases} d_0 & c \geq c_P \\ d_B & \text{otherwise} \end{cases} \tag{3.2.1}$$

where

$$d_B > d_{Bm} \equiv u(k) \ , \tag{3.2.2}$$

so below the threshold, growth is negative.

When a threshold is applied to an oscillatory system one of two things can happen behind the front. If the threshold is low, the invasion persists and a wave train follows the initial invasion wave, as shown in Figure 3.1 (a). If the threshold is high enough, the low density populations in the first trough of the wave train become extinct, so there is only a single wave of predators from the point of introduction, a soliton wave, as shown in Figure 3.1 (c). Once the wave has passed through the arena there are no predators within the arena and the prey return to carrying capacity.

Addition of a threshold to the predator growth function reduces the velocity of the wave. As $d_B \to \infty$ the invasion halts altogether and as $d_B \to 0$, $v \to v_0$ as

36

shown by figure 3.3.

The development of methods to estimate the properties of waves with small thresholds has already been carried out (Gurney et al. 1998). d_B can be chosen to be very slightly larger than d_{Bm}, halting in situ regrowth while keeping velocity reduction to a minimum, so the method used for estimating the velocity of the non-thresholded case can still be used to describe these waves.

Predictions about the shape of the wave can also be made. The leading edge of the front can still be treated as in the non threshold case. At the trailing edge of predator band, the prey density is zero. The predator dynamics can therefore be described as in the non threshold model with $\varepsilon u(k) - d$ replaced with $-d$. The solution sought is of the form $e^{\lambda' z}$. The front velocity, v, and the exponential growth rate λ' are related by

$$v = \frac{d}{\lambda'} - \lambda',\tag{3.2.3}$$

implying that this part of the wave can travel at any speed as long as λ' is chosen accordingly. It must travel at the same velocity as the leading edge of the wave, so the exponential growth rate in the tail of the wave, λ_t, must be the positive solution of

$$\lambda_t^2 + v\lambda_t - d = 0,\tag{3.2.4}$$

which is

$$\lambda_t = \sqrt{\varepsilon u(k)} - \sqrt{\varepsilon u(k) - d}.\tag{3.2.5}$$

It is now assumed that these equations apply right to the peak of the predator outbreak. $z = 0$ where $c(z) = c_m$ the maximum of the peak, so there is a solution of the form

$$c(z) \simeq \begin{cases} c_m e^{-\lambda_c z} & z \geq 0 \\ c_m e^{\lambda_t z} & \text{otherwise} \end{cases}.\tag{3.2.6}$$

This allows estimation of the characteristic spatial scale of the predator outbreak. w_c is the distance over which c exceeds 10% of c_m, so

$$w_c \simeq \ln(10)\left(\frac{1}{\lambda_c} + \frac{1}{\lambda_t}\right).\tag{3.2.7}$$

This gives an approximate relationship between the total consumer population,

T_c, and c_m,

$$T_c = \int\limits_{-\infty}^{\infty} c(z)dz \simeq c_m \left(\frac{1}{\lambda_c} + \frac{1}{\lambda_t} \right). \tag{3.2.8}$$

To find c_m, T_c is assumed to be constant over time, possible only if the totals of reproduction and mortality balance, that is $dT_c = \varepsilon u_t$, where u_t represents the total rate of prey uptake by the predator population. As ahead of the predator outbreak the prey is at carrying capacity and behind the predator outbreak the prey are at zero density, a lower bound can be put on u_t by assuming that it corresponds to the rate the predators engulf unexploited territory multiplied by the prey density on the territory, so $u_t \approx k v_R$.

The prey are then assumed to increase linearly with z, starting from zero at $z = 0$ and reaching k at the point where $c = 0.05c_m$, which can be approximated as $z = 3/\lambda_c$. Integrating net prey production from $z = 0$ to $3/\lambda_c$ shows that the total prey reproduction in the region is $k/(2\lambda_c)$. Hence $u_t \approx k v_c + k/(2\lambda_c)$, which implies

$$dT_c = \varepsilon k \left(v_R + \frac{1}{2\lambda_c} \right) \tag{3.2.9}$$

Using equation (3.2.8) and substituting for λ_t, λ_c and v_R gives

$$c_m \approx 2\varepsilon k \left(1 - \sqrt{1 - \frac{d}{\varepsilon u(k)}} \right) \left(\frac{\varepsilon u(k)}{d} - 1 + \frac{1}{4d} \right). \tag{3.2.10}$$

To calculate the width of the region of prey depletion, the transformed dynamic equation (3.1.15) must be reconsidered. When predators are at their peak density, the prey have already been depleted to densities below their carrying capacity and half saturation level. Hence the scaled production of new prey is approximately f and scaled uptake function of the predators is approximately $u_m f$. Putting these back into the transformed equation and remembering that in the region of interest $c(z) \simeq c_m e^{\lambda_t z}$,

$$\frac{1}{f} \frac{df}{dz} = -\frac{1}{v_R} + \frac{u_m}{v_c} c_m e^{\lambda_t z}. \tag{3.2.11}$$

This can be integrated to give an approximate closed form solution for $f(z)$ which can be used to calculate the distance between the predator peak and the point where the prey population returns to k, w_f. It is assumed that $f(0) = k$, so w_f

38

is a solution of

$$\frac{w_f}{w_{fm}} = 1 - \exp\left(-(u_m c)\frac{w_f}{w_{fm}}\right), \quad w_{fm} \equiv \frac{u_m c_m}{\lambda_t}. \tag{3.2.12}$$

Provided that $u_m c_m > 3$, the solution of the equation is well approximated by $w_f = w_{fm}$, as shown by Gurney et al. (1998), so

$$w_f = \frac{u_m c_m}{\lambda_t}. \tag{3.2.13}$$

ε	c_P	Predicted Values				Observed Values			
		v	c_m	w_c	w_f	v	c_m	w_c	w_f
0.05	1×10^{-2}	0.42	3.7	35	76	0.39	3.17	40	61
0.075	1×10^{-2}	0.61	4.0	39	109	0.56	3.78	41	98
0.1	2×10^{-3}	0.75	4.4	43	142	0.74	4.40	46	145
0.15	3×10^{-5}	0.97	5.3	52	216	0.95	5.61	51	229
0.2	3×10^{-6}	1.15	6.3	59	300	1.14	6.75	61	323
0.3	3×10^{-7}	1.44	8.3	71	489	1.45	8.97	74	532
0.5	3×10^{-7}	1.89	12.2	91	938	1.93	13.29	94	1032

If $d_B >> d_{Bm}$ then the above methodology does not work because the assumption that the wave is minimally affected by the threshold no longer applies. An extension of the Shooting method, developed in chapter 2, can be used to predict the characteristics of the waves in this case. The model is transformed into a moving frame of reference, moving from left to right with velocity $-v_R$, in the same way as the non-thresholded model in equations (3.1.15) and (3.1.2), so again f and c are only dependent on $z \equiv x + v_R t$.

If $z = 0$ placed at some point, c_0, in the front where $c << c_P$ and $f \approx k$, then for all populations to the left of $z = 0$,

$$\frac{d^2 c}{dz^2} - v_R \frac{dc}{dz} - d_e c = 0, \quad \text{where} \quad d_e \equiv d_B - \varepsilon u(k) > 0. \tag{3.2.14}$$

This implies that for $z \leq 0$, a solution for $c(z)$ is sought in the form $c(z) = c(0)e^{\lambda_B z}$, where the exponential decay rate, λ_B is

$$\lambda_B = \frac{1}{2}\left[v_R + \sqrt{v_R^2 + 4d_e}\right]. \tag{3.2.15}$$

To the right of $z = 0$,

$$\frac{d^2c}{dz^2} - v_R\frac{dc}{dz} - (\varepsilon u(f) - d_0)c = 0 . \quad (3.2.16)$$

If $dc/dz \equiv \phi$, the transformed model can be rewritten as a triplet of coupled first-order ODEs

$$\frac{dc}{dz} = \phi, \quad \frac{d\phi}{dz} = v_R\phi - (\varepsilon u(f) - d_0)c \quad \text{and} \quad \frac{df}{dz} = \frac{1}{v_R}\left(p(f) - u(f)c\right), \quad (3.2.17)$$

Equations (3.2.17) are solved, subject to the initial conditions

$$c(0) = c_0, \quad c'(0) = \lambda_B c_0 \quad \text{and} \quad f(0) = k. \quad (3.2.18)$$

Figure 3.1 (b) and (d) shows that within the moving frame of reference the trajectories of c head monotonically to infinity if v_R exceeds the velocity of the wave front, v, but if $v_R < v$ then the trajectory initially dips below zero, as was proved for the Fisher model in the previous chapter. A bisection search similar to the one described in subsection 2.2.1 can then be used to find v. In this case the starting bracket for v_R is chosen as $(0 \rightarrow v_0)$. If n dips below zero or rises above 100 then $\phi = 0$, the resulting value of n at the end of the simulation is used as the criterion for the bisection search. The bisection search is terminated when the high and low ends of the bracket for v_R produce identical solutions up to the peak of the wave front.

The Shooting method can also find the peak predator density and therefore the width of the front. Figure 3.1 (b) and (d) shows that, as in the single species model in Chapter 2, as $v_R \approx v$, the trajectories of the solutions follow the shape of the wavefront, so measurement of the region where $\phi > 0$ can be used to predict the width of the wavefront. The correct velocity of the wave front, v, can be substituted into equation (3.2.5), for λ_t, instead of v_0, so an improved estimate of the shape of the back of the wave front can be made. The new estimate of λ_t can then be substituted into the calculations for the peak height and the width of the soliton wave. The new estimates for the peak height and λ_t can then be used in the calculation for the prey recovery width.

Table 3.1 shows that the velocities of the simulations are all predicted to within 1% by the Shooting method. Substitution of the values of v, c_m and w_f predicted
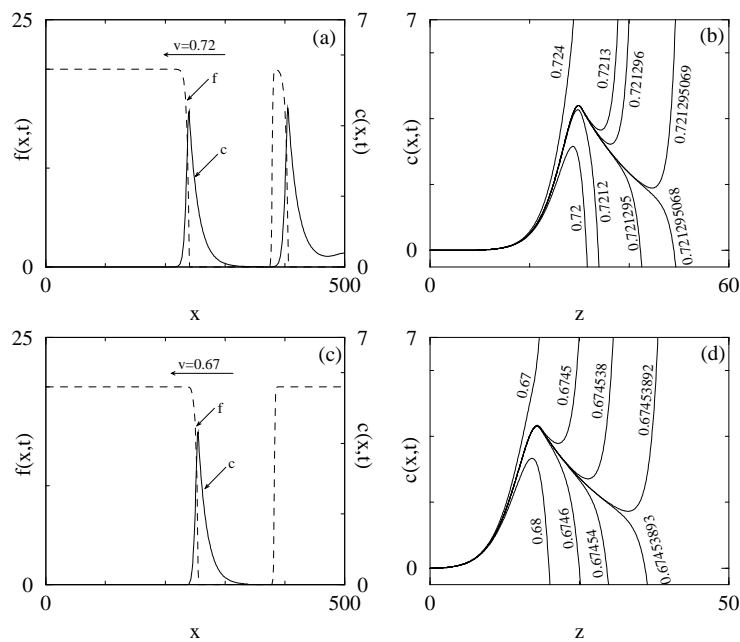
Figure 3.1: *Predator-prey model with a threshold, $k = 20$, $u_m = 2$, $d = 0.05$ and $\varepsilon = 0.1$. (a) A wave train travelling from right to left with $v = 0.72$ at time 350. $c_P = 10^{-4}$. (c) A soliton travelling from right to left with velocity $v = 0.67$ at time 350. $c_P = 10^{-2}$. In both these simulations, $\Delta x = 0.5$, the time increment varies between $\Delta t = 0.001 \to 0.1$ and a numerical integration tolerance of 0.00001. (b) and (d) show equivalent solutions in frames of reference moving at different velocities as marked. To obtain these, equation (3.2.17) was solved with the initial conditions in equation (3.2.18) and using RK4 with allowed error of 10^{-6}.*

by the Shooting method, into the calculations developed by Gurney et al. (1998),

c_P	Predicted Values				Observed Values			
	v	c_m	w_c	w_f	v	c_m	w_c	w_f
0.05	0.59	2.21	38	59	0.58	2.21	40	72
0.1	0.55	2.17	36	55	0.54	2.17	37	59
0.2	0.48	2.09	33	47	0.47	2.08	31	48
0.3	0.42	2.02	30	42	0.40	2.00	22	40
0.4	0.36	1.93	27	36	0.33	1.90	17	35
0.5	0.29	1.84	25	30	0.28	1.81	14	32

Table 3.1: *Comparisons between wave characteristics predicted by the Shooting method and those observed from simulations of the predator-prey model with a threshold. $\Delta x = 0.1$, the numerical integration tolerance is 0.000001, the time step varies between $\Delta t = 0.00001..0.001$, $k = 10$, $u_m = 2$, $\varepsilon = 0.1$, $d = 0.05$ and $d_B = 0.5$. v is the velocity of the wavefront, c_m is the maximum density of predators at the peak of the wavefront, w_c is the width of the wave front, measured from $c = c_m$ to $c = c_m/10$, and w_f is the recovery time of the prey.*

increases the accuracy of the predictions of the wave front characteristics when the solution of the system is a soliton.

The Shooting method predictions should be correct to arbitrary accuracy. The discrepancy is due to the discontinuity in both value and slope in the threshold formulation of the growth function. This discontinuity causes problems with the numerical simulations of the model which are used to produce the observed wave characteristics. As it was shown in Chapter 2 that using an Allee effect formulation for the Fisher model reduced this error, a formulation of the predator-prey model where regrowth from low densities is stopped by an Allee effect is now considered.

3.3 Decreased Prey Conversion Efficiency in Predators due to an Allee Effect

Now a model where the negative growth of populations with low densities is achieved by an Allee effect is considered, to reduce the error in the numerical simulations. Whereas previously the efficiency of conversion of prey into new predators was a constant, ε, in this formulation, the conversion efficiency, E, is

dependent on the density of predators. If predators never become scarce then $E = E_0$ (Cruickshank et al. 1998). If reproduction is sexual then at low densities mating is rare, so the conversion efficiency is reduced. To represent this in the model, E is proportional to of C up to a maximum, E_0, hence the dynamics of this system are described by

$$\frac{\partial F}{\partial T} = RF\left(1 - \frac{F}{K}\right) - U(F)C \quad \text{and} \quad \frac{\partial C}{\partial T} = (EU(F) - D)C + \Psi\frac{\partial^2 C}{\partial X^2} , \quad (3.3.1)$$

where

$$E = \begin{cases} E_0 & C \geq C_P(E_0U_m/D) \\ DC/(U_mC_P) & \text{otherwise} \end{cases} . \quad (3.3.2)$$

The steady states are identical to those of the original predator-prey model (with ε set to E), described in equation (3.1.4) if

$$C_P \leq \frac{RHD(DK + DH - KE_0U_m)}{KU_m(-E_0U_m + D)^2} . \quad (3.3.3)$$

R^{-1}, $\sqrt{\Psi/R}$, H and E_0H are identified as the natural scales of time, space, prey population and predator population respectively. The model is re-expressed in terms of dimensionless variables $t \equiv RT$, $x \equiv X\sqrt{R/\Psi}$, $f \equiv F/H$, $c \equiv c/(E_0H)$ and the parameter groups $k \equiv K/H$, $u_m \equiv U_m/R$ and $C_P \equiv c_P/(E_0H)$, giving

$$\frac{\partial f}{\partial t} = f\left(1 - \frac{f}{k}\right) - u(f)c \quad (3.3.4)$$

and

$$\frac{\partial c}{\partial t} = (eu(f) - d)c + \frac{\partial^2 c}{\partial x^2} \quad (3.3.5)$$

where

$$u(f) = \frac{u_m f}{f + 1} \quad (3.3.6)$$

and

$$e = \begin{cases} 1 & c \geq c_P u_m/d \\ dc/(u_m c_P) & \text{otherwise} \end{cases} . \quad (3.3.7)$$

This model's spatially homogeneous external steady state is identical to that of the non threshold model, and the internal steady state is

$$f^* = \frac{d}{u_m - d} , \quad c^* = \left(\frac{f^* + 1}{u_m}\right)\left(1 - \frac{f^*}{k}\right) , \quad (3.3.8)$$

43

only if

$$c_P \leq \frac{d}{u_m - d} \left(1 - \frac{d}{k(u_m - d)} \right). \tag{3.3.9}$$

As in the threshold formulation model, if the dynamics are non-oscillatory or the threshold density is low, eventually the predator and prey populations reach the stable coexistence state throughout the whole arena. If the threshold is large and the local dynamics are oscillatory or show weakly damped oscillations, then the wave form is a soliton.

As in the previous section, the model is transformed into a frame of reference travelling from right to left with velocity $-v_R$, so that c and f depend only on $z \equiv x + v_R t$. If $\phi \equiv dc(z)/dz$, equations (3.3.4) and (3.3.5) can be re-expressed as

$$\frac{d\phi}{dz} = v_R g - (eu - d)c, \quad \frac{dc}{dz} = \phi \tag{3.3.10}$$

and

$$\frac{df}{dz} = \frac{1}{v_R} \left[f(1 - f/k) - uc \right]. \tag{3.3.11}$$

If $z = 0$ is placed to the left of the front, where $c(z) = c_0 \ll c_P$, then for all $z < 0$, $f(z) \simeq k$ and hence $c(z) = c_0 e^{\lambda z}$, where

$$\lambda = \frac{1}{2} \left[v_R + \sqrt{v_R^2 + 4d} \right]. \tag{3.3.12}$$

Hence for $z > 0$, equations (3.3.11) and (3.3.10) can be solved subject to the initial conditions

$$c(0) = c_0, \quad f(0) = k \quad \text{and} \quad \phi(0) = c_0 \lambda. \tag{3.3.13}$$

Figure 3.2 shows that as in the thresholded formulation in the transformed predator-prey model with an Allee effect, if v_R is greater than the wave front velocity, v, $c(z) \to \infty$ as z increases. If $v_R < v$ then $c(z) < 0$ at some value of z. Figure 3.2 shows, when $v_R \simeq v$, and there is a travelling wave solution, the shape found must be the shape of the wave front, so estimates of the height of the peak and the width of the front can also be attained from the Shooting method.

44
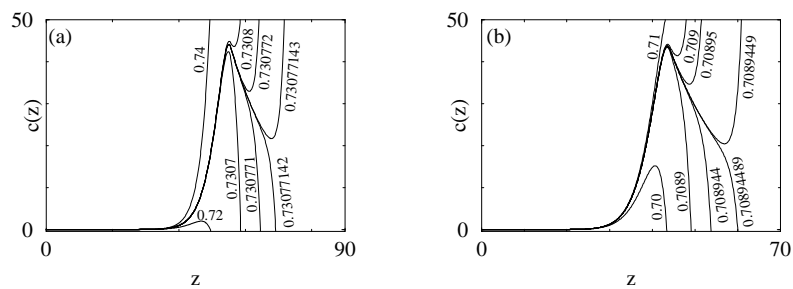
Figure 3.2:   *Solutions in frames of reference moving at different velocities as marked and $k = 20$, $u_m = 0.2$, $d = 0.05$, (a) a wave train with $c_P = 10^{-4}$ (b) a soliton with $c_P = 10^{-2}$. To obtain these, equations (3.3.11) and (3.3.10) were solved numerically with initial conditions as in equation (3.3.13) with an allowed error of 10^{-6}.*

$c_0 = min(0.0001, c_P/10000)$ is chosen as the starting population for the predator population and $f(0) = k$ is chosen as the starting population for the prey population for the bisection search, with $\phi(0)$ calculated from equation (3.3.12). v is then determined by a bisection search. The bracket for v_R is initially chosen to

be the same as in the threshold predator-prey model, as is the criterion for the end of the search.

k	c_P	Predicted Values			Observed Values		
		v	c_m	w_f	v	c_m	w_f
2.5	0.05	0.5180	7.45	13.8	0.5196	7.45	13.8
2.5	0.675	0.3653	7.10	10.7	0.3651	7.10	10.5
2.5	1.622	0.1828	6.62	12.0	0.1826	6.51	12.0
5.0	0.11	0.5826	12.4	11.1	0.5836	12.4	11.1
5.0	1.34	0.4099	11.5	8.77	0.4101	11.5	8.75
5.0	2.86	0.2047	9.92	11.2	0.2040	9.43	11.2
10.0	0.064	0.6535	22.7	10.7	0.6556	22.7	10.7
10.0	2.645	0.4357	20.4	7.73	0.4358	20.4	8.0
10.0	5.29	0.2178	16.9	10.7	0.2184	17.1	10.4
20.0	0.14	0.6744	43.1	9.463	0.6767	43.7	10.1
20.0	5.25	0.4494	38.3	7.324	0.4497	38.3	7.7
20.0	10.14	0.2249	31.0	10.5	0.2197	29.3	10.4

Table 3.2: *Comparisons between wave properties predicted by the Shooting method and those observed from simulations of the predator-prey model with an Allee effect. $\Delta x = 0.05$, the time step varying between $\Delta t = 0.0000001..0.0001$, the numerical integration tolerance is 0.0000001, $u_m = 0.2$ and $d = 0.05$. v is the velocity of the wavefront, c_m is the maximum density of predators at the peak of the wavefront, w_c is the width of the wave front, measured from $c = c_m$ to $c = c_m/10$, and w_f is the recovery time of the prey.*

Table 3.2 shows that for the predator-prey model with an Allee effect the Shooting method is very good at estimating the velocity, peak height and width of wave fronts. It can also be seen that at high thresholds the wave front widens. This is because at these thresholds, the criterion described by equation (3.3.9) is not fulfilled, so the system is no longer oscillatory and a state of coexistence is reached, as shown by figure 3.3.

3.4   Discussion

Both an Allee effect and a threshold have been used to reduce the regrowth of predator populations from very low densities. They successfully removed this effect while maintaining the dynamics of the unthresholded model at higher densities. In the threshold formulation the predators died with an increased mortality

rate, which describes inbreeding depression in real small populations (Kot et al. 1996) and in the Allee formulation the conversion efficiency of prey into new predators was decreased, describing problems of finding mates in small populations of sexually breeding organisms (Gurney et al. 1998).

These modifications to the original predator-prey model can make a large change to the wave form generated. If the system is oscillatory and the density of predators in the first trough behind the front is low enough in relation to the threshold, the predator population in the trough starts to die with the increased mortality rate or becomes less efficient at converting prey to new predators and goes extinct. There is no continuation of the wake after this trough, and the invasion wave becomes a soliton. Once the soliton has passed through the arena the arena returns to a state where there are no predators and the prey are at carrying capacity.

The Shooting method successfully predicts the characteristics of an invasion wave of predators which have negative growth at low densities in a two species predator-prey model. As discussed in Chapter 2, the method is more successful for the Allee formulation than the threshold formulation due to the discontinuities of the growth function.

Figure 3.3 shows that the Shooting method can be used to investigate the dynamics of the 2 formulations of the predator-prey model. $v_0 = 0.6095$, and as the threshold tends to zero the velocity nears v_0. As the threshold increases the wave front stops forming. There cannot be a negative velocity in these models as the wave is narrow. The peak height predictions show that the predator peak is only affected when the threshold is very high and the wave is close to non existence, which is to be expected as only low densities are affected by the threshold. In the Allee formulation, the wave front gets wider at high thresholds. This is because the steady state is changed as inequality (3.3.9) is no longer satisfied and the wave has become non-oscillatory.

Threshold and Allee effect growth function formulations removing regrowth from low densities populations for models describing the invasion of an exotic species.

The Shooting method has been shown to work for these altered models. Maybe other models with spreading waves, for instance, epidemic models, should be considered for this treatment.
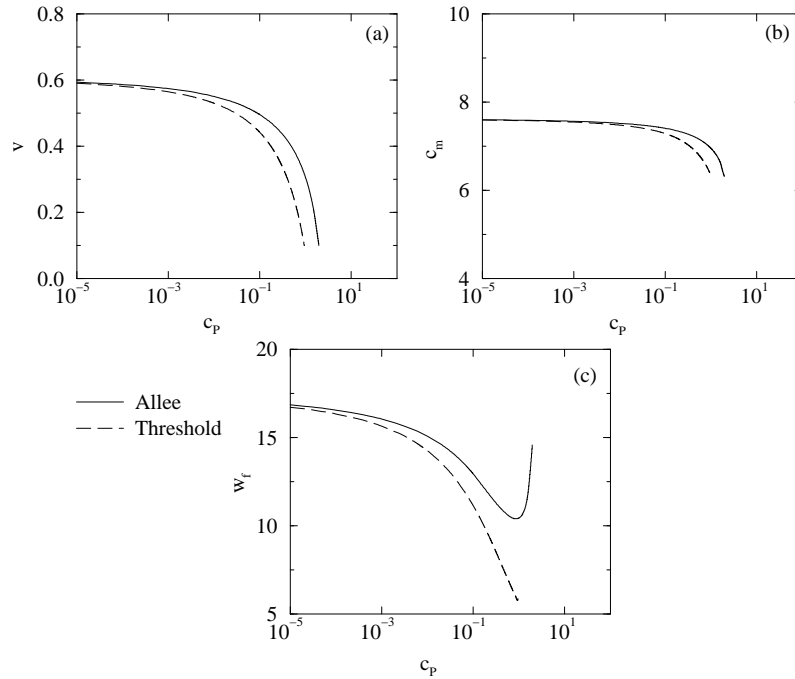
Figure 3.3: *Wave characteristics as predicted by the Shooting method of both the Allee and the threshold formulations of the predator-prey model. (a) shows the velocities, (b) shows the peak heights and (c) shows the front widths. The threshold results have been rescaled to the same scaling as the Allee effect formulation. In the Allee effect formulation model, $k = 2.5$, $u_m = 0.2$, $d = 0.05$ and in the threshold formulation model, $k = 2.5$, $u_m = 0.2$, $d_0 = 0.05$ and $d_B = 2$. For these parameters, $v_0 = 0.6095$.*

Chapter 4

The Two Stage Epidemic Model

Having looked at two forms of models where there is an invasion of a species into new regions, now a two stage epidemic model is considered. A threshold removing reinfection at low densities and a reduction in infectivity at low densities are applied to the epidemic model. If this is the case, the Shooting method can then be used to predict characteristics of the wave front in the resultant model.

4.1   Introduction

4.1.1   The Two Stage Epidemic Model

The 2 stage epidemic model was developed to describe the transmission of rabies in European foxes (Anderson et al. 1981). At a given time, T, there are two possible stages of infection; the susceptible stage, $S(T)$, in which an individual is healthy and can be infected, and the infective stage, $I(T)$, in which an individual is rabid. Susceptibles grow logistically with per capita rate of growth, R, to a carrying capacity, K. Infectives infect all susceptibles they contact with per capita contact rate B. Once infected, the individual goes on to infect susceptibles, and then dies with per capita mortality D. This produces the model

$$\frac{\partial S}{\partial T} = RS\left(1 - \frac{S}{K}\right) - BIS \tag{4.1.1}$$

49

and

$$\frac{\partial I}{\partial T} = BIS - DI. \tag{4.1.2}$$

This model has exterior steady states at $(0,0)$, $(K,0)$ and an interior steady state at (S^*, I^*) where

$$S^* = \frac{D}{B} \quad \text{and} \quad I^* = \frac{R}{B}\left(1 - \frac{S^*}{K}\right). \tag{4.1.3}$$

For both the infective and susceptible populations to be real and positive,

$$K > \frac{D}{B}. \tag{4.1.4}$$

4.1.2 The Spread of Rabies

As foxes have territories, and as after recruitment to the adult population they do not disperse, susceptibles are assumed to be immobile. This obviously inaccurate assumption can made because in terms of the spread of rabies, it is not the dispersal rate of foxes that is important, but the rate of contact between rabid and susceptible foxes which causes the spread of the disease. The infectives who do not contract the paralytic form of the disease wander aimlessly, and so disperse with diffusion coefficient Ψ (Källén et al. 1985). The population of susceptibles at position X, is $S(X,T)$, and the local density of infectives is $I(X,T)$. As the susceptible equation contains no spatial component, the equation for the susceptible population remains as in equation (4.1.1) and equation (4.1.2) becomes

$$\frac{\partial I}{\partial T} = BIS - DI + \Psi\frac{\partial^2 I}{\partial X^2}. \tag{4.1.5}$$

This model is scaled by using R^{-1} as the natural scale of time, T_0, K as the natural scale of population, S_0, and $\sqrt{\Psi/R}$ as the natural scale of space, X_0. This process results in the scaled variables $s \equiv S/S_0$, $i \equiv I/S_0$, $x \equiv X\sqrt{R/\Psi}$ and the parameter groups $b \equiv BK/T_0$ and $d \equiv D/T_0$, giving the equations

$$\frac{\partial s}{\partial t} = s(1 - s) - bis \tag{4.1.6}$$

and

$$\frac{\partial i}{\partial t} = bis - ds + \frac{\partial^2 i}{\partial x^2}. \tag{4.1.7}$$

50

The exterior steady states of this model are $(0,0)$, $(1,0)$ and the interior steady state is (s^*, i^*), where

$$s^* = \frac{d}{b} \quad \text{and} \quad i^* = \frac{b-d}{b^2} \tag{4.1.8}$$

which is positive and locally stable as long as $b > d$. If

$$b - d < \frac{d}{b} \tag{4.1.9}$$

the front has at most one overshoot before settling to the steady state. If not, there is a trail of damped oscillations behind the front (Källén et al. 1985).

The same method described in Chapter 3, developed from (Dunbar 1983), allows the calculation of the velocity of the wave front, where the introduction of a small propagule of infected individuals into an universe previously inhabited by susceptible individuals will eventually result in a wave travelling with velocity, v_0,

$$v_0 = 2\sqrt{b-d}. \tag{4.1.10}$$

With the rabies parameters suggested by Källén et al. (1985), this model always has a velocity greater than 242 km yr^{-1}. In nature a rabies epidemic has an observed velocity of around 30 to 60 km yr^{-1}. This suggests that this model does not accurately describe a rabies epidemic. This idea is explored in the next chapter. The wake behind the initial invasion wave can dip to very low densities of infectives, densities which are not biologically realistic, and persistence of the epidemic behind the wave front could be caused by in situ growth of these low density populations rather than through re-invasion of these areas (Mollison 1991), known as the "Atto-Fox" effect. The model is altered so that at very low densities of infectives, the individuals do not infect susceptibles locally. This in itself will reduce the velocity of the wavefront of this system. Two methods of removing reinfection by low density populations from this model are investigated.

4.2 Removal of Infection of Susceptibles by Infectives below a Threshold Density

The model can be altered so that densities of infectives below a threshold, I_P, are no longer infective, so the contact rate becomes a function, $B(I)$, the above threshold contact rate is B_0 and below the threshold $B = 0$. These parameters have the dimension of population and are scaled, so $i_P = I_P/S_0$ and $b_0 = B_0/S_0$, and the scaled function is termed b. So the model described in equations (4.1.6) and (4.1.7) is modified so that when the density of infectives falls below i_P, the contact rate of infectives with susceptibles is zero, so in equations (4.1.6) and (4.1.7),

$$b = \begin{cases} b_0 & i > i_P \\ 0 & \text{otherwise} \end{cases} . \tag{4.2.1}$$

This model has the same internal stationary state as the non thresholded model in equation (4.1.8) as long as $i^* > i_P$.

If the threshold density is low, the wake of the epidemic front is the same as in the non thresholded version of the model, and eventually there is persistence of the epidemic behind the front and the interior steady state is reached, as shown in figure 4.1 (a). If the threshold is increased, low densities of infectives in the wake behind the front do not infect susceptibles, there is no persistence of the epidemic and the epidemic wave becomes a soliton as shown by figure 4.1 (c) . So the persistence of rabies epidemics in this model is created by re-infection of susceptibles in areas with an unbiologically low density of infectives.

In the previous chapter, a method was developed to predict the shape of a whole soliton of a predator-prey model; the shape of the leading and trailing edges, the time it took for the prey to recover and the maximum density of predators in the peak. This method cannot be applied to the 2 stage epidemic model as the method relies on the assumption that the prey density falls to $f \approx 0$. In an epidemic, the susceptible density rarely falls to zero; this would cause the extinction of the infection. Therefore only the Shooting method can be used to make predictions about the characteristics of the wave front.

The Shooting method is altered so as to make predictions about the wave front characteristics of the 2 stage epidemic model. The model is transformed into a frame of reference travelling from left to right with velocity $-v_R$ and s and i depending only on $z \equiv x + v_R t$. This results in the transformed model

$$\frac{d^2 i}{dz^2} - v_R \frac{di}{dz} + g(i) \quad \text{and} \quad \frac{ds}{dz} = \frac{1}{v_R}\left[s(1-s) - bsi\right] \tag{4.2.2}$$

where

$$g(i) = \begin{cases} b_0 si - di & i > i_P \\ -di & \text{otherwise} \end{cases} . \tag{4.2.3}$$

If $\phi \equiv di/dz$ then equations (4.1.6) and (4.1.7) can be re-expressed as

$$\frac{d\phi}{dz} = v_R \phi - g(i), \quad \frac{di}{dz} = \phi \quad \text{and} \quad \frac{ds}{dz} = \frac{1}{v_R}\left[s(1-s) - bsi\right] , \tag{4.2.4}$$

If $z = 0$ is placed where $i(z) = i_P$, for all $z < 0$, $s(z) \approx 1$ and $i(z) = i_P e^{\lambda z}$ where

$$\lambda = \frac{1}{2}\left[v_R + \sqrt{v_R^2 + 4d}\right] . \tag{4.2.5}$$

Hence, for $z > 0$, equation (4.2.4) can be solved subject to the initial conditions,

$$s(0) = 1, \quad i(0) = i_P \quad \text{and} \quad \phi(0) = i_P \lambda . \tag{4.2.6}$$

Figure 4.1 shows that the trajectories of the solutions in the moving frame of reference are similar to those of the predator-prey model, so the Shooting Method bisection search can be used with the same criteria as used for the predator-prey model and equation (4.2.4) solved with initial conditions as set in equation (4.2.6).

There is again the problem of a discontinuity in the growth function in the simulation of the untransformed model, but there is no longer a discontinuity in the simulations of the z transformed model, as the simulations are initiated at the threshold. The predictions of the Shooting method are more accurate than in the predator-prey model formulated with a threshold. To reduce the affect of the discontinuity in the simulation, a formulation in which the value of the population is continuous is used instead of a threshold.

i_P	Predicted Values			Observed Values		
	v	i_m	w_f	v_f	i_m	w_f
1×10^{-8}	23.717	0.1531	0.5545	23.349	0.1531	0.5512
1×10^{-7}	23.563	0.1530	0.5460	23.349	0.1530	0.5429
1×10^{-6}	23.323	0.1530	0.5460	23.237	0.1530	0.5795
1×10^{-5}	22.918	0.1529	0.5295	22.906	0.1529	0.5380
1×10^{-4}	22.174	0.1526	0.5050	22.171	0.1527	0.5130
1×10^{-3}	20.645	0.1519	0.4635	20.655	0.1519	0.4635
1×10^{-2}	16.819	0.1464	0.3640	16.780	0.1464	0.3560

Table 4.1: *Comparisons between wave characteristics calculated by the Shooting method and those observed from simulations of the 2 stage epidemic model with a threshold. $\Delta x = 0.1$, the time step varies between $\Delta t = 0.00001 \cdots 0.001$, the numerical integration tolerance is 0.00001, $b = 292$ and $d = 146$. v is the velocity of the wavefront, w_f is the width of the wavefront and i_m is the maximum density of rabid individuals in the wavefront peak.*

4.3 Reduced Infection of Susceptibles by Low Densities of Infectives

As there is a small difference between the Shooting method predictions and the observed wave front characteristics from simulations for the 2 stage epidemic model with a threshold, a growth function is formulated as an alternate to the threshold formulation of the 2 stage epidemic model. The growth function is continuous in value but not in slope.

At high densities of infectives the force of infection is constant, B_0, while at low densities the force of infection rises linearly with infective densities (Cruickshank et al. 1998). So in equations (4.1.1) and (4.1.5),

$$B = \begin{cases} B_0 & I \geq I_P(B_0 K/D) \\ (D/K)(I/I_P) & \text{otherwise} \end{cases} . \qquad (4.3.1)$$

I_P is the infective density below which the infective population cannot reinfect. The steady state values for this model are the same as those of the original unmodified model as described in equation (4.1.3), as long as

$$I_P \leq \frac{RD(B_0 K - D)}{B_0^3 K^2} . \qquad (4.3.2)$$

Defining scaled variables $s \equiv S/K$, $i \equiv I/K$, $t \equiv RT$, $x \equiv \sqrt{R/\Psi}$ and parameter

groups $b_0 \equiv B_0 K/R$, $d \equiv D/R$ and $i_P \equiv I_P/K$ allows re-expression of the model as

$$\frac{\partial s}{\partial t} = s(1-s) - bsi \quad \text{and} \quad \frac{\partial i}{\partial t} = (bs-d)i + \frac{\partial^2 i}{\partial x^2} \qquad (4.3.3)$$

where

$$b = \begin{cases} b_0 & i \geq (b_0 i_P/d) \\ di/i_P & \text{otherwise} \end{cases} . \qquad (4.3.4)$$

There are 4 stationary states, $(0,0)$, $(1,0)$, high s^* and low i^*, low s^* and high i^*. Provided

$$i_P \leq (d/b_0^2)(1 - d/b_0) , \qquad (4.3.5)$$

the high i^* steady state is identical to that of the equivalent un-thresholded model,

$$s^* = \frac{d}{b_0} \quad \text{and} \quad i^* = \frac{b_0 - d)}{b_0^2}. \qquad (4.3.6)$$

As long as i^* is positive it is locally stable.

When local dynamics are non-oscillatory, or i_P is small, the behaviour of the modified model is unchanged except for a reduction in velocity. If i_P is larger than the infective density in the first trough behind the initial epidemic in the "no threshold" model, then the infective population does not recover from the trough but declines asymptotically to zero. The susceptible population then recovers to carrying capacity. So in addition to reducing the velocity of the front, the post-epidemic state of the system is also changed.

The behaviour of this system is investigated in a frame of reference moving with velocity $-v_R$. Looking for a constant shape solution, assuming that s and i depend only on $z \equiv x + v_R t$ and defining $\phi(z) \equiv di(z)/dz$, equation (4.3.3) is re-expressed as

$$\frac{di}{dz} = \phi, \frac{d\phi}{dz} = v_R \phi - (bs-d)i \qquad (4.3.7)$$

and

$$\frac{ds}{dz} = v_R^{-1} [s(1-s) - bsi] , \qquad (4.3.8)$$

where b is defined as in equation (4.3.1). If $z = 0$ is placed to the left of the front where $i(z) = i_0 << i_P$, then for all $z < 0$, $s \approx 1$ and hence $i(z) = i_0 e^{\lambda z}$ where

$$\lambda = \frac{1}{2}\left[v_R + \sqrt{v_R^2 + 4d}\right] . \qquad (4.3.9)$$

55

So for $z > 0$ equations (4.3.7) and (4.3.8) can be solved subject to the initial conditions

$$s(0) = 1 \quad , \quad i(0) = i_0 \quad \text{and} \quad \phi(0) = \lambda i_0 . \qquad (4.3.10)$$

In figure 4.2 the solutions produced are reminiscent of those in the threshold formulation of the model. They follow the true shape of the wavefront for a distance, depending on how close the frame of reference velocity is to the velocity of the wavefront. If the frame of reference velocity is less than that of the front velocity then the trajectory eventually dips below zero whereas if the frame of reference velocity is greater than that of the wave front the infective density diverges to ∞.

This allows a bisection search for the wave front velocity. $i_0 = min(0.0001, i_P/10000)$ is chosen as the starting population for the infective population and $s(0) = 1$ is chosen as the starting population for the susceptible population for each run, with $\phi(0)$ calculated from equation (4.3.10) and solving equations (4.3.7) and (4.3.8). The bisection search criteria are again identical to those used for the predator-prey model.

b_0	i_P	Predicted Values			Observed Values		
		v	w_f	i_m	v	w_f	i_m
4.5	6.7×10^{-5}	1.2020	9.82	0.02484	1.1925	9.8	0.02484
4.5	1.5×10^{-3}	0.8156	7.18	0.02469	0.8156	7.2	0.02470
5	4×10^{-5}	1.8041	6.32	0.04689	1.80	6.3	0.04689
5	4×10^{-3}	1.1808	3.97	0.04399	1.18	3.95	0.04399
12	4×10^{-4}	5.0831	2.15	0.3317	5.08	2.15	0.3316
12	0.033	3.3754	1.35	0.3066	3.38	1.35	0.3068
40	1.3×10^{-3}	10.209	1.06	0.6821	10.204	1.06	0.6822
40	0.0355	6.60	0.72	0.6542	6.605	0.72	0.6543

Table 4.2: *Comparisons between wave characteristics predicted by the Shooting method and those observed from simulations of the 2 stage epidemic model with the contact rate varying with slope at low densities. $\Delta x = 0.05$, the time step varies between $\Delta t = 0.000001..0.0001$, the numerical integration tolerance is 0.0000001 and $d = 4$ in all runs. v is the velocity of the wavefront, w_f is the width of the wavefront and i_m is the maximum density of infectives in the peak of the wavefront.*

There is a good agreement between the Shooting method and the values observed from simulations. There is a difference, which is again due to difficulties of simulating a model with a discontinuity in the growth function. The effect is reduced, as there is only a discontinuity in slope but not in value in this formulation. The use of a formulation which is continuous in value to remove infection of susceptibles from unbiological densities of rabid individuals has not changed the dynamics of the system above the threshold and it has improved the agreement between the Shooting method predictions and observations from simulations. Oscillatory behaviour is reduced by large thresholds.

4.4   Discussion

Figure 4.3 shows that when the threshold is low the velocity tends to v_0. When the threshold is high the wave becomes a soliton. Because of the soliton shape of the wave, it cannot retreat, as this would be equivalent to there being no travelling wave solution, so the velocity cannot be negative at high thresholds as in the Fisher model. The peak height is only affected by the threshold when the threshold is nearly high enough so stop the formation of the wave. The width of the wave decreases as the velocity decreases. There is a slight upturn in the Allee wave front width just before the wave stops forming as the steady state becomes dependent on the threshold density, i_P, as predicted by inequality (4.3.5). Otherwise the wave characteristics of the 2 models are very similar.

The Shooting method accurately predicts the velocities, wave heights and widths of the wave front observed from simulations. There is less of a discrepancy for the formulation which is continuous in value than in the formulation with a threshold. Again this is attributed to the discontinuity in the in both value and slope in the threshold formulation growth function, which cannot accurately be modelled in the numerical simulations of the model.

The effective removal of low density populations of infectives from the dynamics of the model may provide the reduction in velocity necessary for the model

to correctly predict the correct velocity of an epidemic wave of rabies in European foxes, but another improvement on the model may also provide this. This improvement is based on the life history of the diseased animals and shall be discussed in the next chapter.
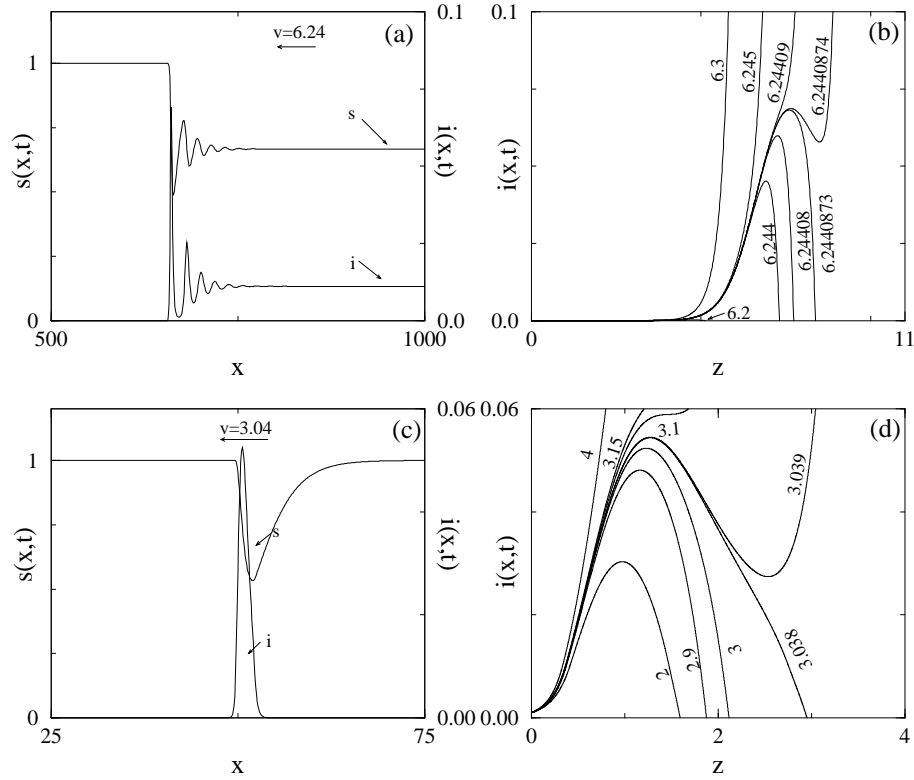
Figure 4.1: *Epidemic waves in the 2 stage epidemic model with a threshold.* $b_0 = 30$ *and* $d = 20$. *(a) shows a wave followed by a wake travelling from right to left with* $v = 6.24$ *and* $i_P = 1 \times 10^{-10}$, $\Delta x = 1$, *the time step varying between* $\Delta t = 0.001 \rightarrow 0.1$ *and a numerical integration tolerance of* 0.0001. *(c) shows a soliton travelling from right to left with* $v = 3.04$ *and* $i_P = 0.01$ *and* $\Delta x = 0.1$, *the time step varies between* $\Delta t = 0.00001 \rightarrow 0.001$ *and a numerical integration tolerance of* 0.00001. *Frames (b) and (d) show solutions in frames of reference moving with the marked velocities for* $i_P = 1 \times 10^{-10}$ *and* $i_P = 10^{-6}$ *respectively, attained by solving equation (4.2.4) with the initial conditions in equation (4.2.6).*

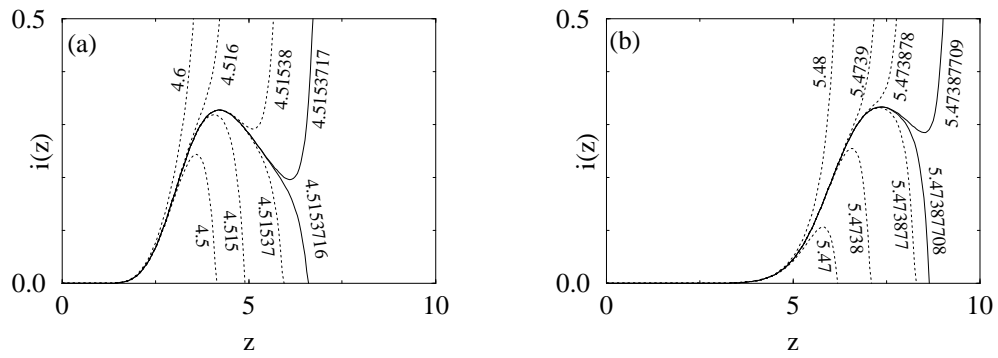Figure 4.2: *The 2 stage epidemic model with a contact rate varying with slope at low densities, with $b_0 = 12$ and $d = 4$. Frames (a) and (b) show solutions in frames of reference moving with the marked velocities for 5×10^{-3}, which forms a wave train, and $i_P = 10^{-6}$, which forms a soliton, respectively, with equations (4.3.7) and (4.3.8) solved with the initial conditions in equation (4.3.10).*
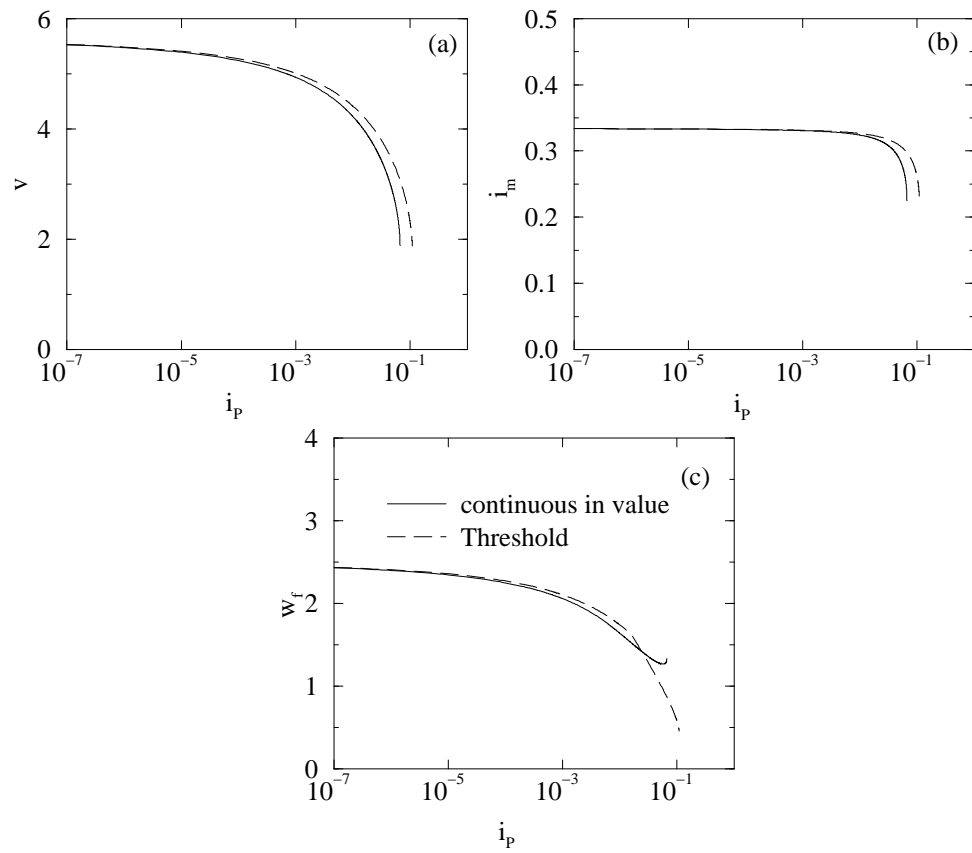
Figure 4.3: *Wave front characteristics of both new formulations of the 2 stage epidemic model as predicted by the Shooting method. In the both formulations, $b_0 = 12$ and $d = 4$ (a) shows the predicted velocity of the wave front, (b) the height of the wave front peak and (c) the width of the wave front as a function of threshold. For these parameters, $v_0 = 5.66$.*

Chapter 5

The Three Stage Epidemic Model

In the previous chapter, a 2 stage model for a rabies epidemic was considered. However, when a fox catches rabies there is an initial latent period when the infected individual shows no symptoms and does not infect others. A model hoping to describe the dynamics of the disease should include this latent period. A 3 stage epidemic model was devised by Murray et al. (1986). The model to be considered is very similar to this.

The growth function of the infectives is altered so that a threshold and a formulation which is continuous in value but not slope are used to reduce the infectivity of the infectives. The Shooting method is then altered so it can be used for this model, and the ability of this method to make predictions about the epidemic wave front of a 3 stage rabies model with no reinfection at low densities is assessed.

5.1 Introduction

5.1.1 The 3 Stage Epidemic Model

At time T, the dynamics of susceptible foxes, $S(T)$, remains unchanged from the 2 stage model, but Q is used as the per capita growth rate parameter. All susceptible foxes contacted with rate B becomes latently infected and are asymp-

tomatic carriers of the disease. Individuals in the incubating population, $I(T)$, have a probability per unit time, L, of becoming rabid. During this latent period the mortality rate of incubating individuals is unaffected by the progress of the disease and have the die with the *per capita* mortality rate , M. In the infective population, $R(T)$, a fox either contracts the paralytic form of the disease or goes on to infect susceptibles. The infectives then die with per capita mortality rate D. This produces a model where

$$\frac{\partial S}{\partial T} = QS\left(1 - \frac{S}{K}\right) - BSR\,, \tag{5.1.1}$$

$$\frac{\partial I}{\partial T} = BSR - (L + M)I \tag{5.1.2}$$

and

$$\frac{\partial R}{\partial T} = LI - DR. \tag{5.1.3}$$

The model has two external steady states at $(0, 0, 0)$ and $(K, 0, 0)$, and has a single internal steady state, at (S^*, I^*, R^*), where

$$S^* = \frac{D}{B}\left(\frac{L + M}{L}\right), \quad I^* = \frac{D}{L} \quad \text{and} \quad R^* = \frac{Q}{B}\left(1 - \frac{S^*}{K}\right). \tag{5.1.4}$$

For the internal steady state to exist,

$$K > \frac{D}{B}\left(\frac{L + M}{L}\right). \tag{5.1.5}$$

If this inequality is not fulfilled the model returns to the state where there are no rabid or incubating individuals and the susceptible foxes are at carrying capacity.

5.1.2 The Spread of Rabies

Susceptible and incubating foxes reside in territories after recruitment to the adult population, and these territories are assumed to always be filled, so it is assumed there is no net movement of non rabid foxes. Once rabid, the fox is assumed to run erratically. This is described as diffusion in this model (Murray et al. 1986) (Skellam 1951), spreading the disease with diffusion constant Ψ , so equation (5.1.3) becomes

$$\frac{\partial R}{\partial T} = LI - DR + \Psi\frac{\partial^2 R}{\partial X^2}. \tag{5.1.6}$$

K is chosen as the natural scale of population, S_0, Q^{-1} as the natural scale of time, T_0, and $\sqrt{\Psi/Q}$ as the natural scale of distance, X_0, giving dimensionless variables $s \equiv S/S_0$, $i \equiv I/S_0$, $r \equiv R/S_0$, $t \equiv T/T_0$, $x \equiv X/X_0$ and the parameter groups $l \equiv L/T_0$, $d \equiv D/T_0$, $m \equiv M/T_0$ and $b \equiv BK/T_0$. This scaling process results in the equations

$$\frac{\partial s}{\partial t} = s(1 - s) - bsr, \tag{5.1.7}$$

$$\frac{\partial i}{\partial t} = bsr - (l + m)i \tag{5.1.8}$$

and

$$\frac{\partial r}{\partial t} = li - dr + \frac{\partial^2 r}{\partial x^2} . \tag{5.1.9}$$

The scaled spatial model has external steady states at $(0, 0, 0)$ and $(1, 0, 0)$ and an internal steady state at (s^*, i^*, r^*) where

$$s^* = \frac{d}{b}\left(\frac{l + m}{l}\right), \quad i^* = \frac{d}{l} \quad \text{and} \quad r^* = \frac{1}{b}(1 - s^*) . \tag{5.1.10}$$

The scaled criterion for the system to reach the internal steady state is,

$$\frac{b}{d} > \left(\frac{l + m}{l}\right) . \tag{5.1.11}$$

The method for determining the velocity of the epidemic wave, v_0, in this model has been devised by Murray et al. (1986) Murray (1989). The resulting calculation for this model is not described here due to mathematical complexity.

As in the 2 stage epidemic model, there is a wake behind the initial invasion front where the population of infectives reaches low densities in the troughs. These populations can be too small to be biologically realistic. Dynamics of the wave are thought to depend on reinfection of susceptibles by these small populations (Mollison 1991). To remove reinfection from low densities of infectives in the 3 stage epidemic model, a threshold density is chosen, beneath which rabid individuals are unable to infect susceptibles in the next section, and then the contact rate is varied with slope at low densities in the third section of this chapter.

5.2 Removal of Infection of Susceptibles by Infectives below a Threshold Density

The contact rate, B, becomes a function of population, so that below a threshold density, R_P, $B \approx 0$, so there is no infection of susceptibles locally. Above the threshold, $B = B_0$, B_0 being constant. Below the threshold the rabid population decreases exponentially with per capita mortality rate D after recruitment from the incubating population stops. These new parameters have the dimension of population, and are scaled to S_0, so $b = B/S_0$, $r_P = R_P/S_0$ and $b_0 = B_0/S_0$. In this situation, in equations (5.1.7) and (5.1.9),

$$b = \begin{cases} b_0 & r \geq r_P \\ 0 & \text{otherwise} \end{cases} \quad . \tag{5.2.1}$$

As in the 2 stage epidemic model, there are two outcomes of using a threshold formulation in the 3 stage epidemic model. At low threshold densities, as demonstrated in figure 5.1 (a), the wake is not affected by the threshold and the rabies epidemic persists behind the epidemic front. If the threshold is increased, as in figure 5.1 (c), the rabies epidemic dies out in the first trough following the front, forming a soliton wave.

The approximations developed by Gurney et al. (1998) for calculating characteristics of a soliton wave for a 2 species predator prey model cannot be applied to the 3 stage epidemic model as there is an extra stage in the system and the calculations depend on the assumption that the prey/susceptibles are approximately zero behind the initial invasion front. The Shooting method is the only tool that can be used to make predictions about the characteristics of the epidemic front.

As in previous chapters, the equations are transformed into a moving frame of reference, moving from right to left with velocity $-v_R$, where $z \equiv x + v_R t$, resulting in the set of equations

$$\frac{ds}{dz} = \frac{1}{v_R}\left(s(1-s) - bsr\right) \, , \tag{5.2.2}$$

$$\frac{di}{dz} = \frac{1}{v_R}\left(bsr - (l+m)i\right) \tag{5.2.3}$$

and

$$\frac{d^2r}{dz^2} - v_R\frac{dr}{dz} + (li - dr) = 0 \ , \tag{5.2.4}$$

which can be decoupled into

$$\phi = \frac{dr}{dz} \quad \text{and} \quad \frac{d\phi}{dz} = v_R\phi - (li - dr) \ . \tag{5.2.5}$$

$z = 0$ is positioned so that $z(0) = r_P$, so for $z < 0$, $s \approx 1$, $i \approx 0$ and

$$\frac{d^2r}{dz^2} - v_R\frac{dr}{dz} - dr = 0. \tag{5.2.6}$$

This has a solution $r(z) = r_Pe^{\lambda z}$, with $r(z) \to 0$ as $z \to -\infty$ provided $\lambda > 0$. This requires that

$$\lambda = \frac{1}{2}\left(v_R + \sqrt{v_R^2 + 4d}\right) \ . \tag{5.2.7}$$

For $z > 0$ equations (5.2.2), (5.2.3) and (5.2.5) are solved subject to the initial conditions

$$s = 1, \quad i = 0, \quad r = r_P \quad \text{and} \quad \phi = \lambda r_P \ . \tag{5.2.8}$$

Figure 5.1 (b) and (d) shows that if v_R is greater than the wave front velocity, v, then the $r(z) \to \infty$ and if $v_R < v$ then the population dips below zero, as in the 2 stage model. This means that the same bisection search algorithm can be used to find v. Also, the closer v_R is to v the further the trajectory follows the shape of the wave front, so the peak height and wave front width can be estimated.

v is then determined by the same bisection search as described for the predator-prey model, with equations (5.2.2), (5.2.3) and (5.2.5) solved with the initial conditions as set in equation (5.2.8).

The Shooting method can be used to predict the velocity, peak height and width of wave front. There is, however a discrepancy between the predicted and the observed results. As the threshold density is increased, the accuracy of the prediction of the width of the wave front decreases. From experiments in Chapter 2 it is known that this is due to the discontinuity in growth function causing inaccuracies in the simulations. This discrepancy can be reduced by using a growth function in which the contact rate is a function of slope at low densities, as it is continuous in value if not in slope.

b_0	r_P	Predicted Values			Ob served Values		
		v	w_f	r_m	v	w_f	r_m
240	2×10^{-5}	2.885	0.782	0.01219	2.893	0.786	0.01220
240	9×10^{-4}	1.743	0.409	0.01073	1.628	0.428	0.01049
320	1×10^{-4}	4.055	0.630	0.02559	4.066	0.632	0.02556
320	2×10^{-3}	2.610	0.360	0.02318	2.461	0.376	0.02277
480	1.5×10^{-4}	6.069	0.556	0.04618	6.119	0.561	0.04627
480	4×10^{-3}	3.846	0.315	0.04221	3.791	0.354	0.04207
640	1×10^{-3}	6.662	0.447	0.05897	6.632	0.448	0.05886
640	6×10^{-3}	4.649	0.279	0.05460	4.573	0.328	0.05430

Table 5.1: *Comparisons between wave properties predicted by the Shooting method and those observed from simulations of the 3 stage epidemic model with a threshold. $\Delta x = 0.1$, the time steps vary between $\Delta t = 0.00001..0.001$, the numerical integration tolerance is 0.00001, $d = 146$, $l = 26$ and $m = 1$ in all runs. v is the velocity of the wavefront, w_f is the width of the wavefront and r_m is the maximum density of rabid individuals in the peak of the front.*

5.3 Contact Rate varying with Slope at Low Densities

Now the contact rate is varied to reduce reinfection from unbiological populations (Cruickshank et al. 1998). As in the threshold formulation, the contact rate is altered so that there is little infection of susceptibles in the locality of very low densities of rabid animals. The force of infection B_0 is assumed to be constant at high densities but at low densities it rises linearly with small rabid densities.

$$\frac{\partial S}{\partial T} = QS\left(1 - \frac{S}{K}\right) - BSR, \quad \frac{\partial I}{\partial T} = BSR - (L + M)I \,, \qquad (5.3.1)$$

$$\frac{\partial R}{\partial T} = LI - DR + \Phi\frac{\partial^2 R}{\partial X^2} \,. \qquad (5.3.2)$$

where

$$B = \begin{cases} B_0 & R \geq KB_0R_PL/(D(L+M)) \\ (L+M)DR/(LKR_P) & \text{otherwise} \end{cases} \;. \qquad (5.3.3)$$

If

$$R^* \geq KB_0R_PL/(D(L+M)) \,, \qquad (5.3.4)$$

then the steady states of the model are the same as those of the unmodified model, as described by equation (5.1.4).

This as scaled in the same manner as the original unmodified 3 stage epidemic model, so that in equations (5.1.7), (5.1.8) and (5.1.9),

$$b = \begin{cases} b_0 & r \geq b_0 r_P l / d(l+m) \\ dr/r_P(1 - m/l) & \text{otherwise} \end{cases} . \qquad (5.3.5)$$

When r^* is greater than the density at which the contact rate changes, ie

$$r^* \geq b_0 r_P l / d(l+m) , \qquad (5.3.6)$$

the stationary states are as those of the unmodified scaled model, as described by equation (5.1.10).

Again, the Shooting method can be used to make predictions about characteristics of the epidemic wave front.

Assuming the wave is originally moving from right to left, the model is transformed into a moving frame of reference travelling from right to left with velocity $-v_R$, giving equations (5.2.2), (5.2.3) and (5.2.5), with b as described by equation (5.3.5).

$z = 0$ is placed to the left of the wave front, where $r(z) = r_0 \ll r_P$, so that for all $z < 0$, $s(z) \approx 1$, $i \approx 0$ and

$$\frac{d^2 r}{dz^2} - v_R \frac{dr}{dz} - dr = 0 \qquad (5.3.7)$$

and hence $r(z) = r_0 e^{\lambda z}$ in the tail of the wave front, where λ is as in the previous section. The equations (5.2.2), (5.2.3) and (5.2.5) are then solved subject to the initial conditions

$$s = 1, \quad i = 0, \quad r_0 \ll r_P \quad \text{and} \quad \phi = r_0 \lambda . \qquad (5.3.8)$$

Figure 5.2 shows that the trajectories in this formulation show the same relationship between v and v_R as in threshold case, so a bisection search can be used to find the velocity of the wavefront, the peak height and the width of the wavefront.

$r_0 = min(0.0001, r_P/10000)$ is chosen as the starting population for the predator population. determined by a bisection search, with equations (5.2.2), (5.2.3) and (5.2.5) solved with the initial conditions as set in equation (5.3.8).

68

K	R_P	Predicted Values			observed Values		
		V	W_f	R_m	V	W_f	R_m
1.2	1.2×10^{-7}	20.35	23.20	0.004957	20.39	23.24	0.004958
1.2	2.28×10^{-5}	17.61	19.02	0.004873	17.60	19.03	0.004873
1.2	5.16×10^{-4}	10.44	10.87	0.004113	10.37	10.81	0.004104
4	4×10^{-6}	85.98	11.92	0.2426	86.14	11.95	0.2427
4	2.84×10^{-4}	76.94	10.5	0.2401	77.26	10.56	0.2398
4	1.396×10^{-2}	44.25	6.70	0.2141	43.81	6.66	0.2127

Table 5.2: *Comparison between predictions made by the Shooting method and observations from simulations of the 3 stage epidemic model with varying contact rate, with $B_0 = 80$, $L = 13$, $M = 0.5$, $Q = 0.5$, $D = 73$. In the simulations, $\Delta x = 0.05$, the time step varies between $\Delta t = 0.000001 \rightarrow 0.0001$ and the numerical integration tolerance is 0.000001.*

Table 5.2 shows that the Shooting method accurately predicts the velocity and shape of wave fronts formed by the 3 stage epidemic model with a varying contact rate.

5.4 Discussion

In this chapter, both threshold and varying contact rate formulations have been used to remove unbiological reinfection of susceptible individuals by tiny fractions of rabid individuals in a 3 stage rabies epidemic model. This was achieved by decreasing the contact rate between susceptible and rabid individuals below a threshold or critical level. Both formulations successfully removed the reinfection. When r_P increases, the epidemic dies out and if $r_P \rightarrow 0$, $v \rightarrow v_0$.

The Shooting method can be used to predict velocity, peak height and wave front width of a 3 stage epidemic model where there is no regrowth from low densities of infectives. There is a lesser discrepancy between the Shooting method predictions and the observed characteristics from the varying contact rate formulation than for the threshold formulation, probably due to the discontinuity only being in slope instead of in value when the contact rate varies, so creating a smaller error in the numerical solutions than in the threshold formulation model.

Figure 5.3 shows that the threshold and varying contact rate formulations have

almost exactly the same dynamics. The velocity at low thresholds tends to V_0 and at high thresholds the wave is stopped as a soliton cannot retreat. The width of the wave decreases with velocity. The peak height is largely unaffected by the threshold until the wave is close to non existence.

Next, this model is to be applied to the rabies epidemic in European foxes. The predictions that the varying contact rate formulation model makes about the epidemic are compared with the velocities and wave forms known to exist in the epidemic.
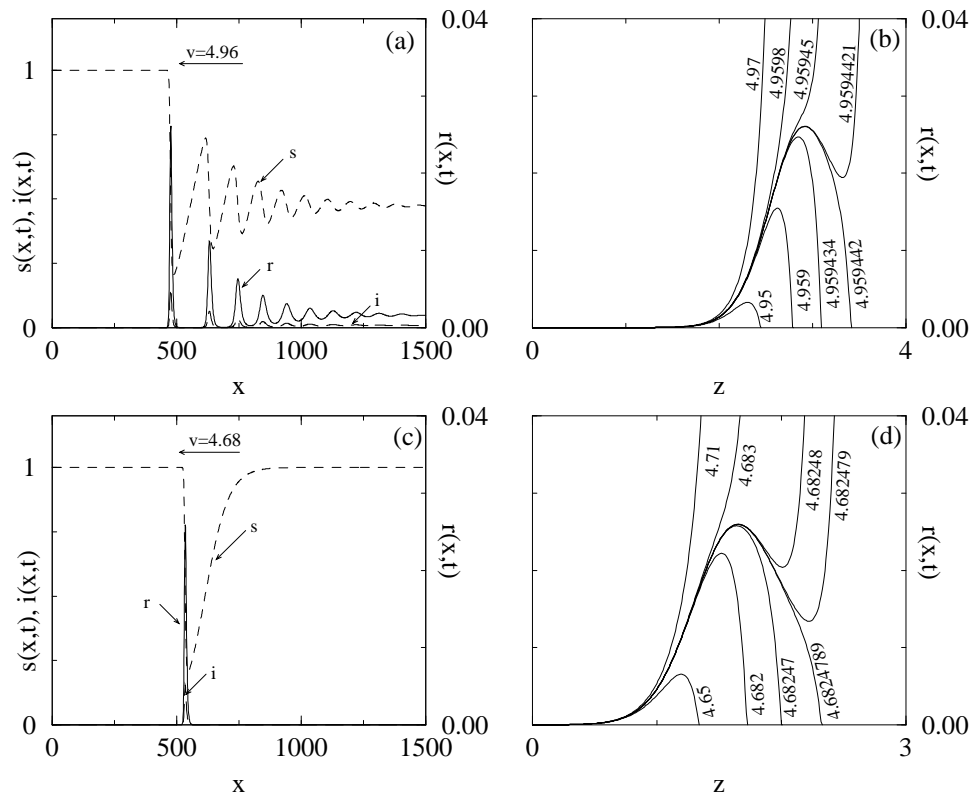
Figure 5.1: *Epidemic waves in the 3 stage epidemic model. $b_0 = 320$, $d = 146$ $l = 26$ and $m = 1$. Frame (a) shows persistence of the epidemic with $r_P = 10^{-10}$. Frame (c) shows a soliton wave with $r_P = 10^{-6}$. In both simulations, $\Delta x = 1$, the time step varies between $\Delta t = 0.001 \rightarrow 0.1$ and the numerical integration tolerance is 0.0001. Frames (b) and (d) show solutions of equations (5.2.2), (5.2.3) and (5.2.5) solved with the initial conditions described in equation (5.2.8) in frames of reference moving with the marked velocities respectively.*
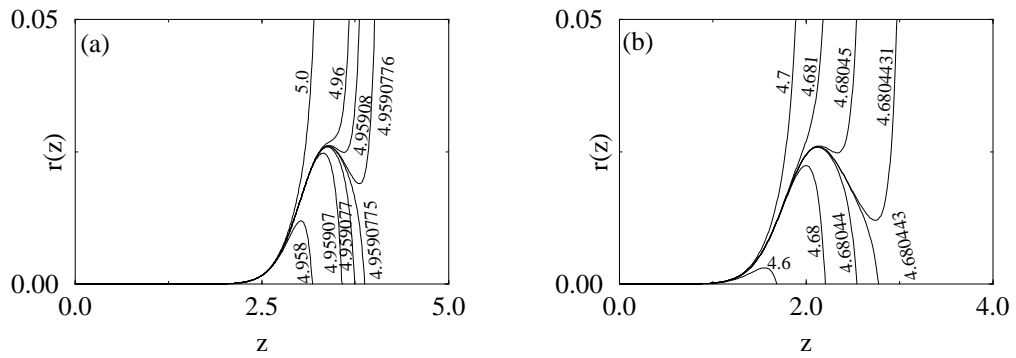
Figure 5.2: *Solutions of the transformed 3 stage epidemic model in frames of reference moving with the marked velocities. $b_0 = 320$ and $d = 146$, $l = 26$ and $m = 1$. Frames (a) and (b) show the solutions for $r_P = 10^{-10}$, which produces a wake, and 10^{-6}, which produces a soliton, respectively.*
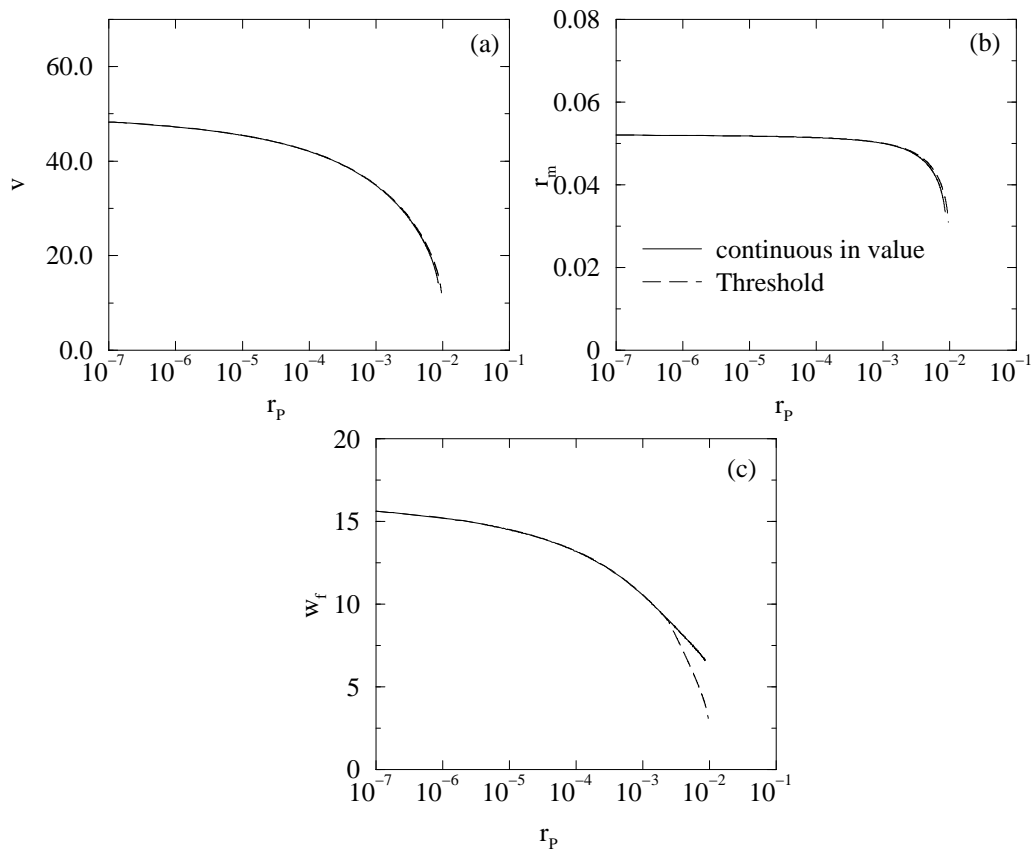
Figure 5.3: *Predictions made about the wave front of the 3 stage epidemic model by the Shooting method. (a) shows the velocity, (b) shows the peak height and (c) shows the width of the wave front as a function of threshold. $K = 2$, $B_0 = 80$, $D = 73$, $Q = 0.5$, $L = 13$ and $M = 0.5$. For these parameters, $V_0 = 5.08$.*

Chapter 6

Overview of Reaction-Diffusion Models of Epidemics and Invasions

6.1 The Shooting Method

The Shooting method can be used to predict the velocity, the width of the wave front and where applicable the peak height of invasion and epidemic waves where the dispersing individuals cannot grow from low densities.

A single species invasion model, a predator-prey model with invasion of predators, a two stage epidemic model and a three stage epidemic model have been considered. Each model has been altered so there is no population growth at low densities. The characteristics of wavefronts in these models can be predicted with the Shooting method. In the epidemic models, the threshold and varying contact rate formulations have near identical wave characteristics. Using the latter formulation increases the accuracy of the Shooting method, so this formulation is now to be used in preference to the threshold formulation in each model.

Now the 3 stage epidemic model, with the contact rate varying at low densities, is going to be applied to a real system.

6.1.1   Accuracy of the Shooting Method

The completely continuous growth function with an Allee effect, used in Chapter 2, shows that when the discontinuity is removed, the velocity predictions are accurate to an arbitrary level. Unfortunately this Allee formulation is not suitable to be used in these models as it effects the dynamics of the populations at high densities as well. For this reason, a formulation which is continuous in value but not in slope has been used to reduce discrepancies between the predictions and observations from simulations. It is known that the numerical simulations of the time and space models miss the threshold. In z transformed models when the simulations have a starting population which is lower than the point of the discontinuity, it is possible that the discontinuity is also missed. This can be checked by reducing the minimum value of Δz until the Shooting results converge.

minimum Δz	v	w_f
0.5	1.8657	8.5
0.3	1.8651	8.4
0.2	1.8652	8.2
0.1	1.8653	8.3
0.01	1.8653	8.3
0.00001	1.853	8.3

Table 6.1:   *Shooting method predictions for the Fisher model with a discontinuous Allee effect, with $a = 1.5$, an integration tolerance of 0.00001 and $n_P = 1 \times 10^{-4}$ and varying the minimum Δz. v is the velocity of the wave front and w_f is the width of the wave front from 0.1 to 0.9.*

Table 6.1 shows that the results converge at $\Delta z = 0.1$. The minimum value of Δz used in all the variants of the Shooting method was 0.00001, so it is unlikely that the Shooting method results are affected by discontinuities in growth functions.

6.2   Rabies Epidemics in 1D

The 3 stage epidemic model described in chapter 5 was formulated to represent the rabies epidemic currently spreading through the European fox population (Murray et al. 1986) (Murray 1987) (Murray 1989). Now the 3 stage epidemic

model with an Allee effect is used, and the velocities predicted by the Shooting method are compared those seen in nature.

To investigate this, a set of parameters for the spread of rabies in European foxes was taken from Murray (1989). At first at the velocity of epidemic waves with no

Parameter	Symbol	Value
average birth rate	a	1 yr^{-1}
average intrinsic death rate	M	0.5 yr^{-1}
average duration of clinical disease	$1/D$	5 days
average incubation time	$1/L$	28 days
force of infection	B_0	80 km$-$2yr^{-1}
carrying capacity	K	$0.2 \rightarrow 4$ foxes km^{-2}
diffusion coefficient	Ψ	200 km^2 yr $^{-1}$

threshold, V_0, is considered. The velocity calculation from Murray (1989) for the 3 stage rabies epidemic was adapted to this formulation of the model to estimate V_0.

K (km^{-2})	V (km yr^{-1})
1.2	22
1.5	34
2	51
3	75
4	93

The results in table 6.2 are very similar to those obtained by Murray in 1986 and 1989, so the small changes between the 3 stage epidemic model formulated in this thesis produce no large difference from Murray et al.'s 3 stage epidemic formulation. Table 6.2 shows that when K is at the higher end of the possible scale the predicted velocities are higher than those observed in nature. This suggests that reducing regrowth of unbiological populations, which would reduce the velocity of the epidemic wave, may be a good idea. An Allee formulation as described in previous chapter is used to effect this as this allows accurate Shooting predictions to be made about the wave characteristics.

A series of runs carried out for the parameters in table 6.2 are shown in figure 6.1. In chapter 5 it has been shown that for the parameters given in table 6.2, with a

threshold of 10^{-6}km^{-2}, the model gives rise to a soliton solution. The predictions of the Shooting method show that with a threshold this low the epidemic is only a few percent slower than the non-thresholded model. Much higher thresholds can cause significant changes in the characteristics of the epidemic.

To estimate the appropriate threshold for a rabies epidemic, it is assumed that no rabid individual is likely to live for more than double the average lifespan, 10 days. The diffusion coefficient is difficult to estimate, but Murray (1989) states that it is unlikely to lie out with the range, $70 \rightarrow 330$ km^{2}yr^{-1}. The root mean square displacement of an rabid individual between becoming infected and dying must therefore be between 2.8 and 6.1 km. Since the probability distribution of this displacement is Gaussian, it seems reasonable to assume that any susceptible individual that does not have at least one rabid individual within three times the root mean square displacement in safe from infection. This implies that R_P lies within the range 1×10^{-3} km^{-2} and 4.5×10^{-3} km^{-2}.

In the calculation of the contact rate, B_0, it is assumed that below a critical value of the carrying capacity, K_P, the epidemic wave cannot form. There is a wide range of observed values for K_P, from $0.25 \rightarrow 1$km^{-2}. B_0 in Table 6.2 is chosen so that the front of the epidemic wave does not form at $K_P = 1$. As this value is at the top of the range for the critical carrying capacity, the centre of the range, $K_P = 0.63$, is chosen as the best estimate for this study. The force of infection, B_0 is calculated so that the epidemic wave cannot form below K_P.

As the smallest value of Ψ differs from the highest by a factor of 5, $\Psi = 150$km^{2}yr^{-1} is chosen as the best estimate of Ψ as it differs from both ends of the range by a factor of ≈ 2.2.

The top two frames of figure 6.2 show that there is a very wide range of velocities and peak heights associated with the uncertainty of the diffusion coefficient. The velocities predicted are too high at large values of K. Because of the adjustment of B_0 to K_P, the predicted velocities differ little from the original predictions of Murray.

The wide range in velocity associated with changes in the carrying capacity are

not observed in nature. To combat this, van den Bosch et al. (1990) suggested that as the environment is always full of fox territories, that the diffusion coefficient should vary inversely with the carrying capacity, so that

$$\Psi = \frac{\Psi_0}{K} \tag{6.2.1}$$

where Ψ_0 is arbitrarily anchored where $K = 2$ in the previous calculations.

The bottom 2 frames of figure 6.2 show that if the diffusion coefficient varies inversely with K, the velocity does not vary with K. For the best estimate of Ψ, the velocity of the epidemic remains within the range of velocities observed in nature. The graph looks similar to that of van den Bosch et al.'s. The largest error is that associated with the uncertainty of the diffusion coefficient.

This suggests that when the 3 stage epidemic model is applied to a rabies epidemic in European foxes, the main features of the epidemic are robust to the removal of reinfection from low densities. The features such as the wake of the epidemic which are not observed in nature are efficiently removed by reducing the infectivity of low densities of infectives.

This representation of a rabies epidemic predicts that behind the initial invasion the epidemic dies out. The epidemic has been shown to persist in nature. The next step in this investigation is to find a mechanism which would allow persistence of the epidemic behind the wave front.
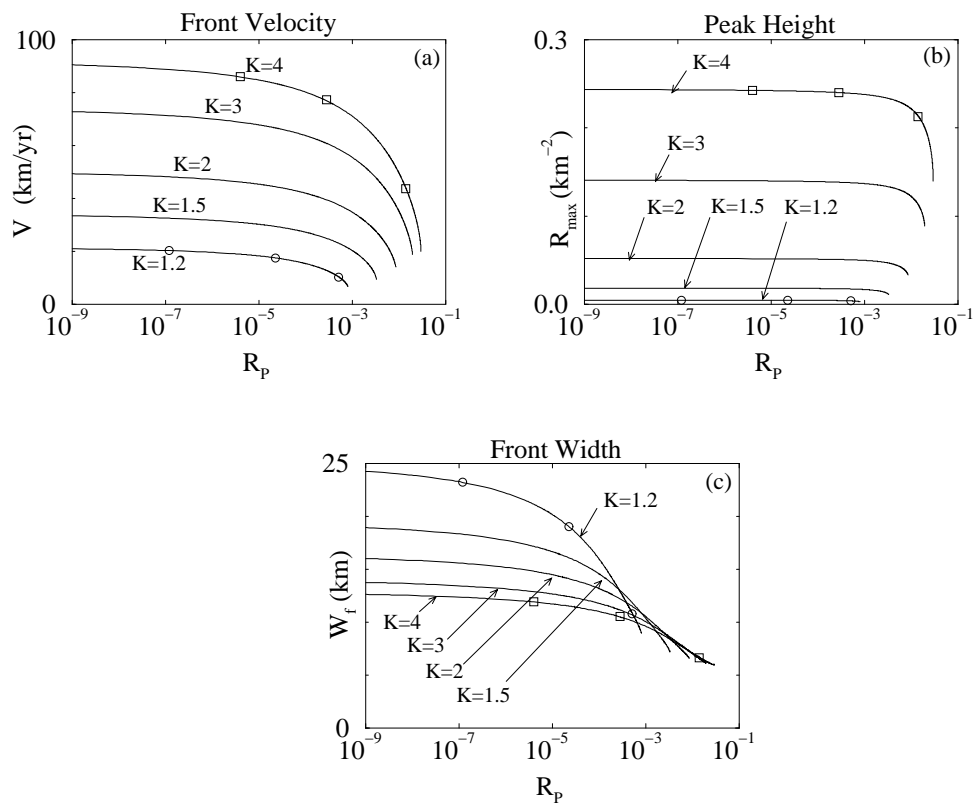
Figure 6.1: *Properties of epidemic fronts as a function of threshold R_P. In the 3 stage epidemic model with an Allee effect, with parameters from table 6.2 appropriate to rabies in the European fox population. Curves derived from the bisection search method for the given values of K. Points show direct simulation results. (a) front velocity, (b) peak rabid density and (c) front width defined as between 5% and 95% r_m.*
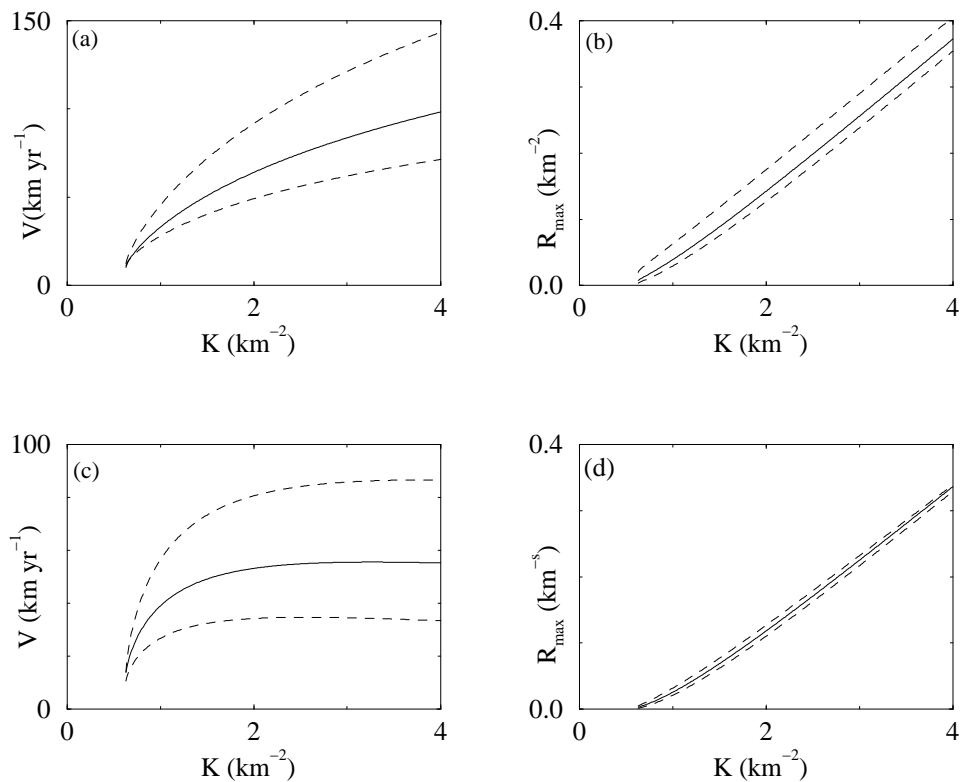
Figure 6.2: *Properties of the epidemic fronts of the 3 stage epidemic model, as a function of carrying capacity, K for rabies in European foxes. Solid curves show best estimates, dotted curves are from extreme values of the diffusion coefficient. Upper frames have constant diffusion coefficient. $\Psi = 150 km^2 yr^{-1}$, $R_P = 2.1 \times 10^{-3} km^{-2}$, $B_0 = 221 km^2 yr^{-1}$. Lower frames have diffusion coefficient proportional to K, with $\Psi_0 = 300 km^2 yr^{-1}$, $R_P = 1.05 \times 10^{-3} km^{-2}$ and $B_0 = 164 km^2 yr^{-1}$.*

Part II

Discrete and Continuous Models

Chapter 7

Single Species Discrete Models

7.1   Motivation

Part I of this thesis showed that in these invasion and epidemic models with either an Allee effect or a threshold term in the growth function of the dispersing component, the invasion or epidemic does not persist behind the front of the wave. As this is known not to be the case in many epidemics and invasions, other mechanisms which are not already included in these models must be at work.

Simulations of the continuous time and space models in 1 spatial dimension take many hours and in some cases, days, to run. The investigation of some of these mechanisms requires the use of two dimensional spatial arenas (Hassell et al. 1994). For reaction-diffusion models these two dimensional simulations may take days or weeks to run until completion. Testing potential mechanisms of persistence behind the invasion or epidemic front may require many simulations. A faster and more computationally efficient method for testing these mechanisms must be used.

Simulations of discrete time and space models are less computationally intensive and take a shorter time to run, as update rules are used to represent the model instead of differential equations. Using update rules means that numerical integration methods are not used in simulations. Using discrete models instead of continuous models would therefore allow a faster and more efficient investigation

of these mechanisms. In order to carry this out, discrete time and space analogues of the reaction-diffusion models described in chapters 2 to 5 must be formulated.

It is important that these discrete models do not show behaviour different to that of the reaction diffusion models and that reasonably large time and space steps can be taken. These models should also be predictable, for instance by the Shooting method.

From now on in this thesis, continuous time and space models are termed continuous models and discrete time and space models are termed discrete models.

This chapter looks at dispersal in a discrete time and space framework. van den Bosch et al. (1990) devised a calculation of the velocity of discrete time continuous space models, generalised so that advection could be taken into account in the calculation. Like the Fisher (1937) - Kolmogorov et al. (1937) velocity calculation, the exponential shape of the toe of the wave is instrumental to the calculation and it therefore cannot be used to calculate the velocity of a wave which has no regrowth from low density populations. A method of predicting the characteristics of waves in discrete time and space is developed by considering a very simple model of invasion (Kot et al. 1996). Then a discrete time and space version of the Fisher model with an Allee effect is formulated and the best method of predicting the velocity and shape of the Fisher wave is investigated.

7.2   Distribution Kernel

A discrete time and space dispersal kernel is sought. In a discrete time and space arena in one dimension,

$$N_{X,T} = \text{ Number of individuals in location } X \to X + \Delta X \text{ at time } T. \quad (7.2.1)$$

A group of individuals, N_0, is released from a single location, $X = 0$, at time $T = 0$, and at time $T + \Delta T$ each spatial segment is searched. A proportion ρ of the survivors from the initial population is the total proportion recaptured.

If ρ is independent of location, the number of individuals expected to be recovered

from segment X is related to the expected number of survivors from the initial population (ξN_0) by

$$C_X = \rho \xi N_0. \tag{7.2.2}$$

If all spatial segments are sampled, then the number of recaptures will be a fraction ρ of the survivors from the original release, that is

$$\sum_{\text{all X}} C_X = \rho \xi N_0 . \tag{7.2.3}$$

The probability of dispersing into segment of distance $\boldsymbol{J}$ from the release site after a single time increment is equal to the proportion of recaptures which occur in the segment, so

$$J_{\boldsymbol{J}} = \frac{C_{\boldsymbol{J}}}{\sum C_{\boldsymbol{J}}}. \tag{7.2.4}$$

Dispersal kernels, such as described by J, share a number of properties. Each survivor must land at exactly one destination. This implies that all valid dispersal kernels must satisfy

$$\sum_{\text{all } \boldsymbol{J}} J_{\boldsymbol{J}} = 1. \tag{7.2.5}$$

For the dispersal kernel being considered here, the dispersal probability is assumed to fall linearly with the magnitude of displacement as in figure 7.2. This is written as

$$J_{\boldsymbol{J}} = \phi \left(1 - \alpha |\boldsymbol{J}|\right)^{+} , \tag{7.2.6}$$

where $+ \equiv max(X,0)$. $J_m \equiv trunc(1/\alpha)$ is used to represent the number of space increments either side of the origin over which the dispersal distribution is non-zero, so

$$\sum_{\text{all } \boldsymbol{J}} J_{\boldsymbol{J}} = \theta \left[J_m + (1 - \alpha J_m)(J_m + 1)\right]. \tag{7.2.7}$$

This is consistent with equation (7.2.5) if and only if θ is chosen appropriately. As this dispersal kernel only disperses the population over a finite area it approximates the diffusion term in reaction-diffusion models.

The mean displacement per time step and the mean square displacement per time step of this dispersal kernel are discussed in full by Gurney and Nisbet (1998).
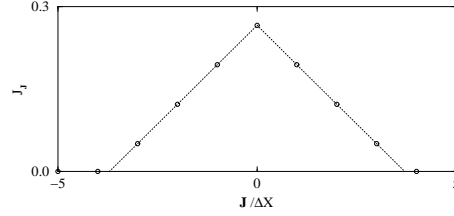
This kernel is symmetrical about the origin, so the mean displacement must be zero.

The above dispersal kernel is dimensional. The continuous time and space models were scaled to increase the speed of computations, so it is only sensible to repeat the scaling process to reduce the dimensions of the dispersal kernel. The non-dimensional version is of the form

$$J_{X_0 \boldsymbol{j}} = \theta(1 - \alpha X_0 |\boldsymbol{j}|)^+ . \tag{7.2.8}$$

To be able to compare the scaled continuous and discrete models, $\alpha' \equiv \alpha X_0$ must be chosen to ensure that the spatial variance increases at the same rate in both models. The dimensional version of this requirement is, from Gurney and Nisbet (1998),

$$2\Psi = \frac{\theta}{\Delta T} \sum_{\text{all } \boldsymbol{J}} |\boldsymbol{J}|^2 (1 - \alpha|\boldsymbol{J}|)^+ = \frac{1}{\Delta T} \frac{\sum |\boldsymbol{J}|^2 (1 - \alpha|\boldsymbol{J}|)^+}{\sum (1 - \alpha|\boldsymbol{J}|)^+}. \tag{7.2.9}$$

Working in 1 dimension means that $\boldsymbol{j} \equiv m\Delta x$. Equation (7.2.9) is then restated

85

as

$$2\Psi \frac{T_0 \Delta t}{X_0^2 \Delta x^2} = \frac{\sum m^2 (1 - \alpha X_0 |m| \Delta x)^+}{\sum (1 - \alpha X_0 |m| \Delta x)^+}. \qquad (7.2.10)$$

If $X_0 = \sqrt{\Psi T_0}$ and $\alpha' \equiv \alpha X_0 \Delta x$ then this becomes

$$\frac{2\Delta t}{\Delta x^2} = \frac{\sum m^2 (1 - \alpha' |m|)^+}{\sum (1 - \alpha' |m|)^+} \qquad (7.2.11)$$

which forms a recipe for working out a value of α' appropriate for a given combination of normalised time and space steps.

For further information on this dispersal kernel, refer to Gurney and Nisbet (1998).

7.3 Piecewise Continuous Approximation to the Fisher Model with an Allee Effect

Kot et al. (1996) developed a method for predicting the spread of a wave with a simple growth function and a threshold in a discrete time continuous space simulation. The organisms have a growth phase, after which they disperse. The growth function used is a piecewise constant approximation to the Fisher model with an Allee effect (see figure 7.1),where if a population's density is above a threshold level the population grows instantaneously to carrying capacity, K, and if the population's density is below the threshold density, N_P, the population instantaneously becomes extinct. A Laplace distribution kernel was used for dispersal of the organisms in Kot et al. (1996).

The method developed in the paper is adapted to a discrete time and continuous space system with the piecewise constant growth function and a tent dispersal kernel as described by equation (7.2.6), so

$$N_{X,T+\Delta T} = \int_{X_{P,T}-1/\alpha}^{X_{P,T}+1/\alpha} K J(X - Y) dY . \qquad (7.3.1)$$

The wave front lies where $N(X,T) = N_P$, and this position is denoted as $X = X_P(T)$. If $1/\alpha$ is the maximum dispersal distance, then after the next time step,
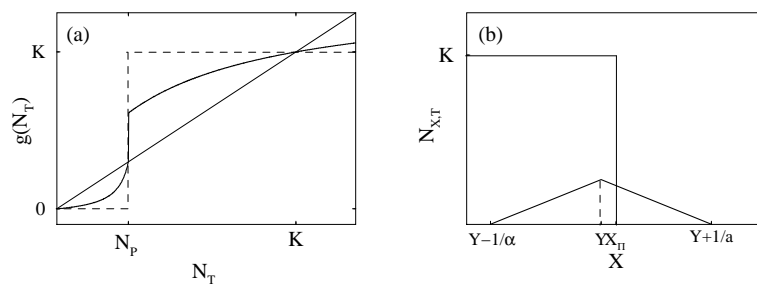
Figure 7.1: *(a) The discrete time Allee Growth function as described by equations (7.4.9) → (7.4.13). The bold line is the function with regards to population density, the diagonal line satisfies $N_{T+\Delta T} = N_T$, and the dotted line is the piecewise constant approximation to the Allee growth function. (b) shows the situation at the front of an invasion wave with the piecewise constant growth function. The bold line shows the application of the tent distribution kernel to the wave front.*

the position of the front, $X_P(T + \Delta T)$ must lie within the region

$$X_P(T) < X_P(T + \Delta T) < X_P(T) + \frac{1}{\alpha} \, . \tag{7.3.2}$$

As $X_P(T + \Delta T) = N_P$,

$$N_P = \int_{X_P(T+\Delta T)-1/\alpha}^{X_P(T)} KJ(X - Y)dY , \qquad (7.3.3)$$

which after some algebra can be written as

$$N_P = \frac{1}{2}K \left(1 - \frac{X_P(T + \Delta T) - X_P(T)}{1/\alpha}\right)^2 . \qquad (7.3.4)$$

Rearrangement of this gives the difference in extent of the invasion wave between times T and $T + \Delta T$,

$$X_P(T + \Delta T) - X_P(T) = 1/\alpha \left(1 - \sqrt{2N_P/K}\right) . \qquad (7.3.5)$$

This predicts the new extent of the invasion at the next time step.

J_m	N_P	predicted spread	observed spread
2	0.1	1	1
3	0.1	2	2
4	0.1	3	3
10	0.1	8	8
10	0.05	8	8
10	0.01	9	9
10	0.005	9	9

Table 7.1: *Comparison between observed and predicted spread of the piecewise continuous approximation of the Fisher model with an Allee effect over one time increment.* $\Delta T = 1$, $\Delta X = 1$ *and* $K = 5$.

Table 7.3 shows that the method devised to predict the rate of spread of the discrete time and space piecewise-continuous approximation of the Fisher model with an Allee effect with the tent dispersal kernel in this section is accurate. Trying to predict the shape of this invasion wave is pointless as the shape is known. Now this method of prediction is applied to the discrete time and space formulation of the Fisher model with an Allee effect.

7.4 Invasions of Logistically Growing Populations

7.4.1 The Discrete Logistic Model - Dynamics in Absence of Dispersal

The well known, analytical solution of the logistic model, is written as

$$N_{T+\Delta T} = \frac{KN_T}{N_T + \Gamma(K - N_T)} ,$$

(7.4.1)

where

$$\Gamma = e^{-R\Delta T}$$

(7.4.2)

where the parameters are equivalent to those described for in the continuous time model described in chapter 2.

As in the continuous model, there are two steady states, $N = 0$ which is unstable, and $N = K$ which is locally stable.

An Allee effect is used to remove the regrowth of low density populations. As in the Fisher model with an Allee growth function, described in subsection 2.2.4, the function is continuous in value but not in slope. So again there is a linearly dependent per capita death rate, D, where

$$D = D_0 + D_1 N ,$$

(7.4.3)

and a fecundity rate B which is a constant, B_0, at high densities but increases linearly with slope B_1 at low densities. With this modification the model becomes

$$N_{T+\Delta T} = \frac{K'N_T}{N_T + \Gamma(K' - N_T)} ,$$

(7.4.4)

where

$$\Gamma = e^{-R'\Delta T} ,$$

(7.4.5)

$$K' = \begin{cases} -(B_1 - D_1)/D_0 & N_T < N_c \\ (B_0 - D_0)/D_1 & \text{otherwise} \end{cases}$$

(7.4.6)

and

$$R' = \begin{cases} -D_0 & N_T < N_c \\ B_0 - D_0 & \text{otherwise} \end{cases}$$

(7.4.7)

where

$$N_c = \frac{B_0}{B_1} \ . \tag{7.4.8}$$

Using the same scaling process as in the continuous model, this can be scaled to

$$n_{t+\Delta t} = \frac{n_t k'}{n_t + \gamma(k' - n_t)} \ , \tag{7.4.9}$$

where

$$\gamma = e^{-r'\Delta t} \ , \tag{7.4.10}$$

$$k' = \begin{cases} n_P & n_t < n_c \\ 1 & \text{otherwise} \end{cases} \tag{7.4.11}$$

and

$$r' = \begin{cases} -a & n_t < n_c \\ 1 & \text{otherwise} \end{cases} \tag{7.4.12}$$

where, as in chapter 2,

$$n_c = \frac{1+a}{1+a/n_P} \ . \tag{7.4.13}$$

7.4.2 The Discrete Fisher Model

Now the model is made explicitly spatial and a scaled dispersal kernel is added. The population has a net per capita growth factor, $g_{x,t}$, which is the sum of the survival probability and the average offspring per individual for the population, $n_{x,t}$, so from equation (7.4.9)

$$g_{x,t} = \frac{k'}{n_{x,t} + \gamma(k' - n_{x,t})} \ , \tag{7.4.14}$$

with γ and k' as defined by equations (7.4.10) and (7.4.11). Combining this growth term with the dispersal term, given by equation (7.2.8), but scaled by the same factor as the continuous model, gives

$$n_{x,t+\Delta t} = \sum_{\text{all } \boldsymbol{j}} J_{\boldsymbol{j}} g_{x-\boldsymbol{j},t} n_{x-\boldsymbol{j},t} \ . \tag{7.4.15}$$

7.4.3 Prediction of Wave Front Properties using Method Developed for Piecewise-Constant Approximation

The method for making predictions about a discrete time and space wavefront as described in section 7.3 is used to predict the velocity of the discrete time and space version of the Fisher model with an Allee effect. The wave shape of the Fisher model is different to that in the piecewise constant approximation, but the wavefront can be manipulated into a similar shape by careful choice of parameter values. The wave front is steepened by increasing the threshold, by increasing the per capita growth rate and by increasing the size of the space step. A number of choices of parameter value are considered.

Δx	n_P	observed v	predicted v
0.25	0.01	1.5761	5
0.25	0.1	1.0599	3
1	0.01	1.5789	2
1	0.1	1.0652	0
2	0.01	1.5754	1
2	0.1	0.9214	1
4	0.01	1.6104	1
4	0.1	1.1150	1

Table 7.2: *Comparisons between wave properties predicted for the piecewise continuous approximation of the model and those observed from discrete time and space simulations of the Fisher model with an Allee effect, with $a = 1.5$ and $\Delta t = 0.25$.*

Table 7.2 suggests that the method devised for the piecewise constant approximation of the Fisher model with an Allee effect works better for simulations with large Δx and large n_P, because within this parameter range the wavefront is similar in shape to the piecewise constant approximation. This method is far from perfect though. The calculation for the prediction results in 2 roots; if both are real and positive then an arbitrary choice has to be made as to which is correct. The piecewise continuous approximation only spreads in integers, so again the calculation is erroneous when applied to the Fisher model. As the waveform this method was formulated to make predictions about has a very set wave shape, this method cannot be used to make predictions about the shape of the wave

front. This method only works on specially chosen waves, so this method cannot be used generally. There is no obvious way of extending its use. Another method for making predictions about the velocity and shape of the wave front must be sought.

7.4.4 Prediction of Wave Properties using the Shooting Method

The Shooting method was devised for a continuous model, so it will only work for the discrete model if it is a good approximation to a continuous model. In chapter 2 it was shown that there will be an error in the simulations as time steps will step over the point were a population transcends from being below n_c to above n_c. A series of simulations were done to investigate the relationship between the discrete model, the time and space steps used, and the continuous model.

Δx	Δt	v	w_f
0.25	0.25	1.5761	7.708
0.25	1	1.4873	7.190
0.25	2	1.4996	7.719
1	0.25	1.5789	7.214
1	1	1.4771	8.246
1	2	1.5000	7.721
2	0.25	1.5754	7.098
2	1	1.4987	7.614
2	2	1.4707	7.574
4	0.25	1.6104	7.420
4	1	1.5385	8.052
4	2	1.6923	9.048

Table 7.3: *The effects of increasing space and time steps on the velocity and shape of the wave front of the discrete Fisher model with an Allee Effect with $a = 1.5$ and $n_P = 0.01$. v is the wave front velocity and w_f is the width of the wavefront measured from $n = 0.1$ to $n = 0.9$. The Shooting method predicts that $v = 1.5708$ and $w_f = 7.071$.*

In table 7.3, for up to around $\Delta t = 0.5$ and $\Delta x = 1$, the observations from the simulations of the discrete model are within 10% of the predictions from the

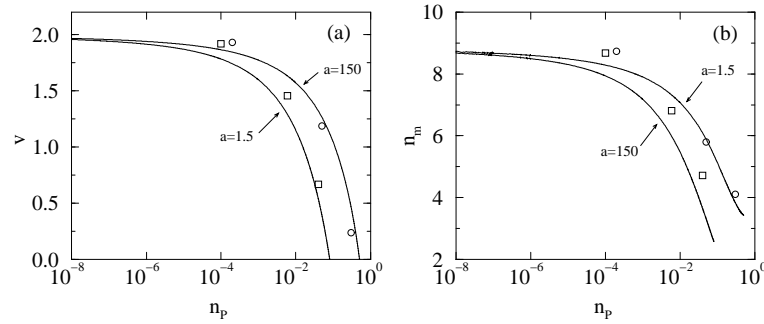Shooting method. Now it is investigated whether this relationship holds up for a range of parameter values.

Figure 7.2: *Comparisons between calculated wave properties and those observed from simulations of the discrete time and space Fisher model with an Allee effect in one dimension, with $\Delta x = 1$ and $\Delta t = 0.5$. v is the velocity of the wavefront, and w_f is the width of the wave front, measured from $n = 0.1$ to $n - 0.9$.*

Figure 7.2 shows that for a range of parameter values observed velocities and wave front widths of the discrete time and space model are within 10% of the predictions from the Shooting method. This suggests that the discrete model is a

good approximation of the continuous model and that the Shooting method can be used to make predictions about invasion waves generated by the model.

7.5   Discussion

A discrete time and space model is needed which is a good approximation of the continuous time and space Fisher model with an Allee effect which is continuous in value but not in slope. There must be a way in which to make predictions about this model.

A distribution kernel, known to approximate diffusion, was chosen. This was based on capture-recapture experiments. Dispersal was assumed to fall linearly with distance from the starting location. This dispersal kernel was termed the Tent dispersal kernel.

In order to derive a method to predict the shape and velocity of an invasion wave in the discrete Fisher model, a piecewise constant approximation to the Fisher model was considered. A method was adapted from Kot et al. (1996) which predicts the velocity of this system. Although the method worked well for the model it was devised for, when applied to the Fisher model with an Allee effect, it only worked for specific cases, when the Fisher wave was forced into the same shape as the approximation. Only the velocity could be predicted. There were other complications associated with the calculation of the predictions. So this method was rejected as a way to make predictions about the Fisher wave with an Allee effect.

The Shooting method was then used to make predictions about the discrete time and space model. It worked for a range of values of space and time steps and for a range of a and n_P. This suggests that within this range of time and space steps the model is a good approximation of the continuous time model.

This exercise was the first step in looking for persistence mechanisms for more complex models where the wave becomes a soliton due to the lack of regrowth from unbiologically small populations. Now discrete versions of the predator prey

model and the 2 and 3 stage rabies epidemic models should be formulated. Once formulated, methods for predicting the shape and velocity of the wave fronts of these models should be sought.

Chapter 8

Formulation of Discrete Multi-Component Models

Now discrete versions of the predator-prey invasion model and the 2 and 3 stage rabies epidemic models are formulated. As with the discrete Fisher model in Chapter 7, these models have to show no behaviour that is qualitatively different from their continuous counterparts at quite large time and space steps, so simulations can be run in as little time as possible. The models also have to be predictable.

In this chapter the formulation of the discrete 2 stage rabies epidemic model is gone through carefully, then the discrete formulations of the 3 stage epidemic model and the predator prey invasion model are considered briefly as these formulations have already been partially described by Gurney et al. (1998) and Gurney and Nisbet (1998). As the Shooting method was so successful at predicting the wave characteristics of the discrete Fisher wave, the Shooting method is now applied to the multi-component models.

8.1   Discrete Time 2 Stage Epidemic Model

It is assumed that the infective population, I, changes slowly compared to the susceptible population. Hence, a solution of equations (4.1.1) and (4.1.2) is sought which is valid over time scales where the infective population is effectively con-

stant. This assumption on its own is not enough to permit a closed form solution for the continuous time equation, but extending the assumption so that BI is constant over the time scale of interest is a better aid to finding a solution. The equation to be solved is

$$\frac{dS}{dT} = RS\left(1 - \frac{S}{K}\right) - BIS. \tag{8.1.1}$$

By defining

$$R' \equiv R - BI \quad \text{and} \quad K' \equiv R'K/R \tag{8.1.2}$$

this can be recast as

$$\frac{dS}{dT} = R'S\left(1 - \frac{S}{K'}\right), \tag{8.1.3}$$

to which the solution is

$$S(T) = \frac{K'S(0)}{S(0) + (K' - S(0))e^{-R'T}}. \tag{8.1.4}$$

K' and R' are either strictly positive or strictly negative but both must have the same sign. They can both simultaneously be zero. In this case the equation becomes the limit of the system as $R' \to 0$,

$$\lim_{R' \to 0} S(T) = \frac{KS(0)}{K + RS(0)T} \tag{8.1.5}$$

which agrees with solving equation (4.1.1) with $R = BI(T)$. Also, as the time step is increased,

$$\lim_{T \to \infty} S(T) = \begin{cases} K' & \text{if} \quad K' > 0 \quad \text{and} \quad R' > 0 \\ 0 & \text{if} \quad K' \le 0 \quad \text{and} \quad R' \le 0 \end{cases}. \tag{8.1.6}$$

The cumulative infection of susceptibles by infectives over a time increment has to be determined. If $U(T)$ denotes cumulative infection by time T, then again working on the approximation that BI is constant over the time scale of interest,

$$U(T) = BI(T) \int_0^T S(x)dx. \tag{8.1.7}$$

If the case where $R' = 0$ is considered,

$$U(T) = BI(T) \int_0^T \frac{KS(0)}{K + RS(0)x}dx = \frac{BI(T)K}{R} \ln\left[\frac{K + RS(0)T}{K}\right], \tag{8.1.8}$$

which can be rewritten as

$$U(T) = \frac{BI(T)K}{R} \ln\left[\frac{S(0)}{S(T)}\right]. \tag{8.1.9}$$

In the general case where $R' \neq 0$,

$$U(T) = BI(T) \int_0^T \frac{K'S(0)}{S(0) + (K' - S(0))e^{-R'T}} dx , \tag{8.1.10}$$

which is

$$U(T) = \frac{BI(T)K'}{R'} \left[R'T - \ln\left(\frac{K'}{S(0) + (K' - S(0))e^{-R'T}}\right)\right] . \tag{8.1.11}$$

As $K'/R' = K/R$, this can be rewritten as

$$U(T) = \frac{BI(T)K}{R} \left[R'T + \ln\left(\frac{S(0)}{S(T)}\right)\right]. \tag{8.1.12}$$

These short term estimates of S(T) and U(T) allow a discrete time model to be written. It is assumed that a fraction ξ_I of the infectives survive each increment. Therefore

$$S_{T+\Delta T} = \frac{K'_T S_T}{S_T + (K'_T - S_T)e^{-R'\Delta T}} \tag{8.1.13}$$

and

$$I_{T+\Delta T} = (\xi_I + U_T)I_T, \tag{8.1.14}$$

where

$$U_T \equiv \frac{BK}{R} \left[(R - BI_T)\Delta T + \ln\left(\frac{S_T}{S_{T+\Delta T}}\right)\right], \tag{8.1.15}$$

$$R'_T \equiv R - BI_T \quad \text{and} \quad K'_T \equiv KR'_T/R. \tag{8.1.16}$$

The steady states of the model are $(0,0)$, $(K,0)$ and (S^*, I^*) where

$$S^* = \frac{1 - \xi_I}{B\Delta T} \quad \text{and} \quad I^* = \frac{R}{B}\left(1 + \frac{\xi_I - 1}{BK\Delta T}\right). \tag{8.1.17}$$

For the existence of the interior steady states (for I^* to be positive),

$$K > \frac{1 - \xi_I}{B\Delta T}. \tag{8.1.18}$$

If this inequality is not fulfilled the system will eventually reach the $(K,0)$ steady state.

If

$$D' \equiv \frac{1 - \xi_I}{\Delta T}, \tag{8.1.19}$$

and the time increment is small enough for $D' \approx D$ in the continuous time model, the steady states are essentially identical to those of the continuous time 2 stage epidemic model.

The infective growth function is then modified so that the contact rate varies with density at low densities. As in the continuous time model described in section 3.4, the force of infection, B, is a constant, B_0 at high densities of infectives, but at low densities B varies linearly with infective density. In equations (8.1.13), (8.1.14) and (8.1.13),

$$B = \begin{cases} B_0 & I_T \geq I_P(B_0 K/D) \\ (D/K)(I_T/I_P) & \text{otherwise} \end{cases}. \tag{8.1.20}$$

Equations (8.1.13) and (8.1.14) can then be scaled. K is chosen as the natural scale of population and M is chosen as the natural scale of time. The choice of scale of time in this model, $T_0 = M$, is different to that of that in the continuous model, R. The mortality rate of rabid animals is very high. The mortality rate is therefore chosen as the scale of time in this formulation since the length of possible time steps is restricted by a high mortality rate. This scaling process produces the new dimensionless variables, $s = S/S_0$, $i = I/S_0$ and $t = T/T_0$ and the parameter groups $i_P = I_P/S_0$, $r = R/T_0$ and $b_0 = B_0 K/T_0$. After scaling, the model becomes

$$s_{t+\Delta t} = \frac{k_t' s_t}{s_t + (k_t' - s_t)e^{-r'\Delta t}} \tag{8.1.21}$$

and

$$i_{t+\Delta t} = (\xi_i + u_t)i_t , \tag{8.1.22}$$

where

$$u_t \equiv \frac{b}{r}\left[(r - bi_t)\Delta t + \ln\left(\frac{s_t}{s_{t+\Delta t}}\right)\right] , \tag{8.1.23}$$

$$r_t' \equiv r - bi_t \quad \text{and} \quad k_t' \equiv r_t'/r , \tag{8.1.24}$$

and

$$b = \begin{cases} b_0 & i_t \geq (b_0 i_P) \\ i_t/i_P & \text{otherwise} \end{cases}. \tag{8.1.25}$$

99

This model has the interior steady state

$$s^* = \frac{1 - \xi_i}{b\Delta t} \quad \text{and} \quad i^* = \frac{r}{b}\left(1 + \frac{\xi_i - 1}{b\Delta t}\right). \tag{8.1.26}$$

The scaled dispersal kernel, as described in the previous chapter, is then applied to the infective individuals, so if the growth of the infective population is described by

$$g_{x,t} = \xi_i + u_{x,t}, \tag{8.1.27}$$

where

$$\xi_i = 1 - \Delta t \tag{8.1.28}$$

and $u_{x,t}$ is described in equation (8.1.23), with mobile infectives and immobile susceptibles. The update equation for the susceptible population becomes

$$s_{x,t+\Delta t} = \frac{k'_{x,t} s_{x,t}}{s_{x,t} + (k'_{x,t} - s_{x,t})e^{-r'\Delta t}} \tag{8.1.29}$$

and the equation for the infective population is

$$i_{x,t+\Delta t} = \sum_{\text{all } j} J_{\boldsymbol{j}} g_{x-d,t} i_{x-d,t}. \tag{8.1.30}$$

In chapter 7 it was shown that the Shooting method developed for a continuous Fisher model with an Allee effect could successfully be used to make predictions about the velocity and shape of the wave front of a discrete version of the model. Predictions made by the Shooting method about the continuous formulation of the model are compared with observations made from simulations of wave fronts in the discrete model.

Table 8.1 shows that up to around $\Delta x = 1$ and $\Delta t = 0.5$, the observed wave front velocity and shape are within 10% of the predictions made by the Shooting method. Δt cannot be larger than 1 as shown by equation (8.1.28).

The relationship between the Shooting method predictions and observations from the discrete model is tested for a wide range of parameter values. Figure 8.1 shows that with $\Delta x = 1$ and $\Delta t = 0.5$, for a range of parameter values the Shooting method is still a good method of making predictions about the model.

Δx	Δt	v	w_f	i_m
0.25	0.125	1.9532	2.625	0.4839
0.25	0.5	1.6784	3.226	0.4686
0.25	1	1.4650	3.774	0.4451
0.5	0.125	1.9440	2.608	0.4830
0.5	0.5	1.6830	3.200	0.4660
0.5	1	1.4678	3.771	0.4442
1	0.125	1.8900	2.614	0.4815
1	0.5	1.6497	3.081	0.4593
1	1	1.4509	3.759	0.4383
2	0.125	1.6452	3.600	0.4334
2	0.5	1.5497	3.898	0.4744
2	1	1.5417	3.712	0.4264

Table 8.1: *Effects of increasing space and time steps on the wave front of the discrete 2 stage epidemic model with $r = 1$, $b = 4$ and $i_P = 0.04$. v is the wave front velocity , i_m is the maximum density of infectives in the peak and w_f is the width of the wavefront measured from 5% to 95% i_m. The Shooting method predicts that $v = 2.0939$, $i_m = 0.4884$ and $w_f = 2.666$.*

This means that the Shooting method can be used to make predictions about the discrete 2 stage epidemic model. As the Shooting method was formulated to make predictions about the continuous model, it also suggests that with small enough time and space steps this model is a good approximation of the continuous time model.

8.2   Predator-Prey Model

The discrete predator-prey model with no Allee effect or threshold is identical to the predator-prey model described by Gurney et al. (1998). In this model is assumed that a fraction ξ_C of the predators survive each time increment, and that consuming U_T prey items during an increment produces EU_T surviving offspring. Using the same arguments as in the 2 stage epidemic model for estimating the total uptake of prey by predators within an increment and for prey growth, the discrete time predator-prey model can be written as

$$F_{T+\Delta T} = \frac{F_T K'}{F_T + (K' - F_T)\Gamma} \tag{8.2.1}$$
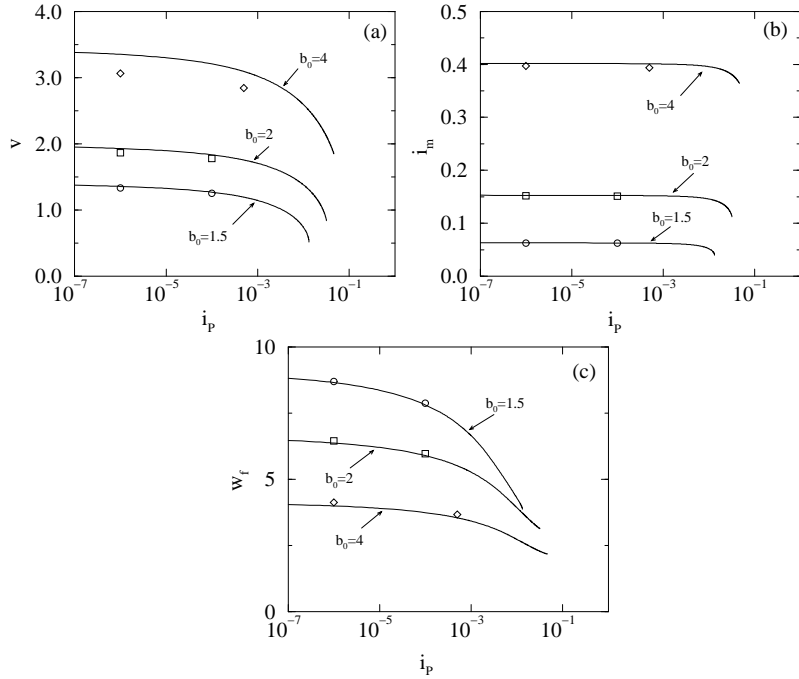
101

Figure 8.1: *Comparisons between wave properties predicted by the Shooting method and those observed from simulations of the discrete 2 stage epidemic model.* $\Delta x = 05$, $\Delta t = 0.125$ and $r = 0.006$. v *is the velocity of the wavefront,* i_m *is the maximum density of predators at the peak of the wavefront and* w_f *is the width of the wave front, measured from 5% to 95% of* i_m.

and

$$C_{T+\Delta T} = (\xi_C + U_T)C_T \ , \tag{8.2.2}$$

where

$$U_T = \frac{EC_T K \mu}{R} \left[R'\Delta T + \ln \left(\frac{F_T}{F_{T+\Delta T}} \right) \right] \ , \tag{8.2.3}$$

$$\mu \equiv \frac{U_m}{F_T + H} , \quad R' \equiv R - \mu C_T , \quad K' = KR'/R \tag{8.2.4}$$

and

$$\Gamma \equiv \exp(-R'\Delta T) \tag{8.2.5}$$

The efficiency for the conversion of ingested prey into predators, E, is a constant, E_0 at high predator densities and at low densities it varies linearly with predator densities, so

$$E = \begin{cases} E_0 & C_T \geq C_P(E_0 U_m/D) \\ DC_T/(U_m C_P) & \text{otherwise} \end{cases} . \tag{8.2.6}$$

The model is scaled as in the continuous case in Chapter 4. The spatial scale is chosen as $X_0 \equiv \sqrt{\Psi/R}$, as in the continuous model. The scaled dispersal kernel (equation(7.2.8)) is then applied to the predator population and the prey are immobile.

$$f_{x,t+\Delta t} = \frac{k'_{x,t} f_{x,t}}{f_{x,t} + (k'_{x,t} - f_{x,t})e^{-r'_{x,t}\Delta t}} \tag{8.2.7}$$

and

$$g_{x,t+\Delta t} = \xi_c + e u_{x,t} , \tag{8.2.8}$$

$$c_{x,t+\Delta t} = \sum_{\text{all } \boldsymbol{j}} J_{\boldsymbol{j}} c_{x-\boldsymbol{j},t} g_{x-\boldsymbol{j},t} \tag{8.2.9}$$

where

$$u_{x,t} \equiv \nu k \left[r'_{x,t}\Delta t + \ln \left(\frac{f_{x,t}}{f_{x,t+\Delta t}} \right) \right] \tag{8.2.10}$$

and

$$\nu_{x,t} \equiv \frac{u_m}{f_{x,t}+1}, \quad r'_{x,t} \equiv 1 + \nu_{x,t} \quad \text{and} \quad k'_{x,t} \equiv kr'_{x,t}. \tag{8.2.11}$$

$$e = \begin{cases} 1 & c_{x,t} \geq c_P u_m/d \\ dc_{x,t}/(u_m c_P) & \text{othe rwise} \end{cases} . \tag{8.2.12}$$

When $r' = 0$ the limit of the expression (8.2.7) must be used, namely

$$f_{x,t+\Delta t} = \frac{k f_{x,t}}{k + f_{x,t}\Delta t}. \tag{8.2.13}$$

The model has exterior steady states at $(0,0)$ and $(k,0)$, and interior steady states at

$$f^* = \frac{d'}{u_m - d'} \quad \text{and} \quad c^* = \frac{R(f^* + 1)}{u_m} \left(1 - \frac{f^*}{k} \right) , \tag{8.2.14}$$

103

where

$$d' \equiv \frac{1 - \xi_c}{\Delta t} \ . \tag{8.2.15}$$

As in the 2 stage epidemic model, if the time increment is small enough that $d' \simeq d$ in the continuous model, these steady states are essentially equal to those in the continuous time model.

The interior steady state can only exist if

$$k > \frac{d'}{u_m - d'} . \tag{8.2.16}$$

The stability analysis carried out by Gurney et al. (1998) shows that the behaviour of the discrete time model is essentially identical to that of the continuous time model for small time increments. This means that the discrete time model can be used as an approximation to the continuous time model.

Δx	Δt	v	w_f	c_m
0.25	0.25	0.7015	11.23	44.28
0.25	1	0.6809	12.00	46.17
0.25	2	0.6570	12.94	48.61
1	0.25	0.7010	11.16	44.12
1	1	0.2814	12.00	46.10
1	2	0.6565	12.92	48.57
2	0.25	0.7082	11.80	45.26
2	1	0.6790	11.82	45.73
2	2	0.6586	14.46	48.77
4	0.25	0.7327	12.26	43.52
4	1	0.7040	13.46	47.65
4	2	0.6696	13.87	48.96

Table 8.2: *Effects of increasing space and time steps on the wave front of the discrete predator-prey model with an Allee effect with $k = 20$, $u_m = 0.2$, $\delta = 0.05$ and $c_P = 0.01$. v is the wave front velocity and w_f is the width of the wavefront measured from 5% to 95% c_m. The Shooting method predicts that $v = 0.7089$, $c_m = 43.74$ and $w_f = 10.07$.*

Table 8.2 shows that with up to $\Delta x = 1$ and $\Delta t = 0.5$ the observed wave shape and velocity is within 10% of the values predicted by the Shooting method. With space and time steps larger than this waves that should be solitons can grow at low densities and a wave train can form. Again, a range of parameter values are

considered to see if this good comparison between the discrete invasion waves and the Shooting method holds up generally. Figure 8.2 shows that this is the case. This means that the Shooting method can be used to make predictions about the discrete predator-prey model with an Allee effect. The Shooting method correctly predicts the wave characteristics of both the continuous model and the discrete model at small values of Δx. This suggests that the wave characteristics of the 2 models are similar.

8.3 Discrete 3 Stage Epidemic Model

The formulation of the discrete time 3 stage epidemic model very similar to that of the 2 stage epidemic model. The unmodified discrete model has already been described in Gurney and Nisbet (1998) but has been repeated here for fullness of explanation. S_T denotes the susceptible population, I_T the incubating population and R the infective population at time T.

$$S_{T+\Delta T} = \frac{S_T K'}{S_T + (K' - S_T)\Gamma} \ , \tag{8.3.1}$$

$$I_{T+\Delta T} = U_T + \xi_T \xi_I I_T \tag{8.3.2}$$

and

$$R_{T+\Delta T} = \xi_R R_T + (1 - \xi_T)\xi_I I_T \ , \tag{8.3.3}$$

where

$$\Gamma \equiv \exp(-Q'\Delta T) \ , \ Q' \equiv Q - \mu \ , \ K' = KQ'/Q \ , \ \mu \equiv BR_T \ , \tag{8.3.4}$$

the cumulative infection of susceptibles, U_T, is

$$U_T = \frac{K\mu}{Q}\left[Q'\Delta T + \ln\left(\frac{S_T}{S_{T+\Delta T}}\right) \right] \ , \tag{8.3.5}$$

and the function for the contact rate is

$$B = \begin{cases} B_0 & R_T \geq KB_0 R_P L/(D(L+M)) \\ (L+M)DR_T/(LKR_P) & \text{otherwise} \end{cases} \ . \tag{8.3.6}$$

Q is the net growth rate of the susceptible population, ξ_T is the proportion of the incubating population which do not become rabid during a time increment,
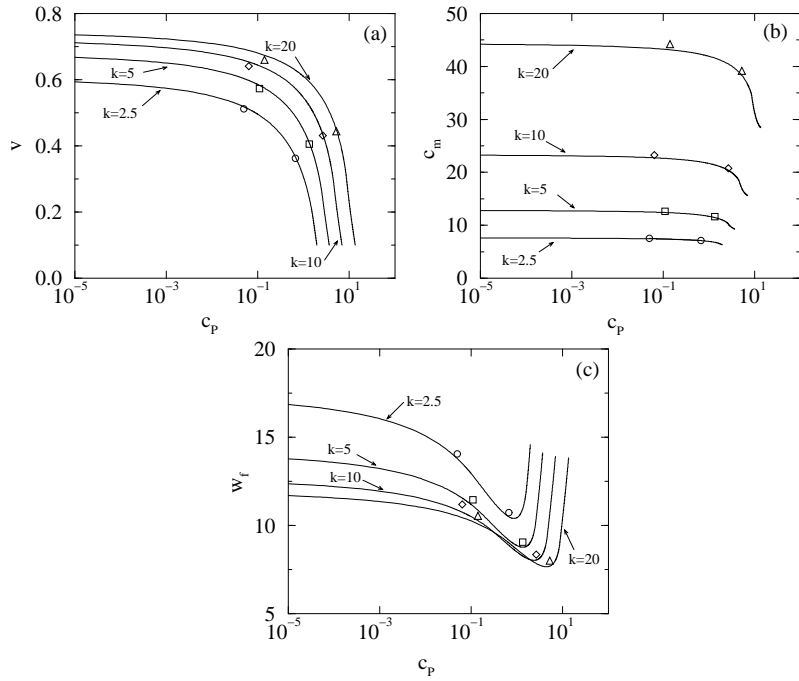
Figure 8.2: *Comparisons between wave properties predicted by the Shooting method and those observed from simulations of the discrete predator-prey model. $\Delta x = 1$, $\Delta t = 0.5$, $u_m = 0.2$ and $d = 0.05$. v is the velocity of the wavefront, c_m is the maximum density of predators at the peak of the wavefront and w_f is the width of the wave front, measured from 5% to 95% to c_m.*

ξ_I is the proportion of the incubating population which survives an increment in time and ξ_R is the proportion of the infective population which survives a time increment. Other parameters are the same as those in the continuous time model.

The model is then scaled, with the scale of time chosen as $T_0 \equiv D$ as opposed to Q

in the continuous model. This is because of the limitations a large mortality rate puts on the possible range of time steps. The populations are scaled to K, the carrying capacity. The distribution kernel is then scaled by $X_0 \equiv \sqrt{\Psi/D}$ to give equation (7.2.8), and applied to the infective rabid individuals. The susceptible and incubating individuals are treated as immobile. The model then becomes

$$s_{x,t+\Delta t} = \frac{k'_{x,t} s_{x,t}}{s_{x,t} + (k'_{x,t} - s_{x,t})e^{-q'\Delta t}} \tag{8.3.7}$$

where

$$\mu_{x,t} \equiv b r_{x,t}, \quad q'_{x,t} \equiv q - \mu_{x,t} \quad \text{and} \quad k'_{x,t} \equiv k q'_{x,t}/r \ . \tag{8.3.8}$$

The proportion of infected individuals who survive a time increment is ξ_i, and the proportion of infected individuals that do not go on to become infectives is ξ_e. Hence if the number of susceptible individuals which are infected within a time increment is $u_{x,t}$, using arguments set out in the section about 2 stage epidemic models, the growth of the infected population is given by

$$i_{x,t+\Delta t} = u_{x,t} + \xi_e \xi_i i_{x,t}, \tag{8.3.9}$$

where

$$u_{x,t} \equiv \frac{\mu_{x,t} k}{q} \left[(q - \mu_{x,t})\Delta t + \ln\left(\frac{s_{x,t}}{s_{x,t+\Delta t}}\right) \right]. \tag{8.3.10}$$

The proportion of infective individuals which survive a time increment is ξ_r, so the update rule for the change in density of the infective population is

$$g_{x,t+\Delta t} = \xi_r r_{x,t} + (1 - \xi_e)\xi_i i_{x,t} \tag{8.3.11}$$

$$r_{x,t+\Delta t} = \sum_{\text{all } \boldsymbol{j}} J_{\boldsymbol{j}} g_{x-\boldsymbol{j},t} r_{x-\boldsymbol{j},t} \tag{8.3.12}$$

where

$$b = \begin{cases} b_0 & r_{x,t} \geq b_0 r_P \sigma/d(l+m) \\ d r_{x,t}/r_P(1 - m/l) & \text{otherwise} \end{cases} . \tag{8.3.13}$$

If large enough,this model had the exterior steady states $(0,0,0)$ and $(1,0,0)$ and the interior steady states

$$s^* = \frac{1 - \xi_r - \xi_e \xi_i + \xi_e \xi_i \xi_r}{b\Delta t \xi_i(\xi_e - 1)}, \quad i^* = \frac{\xi_r - 1}{\xi_i(\xi_e)} r^* \quad \text{and} \quad r^* = \frac{q}{b}(1 - s^*). \tag{8.3.14}$$

107

If
$$\xi_r \equiv 1 - \Delta t, \quad \xi_i \equiv 1 - m\Delta t \quad \text{and} \quad \xi_e \equiv 1 - \frac{l}{\xi_i}\Delta t, \qquad (8.3.15)$$

then these interior steady states are almost equivalent to those of the discrete time model for small Δt if rescaled.

The interior steady states can only exist if

$$1 > \frac{1 - \xi_r - \xi_e\xi_e + \xi_e\xi_i\xi_r}{b\Delta t\xi_i(\xi_e - 1)} \ . \qquad (8.3.16)$$

Δx	Δt	v	w_f	r_m
0.25	0.125	0.7059	7.265	0.06067
0.25	0.5	0.6587	7.075	0.06044
0.25	1	0.5988	6.769	0.05989
1	0.125	0.7121	7.358	0.06074
1	0.5	0.6618	7.073	0.06035
1	1	0.6021	6.754	0.05967
2	0.125	0.7509	7.806	0.06067
2	0.5	0.7494	7.452	0.06061
2	1	0.5989	6.714	0.05950
4	0.125	0.8537	8.44	0.05810
4	0.5	0.7891	8.9	0.06194
4	1	0.7099	7.688	0.05443

Table 8.3: *Effects of increasing space and time steps on the wave front of the discrete 3 stage epidemic model with $b_0 = 4.3836$, $q = 0.00684932$, $m = 0.684932$, $l = 0.17808$ and $r_P = 10^{-6}$. v is the wave front velocity, r_m is the maximum density of rabid individuals in the peak and w_f is the width of the wavefront measured from 5% to 95% r_m. The Shooting method predicts that $v = 0.7115$, $r_m = 0.06066$ and $w_f = 7.202$.*

Table 8.3 shows that as long as $\Delta x \leq 1$ and $\Delta t \leq 0.5$ observations of the velocity and shape of the epidemic wave of the 3 stage epidemic model are within 10% of the predictions made by the Shooting method. Figure 8.3 shows that this remains the case for a range of parameter values. Therefore the Shooting method can be used to make predictions about the discrete 3 stage epidemic model. As the Shooting method was developed for the continuous version of this model, it suggests that for small time and space steps the discrete model is a good approximation of the continuous model.
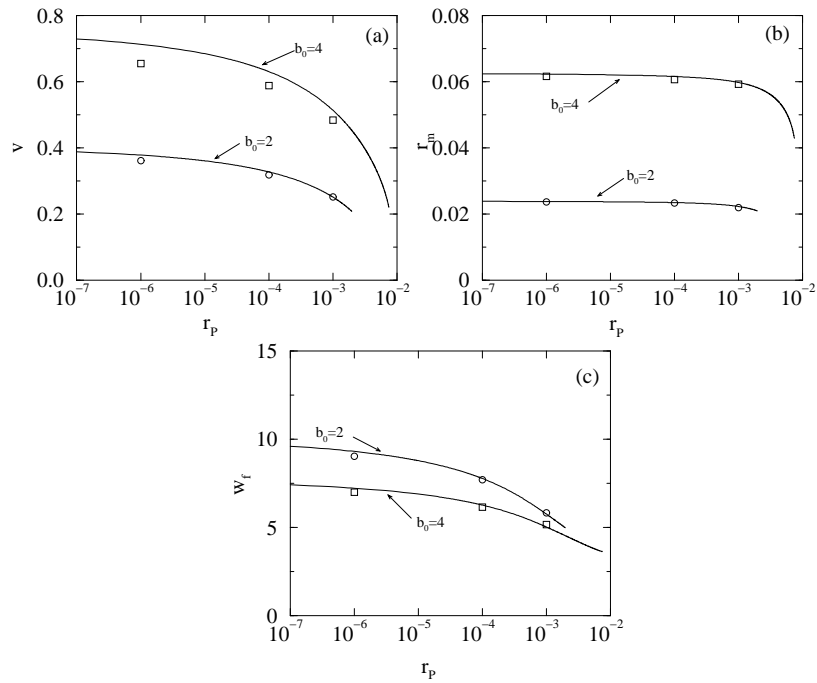
Figure 8.3: *Comparisons between wave properties predicted by the Shooting method and those observed from simulations of the discrete 3 stage epidemic model.* $\Delta x = 1$, $\Delta t = 0.5$, $l = 0.2$, $q = 0.006$ *and* $m = 0.006$. v *is the velocity of the wavefront*, c_m *is the maximum density of predators at the peak of the wavefront and* w_f *is the width of the wave front, measured from 5% to 95%* r_m.

8.4 Discussion

Discrete time and space versions of the predator-prey, 2 stage and 3 stage epidemic models were formulated. For small time steps the steady states and sta-

bility of the models showed no new behaviours to those of the continuous model. The value of c_P which created a soliton wave in the predator-prey model increased. The Shooting method was shown to be a good method of predicting the peak height, the velocity and the width of the wave fronts of the epidemic and invasion waves. This suggested that the discrete spatial models were good approximations of the continuous models.

Discrete approximations of the continuous models have been formulated for 1 dimensional spatial arenas. Before persistence mechanisms for invasions and epidemics which have no regrowth from unbiologically low population densities can be investigated, these discrete formulations have to be extended to 2 dimensional spatial arenas so all possible mechanisms can be studied.

Chapter 9

Discrete Models in Two Dimensions

In part III of the thesis, mechanisms which allow persistence of an epidemic or the establishment of the invading species behind the front when the wave form of the epidemic is a soliton are looked for. Some spatial, biological processes are only realizable when space is considered to have more than one dimension (Hassell et al. 1994). In terrestrial systems, space can be thought of as a 2 dimensional plane (Hanski 1994). Therefore, 2 dimensional arenas are constructed for the discrete spatial models. In this case the arenas are considered to be a form of islands and the boundaries are reflective.

More than one waveform can be generated in a 2 dimensional arena. Plane waves are initialised from a line innoculum of the invading or diseased component at one edge of the arena. They are exact 2 dimensional extensions of the 1 dimensional waves and are not considered likely to have different dynamics from them. Two wave forms, which are not clearly 2 dimensional extensions of the 1 dimensional waves, are going to be considered in this chapter. The first of these is the circular wave (Skellam 1951) (Gurney et al. 1998). Circular waves are interesting as any compact point innoculum generates a circular wave. The second wave form to be considered is the spiral wave (Keener and Tyson 1986) (Kessler and Levine 1989) (Gurney et al. 1998). The spiral wave is initialised from a very carefully set up initial condition. For a spiral to be initialised the wave has to be a soliton.

The spiral wave is important when considering the persistence of the invasion or epidemic (Hassell et al. 1994).

This chapter considers how spiral and circular waves are propagated, how they relate to the persistence problem, and whether or not predictions can be made about their characteristics by the Shooting method.

The Shooting method was developed to predict the wave front characteristics of 1 dimensional wave fronts. These characteristics should be the same as those of the cross section of a plane wave or a circular wave with a large diameter. In this chapter the Shooting method, as developed for the continuous time 1 dimensional models, is used to predict the cross sectional wave characteristics of circular waves with small diameters and spiral waves in 2 dimensional discrete models.

9.1 The Two Dimensional Scaled Dispersal Kernel

The models used in this chapter are basically the same as those formulated in chapters 7 and 8. The scaling of the parameters used in the dispersal kernel, as described in equation (7.2.11), is changed in the 2 dimensional model. The recipe for calculating α' uses the same method as in chapter 7 to produce

$$\frac{4\Delta t}{\Delta x^2} = \frac{\sum\sum(m^2 + n^2)(1 - \alpha'\sqrt{m^2 + n^2})^+}{\sum\sum(1 - \alpha'\sqrt{m^2 + n^2})^+} \tag{9.1.1}$$

and $\mathbf{j} = (m\Delta x, n\Delta x)$. The difference in the calculation for α' is due to the variance increasing at 4 times the rate of the diffusion coefficient in 2 dimensions, as opposed to 2 times, as in 1 dimensional arenas (Gurney and Nisbet 1998).

9.2 Circular Waves

A circular wave is formed by any innoculum with compact support of over a critical size, dictated by the size of the threshold population. The wave expands outwards in all directions at the same velocity when the population is diffusing

(Skellam 1951). The shape of the initial condition is chosen by calculating the square distance of the grid co-ordinates from the centre of the arena, q_{mid}^2, and then choosing the initial density (n_{init}) in the given square with the equation

$$n_{init} = 4n_{max}(1 - 10q_{mid}^2/NN)^+ \qquad (9.2.1)$$

where n_{max} is the highest expected density of the population, given as the highest marked value of the density scale of the arena, and NN is the number of nodes along each axis of the square arena. If the value of the equation is negative, the density in the square is 0.

9.2.1 Single Species Model

In figure 9.1 the simulation was started with the initial condition described by equation (9.2.1). As the wave spreads, the populations in the centre reach carrying capacity and the steady state of $n = 1$ spreads out. Figure 9.2 shows the time series of the mean density of an area of the arena. The area starts off empty, the invasion of the area starts at $t = 130$ and by time $t = 125$ the area is full to carrying capacity. By time $t = 150$ the whole arena is full of organisms at carrying capacity. Persistence of the invading organisms behind the wave front is not an issue in this model.

In table 9.1 the velocities and wave front widths observed from the 2 dimensional simulations are compared with predictions made by the Shooting method devised in chapter 2. The table shows that circular waves have wave characteristics within 10% of those predicted, so the Shooting method can be used to make predictions about circular wave fronts. This also shows if a cross section were to be taken of the wave front, it would be similar in profile to that of the 1 dimensional model.

9.2.2 The Two Stage Epidemic Model

An innoculum of susceptibles, described by equation (9.2.1) is added to an arena of prey at carrying capacity results in a circular soliton which expands (figure 9.3), leaving an area in the centre of the circle where the susceptible density
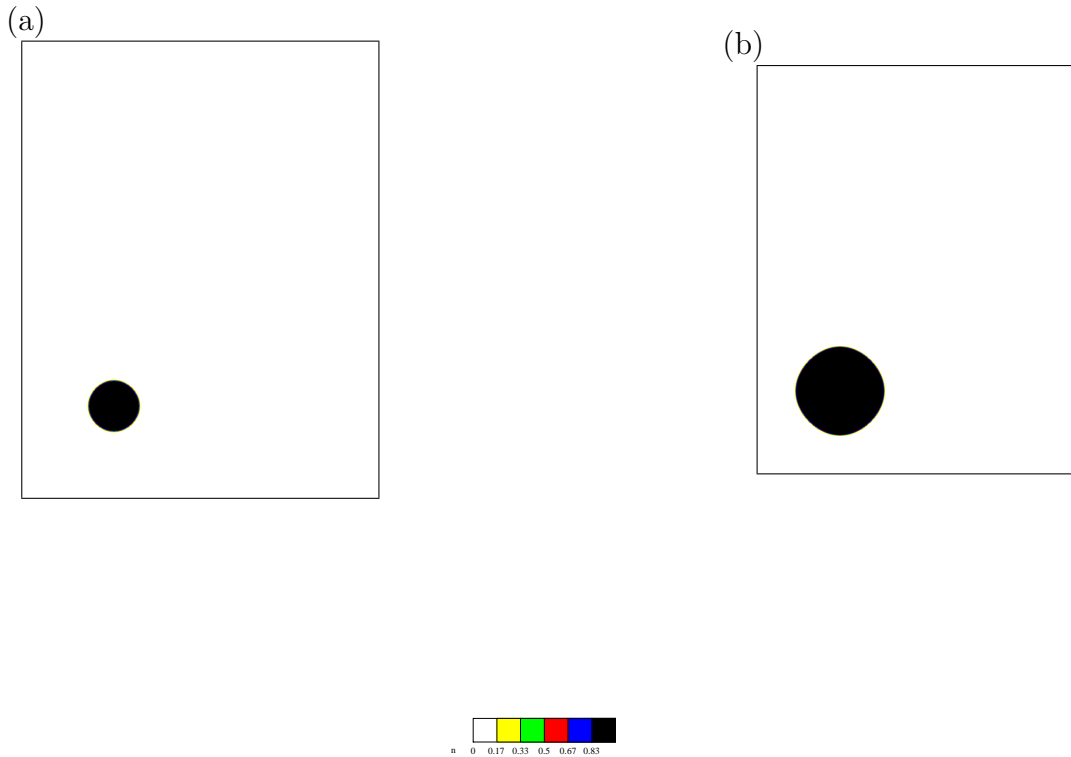
Figure 9.1: *The discrete Fisher model with an Allee effect in 2 dimensions in a* 350×350 *arena.* $a = 1.5$, $n_P = 0.0002$, $\Delta t = 0.25$ *and* $\Delta x = 2$. *(a) is a snapshot of the spatial distribution at* $t = 20$ *and (b) is a snapshot of the spatial distribution at* $t = 65$. *There is a large increase in the spatial range of the population from (a) to (b).*
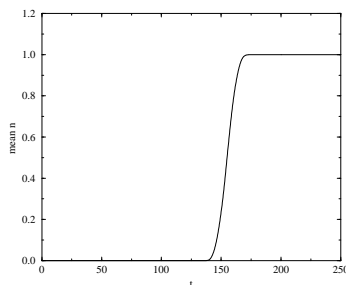
Figure 9.2: *Time series of mean density of n in the Fisher model with an Allee effect, in a 20 × 20 square area of the arena. By time 175 the population has locally reached its carrying capacity.*

a	n_T	Predicted Values		Observed Values	
		v	w_f	v	w_f
1.5	2×10^{-4}	1.8440	8.198	1.9249	8.742
1.5	5×10^{-2}	1.2643	5.888	1.1820	5.715
150	1×10^{-4}	1.7824	7.939	1.9108	8.684
150	6×10^{-3}	1.2889	5.979	1.4546	6.767

Table 9.1: *Comparisons between calculated wave properties and those measured from discrete time and space simulations in 2 dimensions of the Fisher model with $\Delta x = 2$ and $\Delta t = 0.25$. v is the velocity of the wavefront, w_f is the width of the wave front, measured from $n = 0.1$ to $n = 0.9$.*

is low and the infective populations become extinct. As the circle spreads, the susceptibles in the centre of the arena begin to recover. As the soliton reaches the edge of the arena the infectives reflect back into the area of susceptible depletion and dies out. The area of susceptible recovery expands, and eventually the arena reaches a state where susceptibles everywhere are at carrying capacity and the epidemic has died out. Figure 9.11 shows the time series of the mean density of susceptibles and infectives in an area of the arena. At $t = 60$ the soliton wave enters the area and the susceptible density falls. At $t = 80$ the soliton wave leaves the area and the susceptible density begins to rise, reaching the carrying capacity

115

across the area at $t = 125$. So with a circular wave, the epidemic dies out behind the wave front as in the 1 dimensional case.

The Shooting method as described in chapter 4 is used to predict the wave front characteristics of circular waves. The observed wave front width, peak height and velocity were compared with those predicted by the Shooting method. Figure 9.5 shows that the observed values are within 10% of the predicted values, so the Shooting method can be used to predict the wave front characteristics. The cross section of the circular soliton wave of the 2 stage epidemic model is very like the profile of the one dimensional wave.

9.2.3   The Predator-Prey Model

An innoculum of predators, described by equation (9.2.1) with half the diameter as the previous simulations, so the 10 in the equation was replaced with a 20, is added to an arena where the prey are initially at carrying capacity. This results in a circular soliton of predators spreading out from the centre (figure 9.3) (Gurney et al. 1998). As the invasion wave moves away from the centre of the arena the prey return to carrying capacity in the centre. When the soliton reaches the edge of the arena the predators reflect back into the region where prey are scarce and the invasion dies out. Eventually the prey recovers to carrying capacity over the entire arena.

Again the Shooting method as described in chapter 3 is used to make predictions about the velocity, peak height and width of the wave front of this model, and the comparison between the predicted and observed characteristics is shown in figure 9.7. The observed values are within 10% of the predicted values, so again the Shooting method can be used to make predictions about the 2 dimensional discrete predator-prey model with and Allee effect.
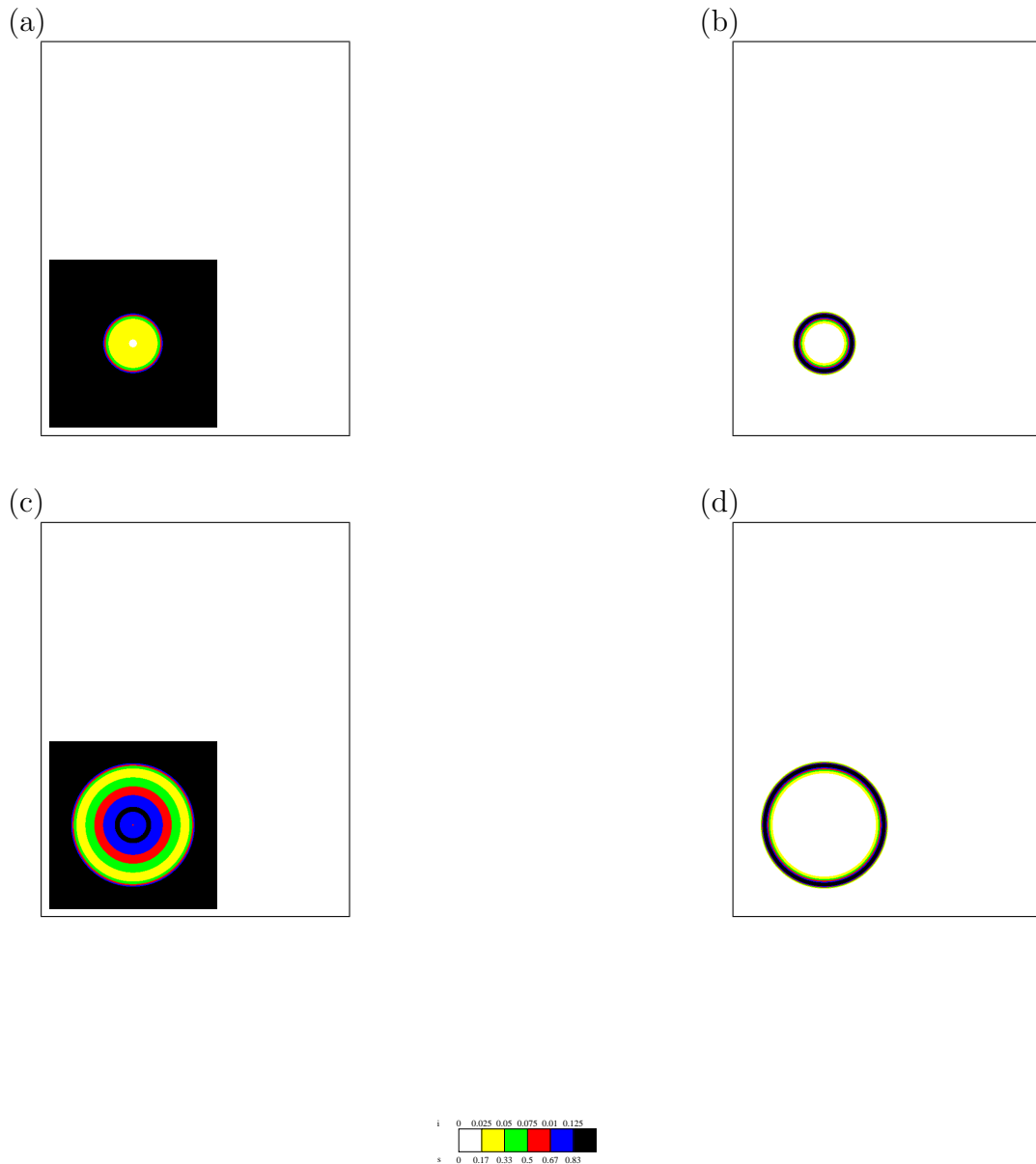
Figure 9.3: *The discrete 2 stage epidemic model with an Allee effect in a 350×350 arena. $b_0 = 2$, $i_P = 0.01$, $r = 0.1$, $\Delta t = 0.125$ and $\Delta x = 0.5$. (a) and (b) are snapshots of the spatial distribution of the susceptibles and infectives respectively at $t = 12.5$. (c) and (d) are snapshots of the spatial distribution of susceptibles and infectives at $t = 37.5$. There is a large increase in the spatial range of the epidemic from $t = 12.5$ to $t = 37.5$.*
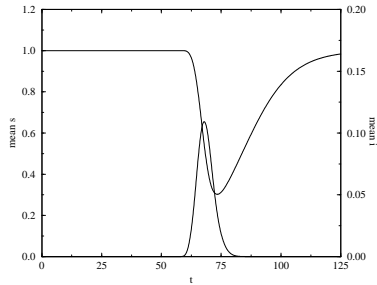
Figure 9.4: *Time series of mean density of susceptibles and infectives in the 2 stage epidemic model in a 20×20 square area of the arena. By time 125 the susceptible population has locally reached its carrying capacity and the soliton wave of infectives has passed out of the area.*

9.2.4 The Three Stage Epidemic Model

As with the previous model, the initial state of the arena is that the susceptible population is at carrying capacity, and the incubating and infective populations initially have the distribution described by equation (9.2.1). A circular soliton wave is formed (figure 9.8) and this wave spreads out from the centre of the arena, leaving an area where there are no incubating individuals and infectives behind it. As the wave spreads away from the centre, the susceptible population begins to recover. When the wave reaches the edge of the arena the infectives are reflected back into the region of susceptible depletion and the epidemic dies out. Eventually the susceptibles recover to carrying capacity over all the arena.

Again the Shooting method, as described in chapter 5, is used to make predictions about the wave front characteristics of circular waves in the 2 dimensional model. Figure 9.9 shows that these predictions are within 10% of the observed velocity, peak height and width of the front, so the Shooting method can be used to make predictions about this model.
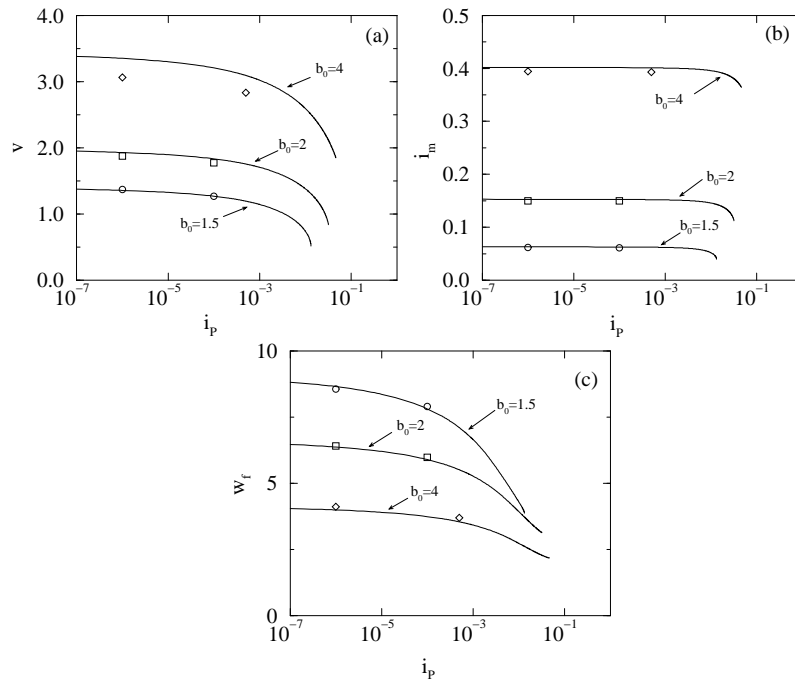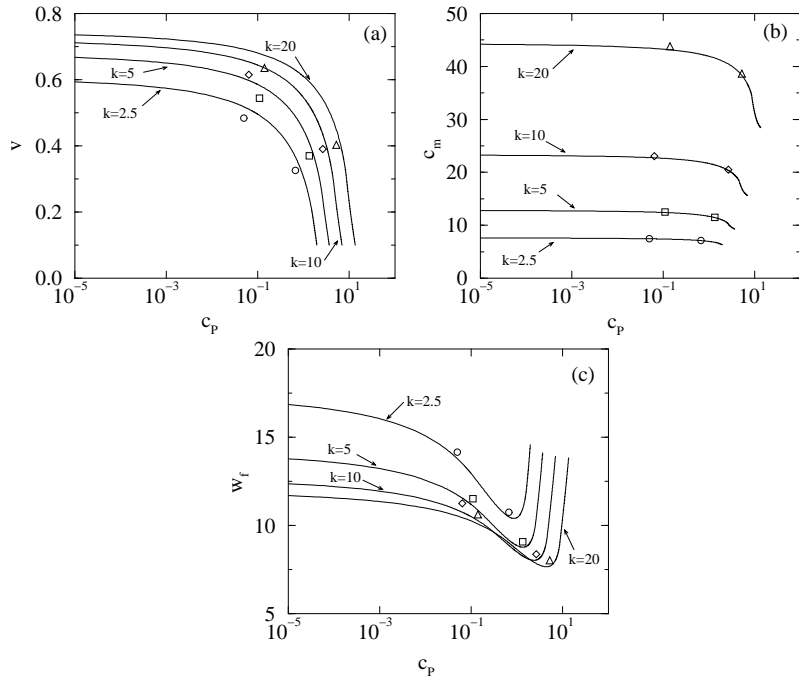
Figure 9.5: *Comparisons between wave properties predicted by the Shooting method and those observed from discrete time and space simulations of the 2 stage epidemic model in 2 dimensions. $\Delta x = 0.5$, $\Delta t = 0.0125$ and $r = 0.05$. v is the velocity of the wavefront, i_m is the maximum density of predators at the peak of the wavefront, w_f is the width of the wave front, measured from $i = i_m * 0.05$ to $i = i_m * 0.95$.*

9.3   Spiral Waves

Now the spiral wave form is considered. A spiral wave is a self organised pattern that forms during very carefully initialised simulations in an excitable medium.
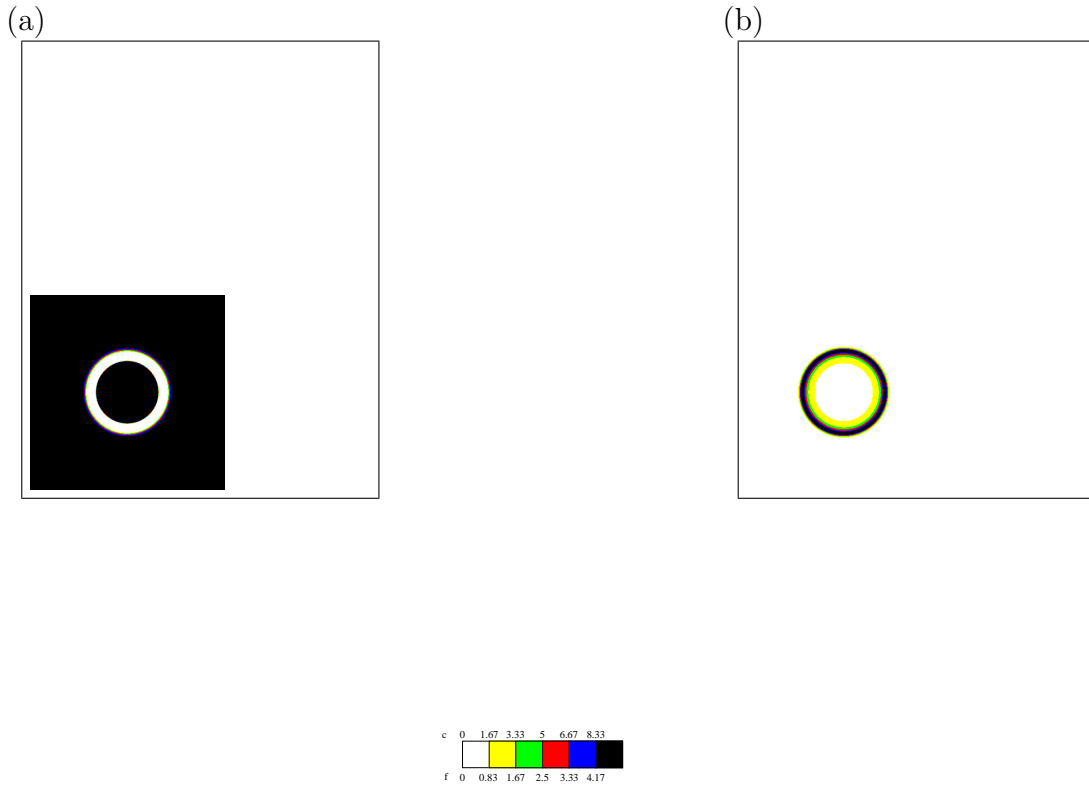
Figure 9.6: *The discrete predator-prey model in a 350×350 arena. $k = 5$, $c_P = 2$, $d = 0.05$, $u_m = 0.2$, $\Delta t = 0.5$ and $\Delta x = 1$. (a) is a snapshot of the prey and (b) is a snapshot of the predators at $t = 210$.*

Figure 9.7: *Comparisons between circular wave properties predicted by the Shooting method and those measured from discrete time and space simulations of the predator-prey model in 2 dimensions.* $\Delta x = 0.5$ *and* $\Delta t = 0.5$. $u_m = 0.2$ *and* $\delta = 0.05$. v *is the velocity of the wavefront,* c_m *is the maximum density of predators at the peak of the wavefront and* w_f *is the width of the wave front, measured from 5% to 95% of* c_m.

Spiral waves cannot be generated in the Fisher model as a soliton solution is required for a spiral to form; only in the multi-component models with Allee effects or thresholds when the thresholds are big enough to cause the wave to become a soliton. The velocity of expansion of the spiral wave perpendicular to the wave

(a)

(b)

(c)

| i (x10²) 0 | 0.23 | 0.47 | 0.7 | 0.93 | 1.17 |
| r (x10³) 0 | 1.17 | 2.33 | 3.5 | 4.67 | 5.83 |

| s | 0 | 0.17 | 0.33 | 0.5 | 0.67 | 0.83 |
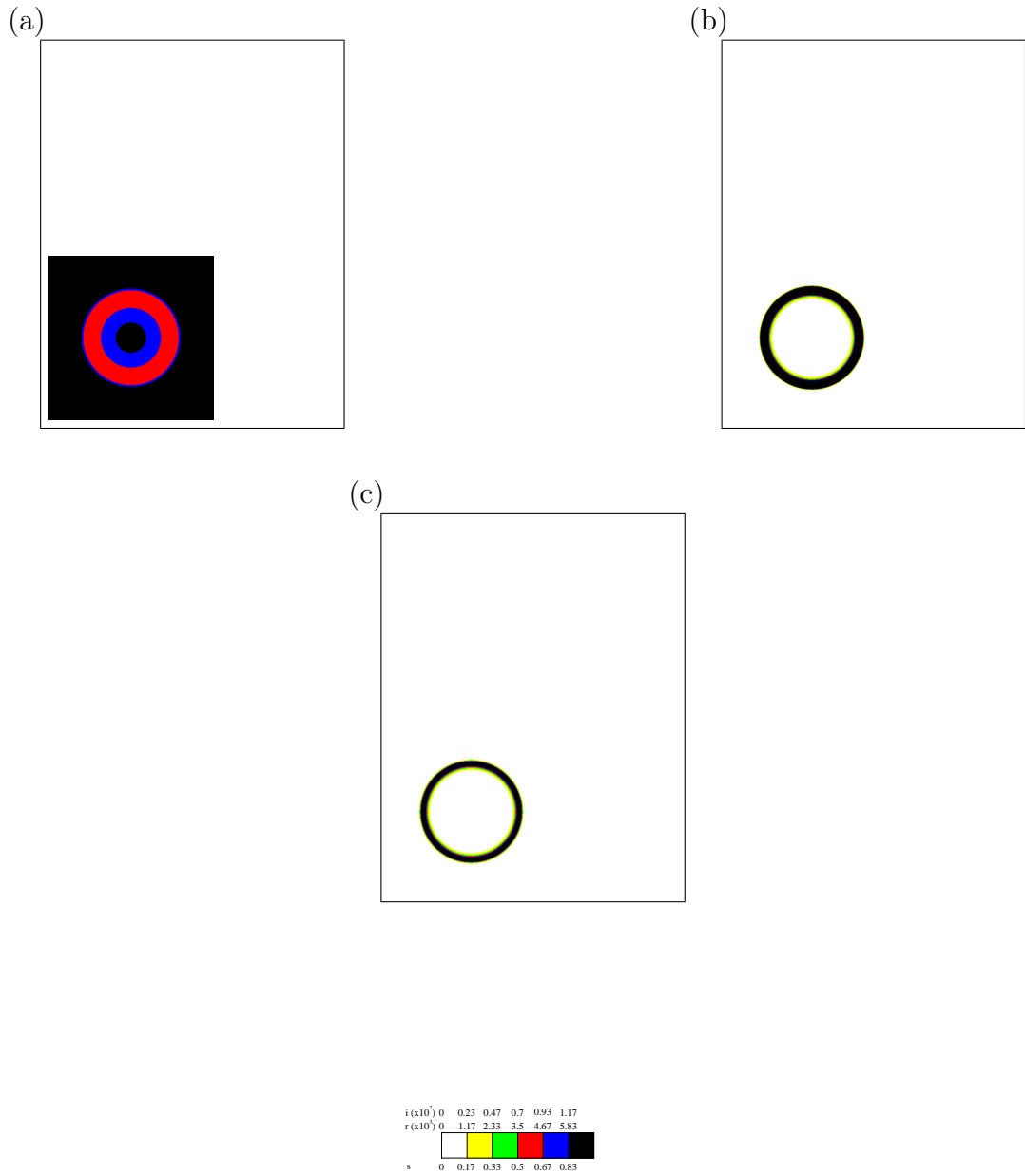
Figure 9.8: *The discrete 3 stage epidemic model in a 350×350 arena. $l = 0.2$, $r_P = 0.0001$, $m = 0.006$, $q = 0.006$, $b_0 = 1.5$, $\Delta t = 0.5$ and $\Delta x = 1$. (a), (b) and (c) are snapshots of the susceptible, incubating and infective distributions respectively at $t = 400$.*
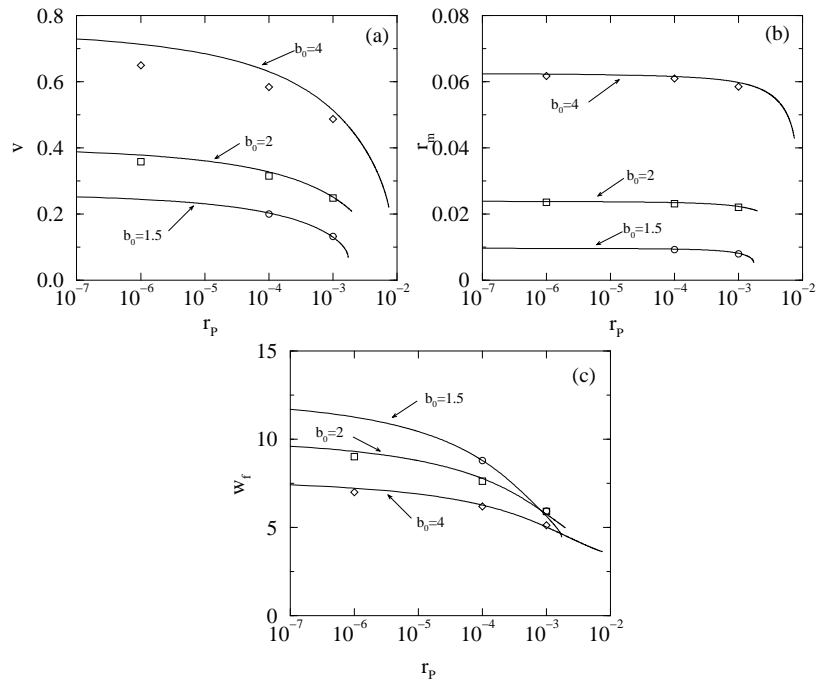
Figure 9.9: *Comparisons between calculated wave properties and those measured from discrete time and space simulations of the 3 stage epidemic model of circular waves, with $\Delta x = 1$ and $\Delta t = 0.5$. $l = 0.2$, $q = 0.006$ and $m = 0.006$. v is the velocity of the wavefront, r_m is the maximum density of predators at the peak of the wavefront and w_f is the width of the wave front, measured from 5% to 95% r_m.*

front is compared with the velocity predicted by the Shooting method which was developed to predict the velocity of wavefronts in continuous, 1 dimensional models. The width of the wavefront and the height of the peak of the wave are also compared with the Shooting method predictions.

123

9.3.1 The Two Stage Epidemic Model

The initial condition used to initiate a spiral wave has been termed the assymetric half line initial condition, as shown by figure 9.10 (a) and (b). This is formed by starting a plane wave of infectives moving from left to right through an arena where in the susceptibles are at carrying capacity. The initial condition used is described by equation (9.2.1), with q_{mid}^2 becoming the distance of the grid point from the left hand side of the arena squared. When the susceptibles start to recover behind the wave front, the top half of the arena is reinitialised so that the susceptibles are all at carrying capacity and there are no infectives. This causes the infectives to form an "umbrella handle" shape as demonstrated by figure 9.10 (c) and (d), where the infectives start to enter the top half of the arena as well as moving from left to right. The tip of the umbrella handle curls down into the region of susceptible recovery behind the wave front. As the wavefront moves to the right, the region of susceptible recovery spreads to the right and the tip follows. The tip also curls upwards as it moves left to right as it creates a region of susceptible depletion below it. This curve forms the core of the spiral, figure 9.10 (e) and (f), which then spreads to fill the whole arena.

Figure 9.11 shows the time series of the mean density of an area in the top left of the arena. At the start of the simulation the soliton used to set up the initial condition passes through the area. At $t = 120$ the first wave of the spiral passes through, followed by the second, at $t = 165$, and so forth. So the epidemic does not die out within the arena as in the circular wave.

Spiral waves are different from the 1 dimensional waves discussed in chapter 8 in a variety of ways. The spatial arena must be large enough for a fully formed spiral to fit into. This may require the use of large space steps. The space steps may be larger than the space steps shown to give a good comparison between the 1 dimensional continuous and discrete models in chapter 8. The wave spins slightly, so only the velocity of spread perpendicular to the wave front can be measured. This is not directly comparable with the velocity of the 1 dimensional wave. Because of these differences, predicting the wave characteristics of spiral
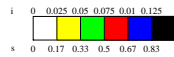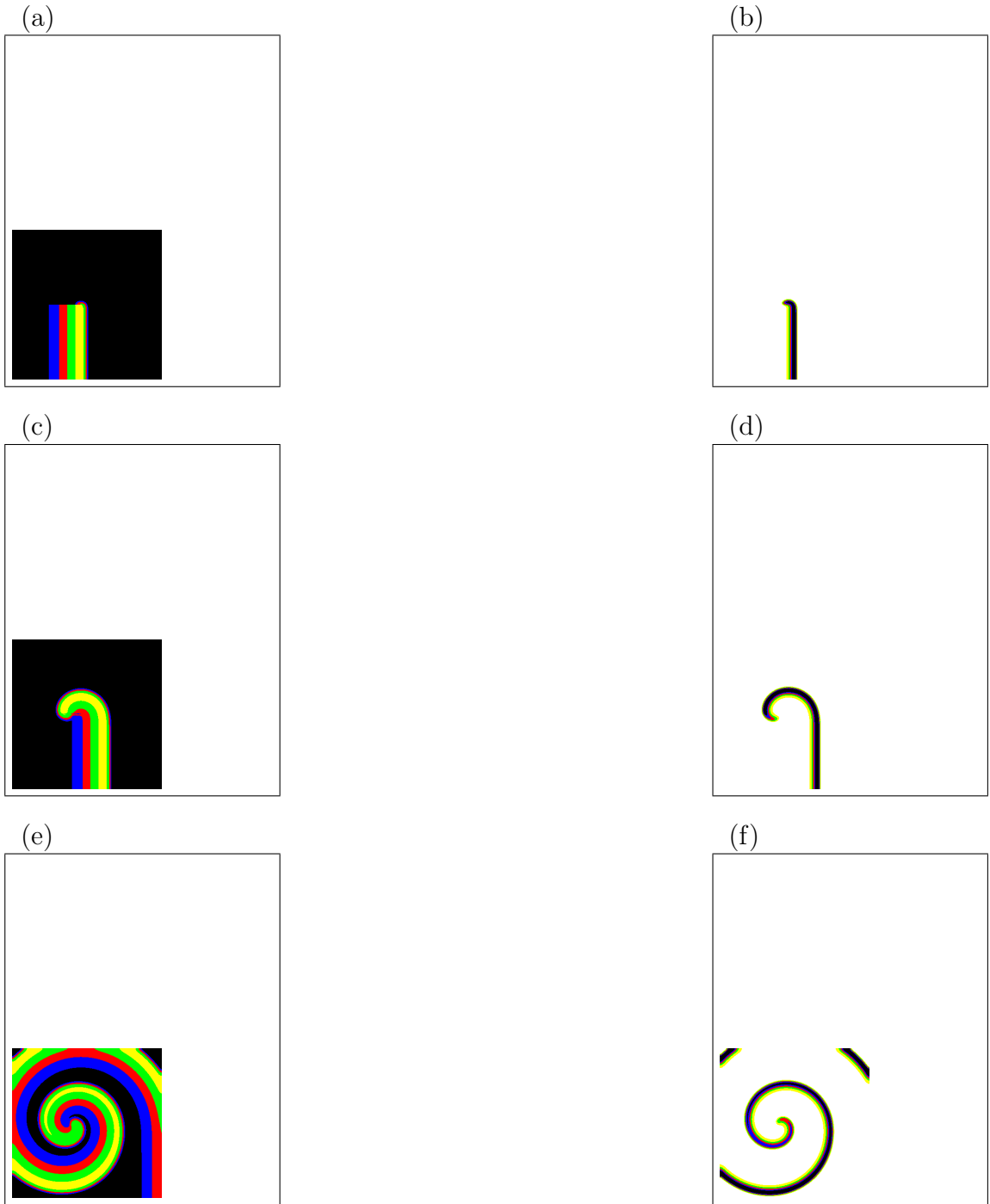
(a)

(b)

(c)

(d)

(e)

(f)

i	0	0.025	0.05	0.075	0.01	0.125

s	0	0.17	0.33	0.5	0.67	0.83

Figure 9.10: *Formation of a spiral wave in the discrete 2 stage epidemic model in*
a 250 × 250 arena, r = 0.1, i = 0.01, b = 3, Δt = 0.125 and Δx = 0.5. (a) and
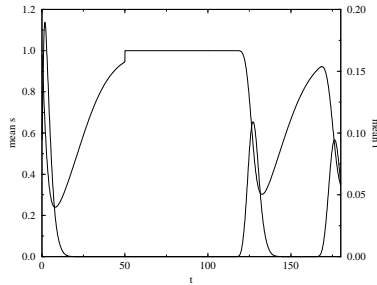
Figure 9.11: *Time series of mean density of susceptibles and infectives of the 2 stage epidemic model in a 20×20 square area of the arena. The population densities oscillate as the spiral waves move through the area.*

waves by using the Shooting method is going to be inexact.

The results of this comparison are shown in table 9.2. The observations from the spiral waves are all around 10% of the predictions made by the Shooting method. So the Shooting method, is able to make reasonable predictions about the velocity, peak height and width of the spiral wave front in the 2 stage epidemic model.

b	i_T	Predicted Values			Observed from Spirals		
		v	w_f	i_m	v	w_f	i_m
2	0.005	1.528	4.966	0.1620	1.370	4.673	0.1404
2	0.01	1.395	4.474	0.1586	1.259	4.109	0.1411

Table 9.2: *Comparisons between wave characteristics of spiral waves observed from simulations of the discrete 2 stage epidemic model in 2 dimensions and predictions made by the Shooting method. $\Delta x = 0.5$, $\Delta t = 0.125$ and $r = 0.1$. v is the velocity of the wavefront, i_m is the maximum density of predators at the peak of the wavefront, w_f is the width of the wave front, measured from 5% to 95% of i_m.*
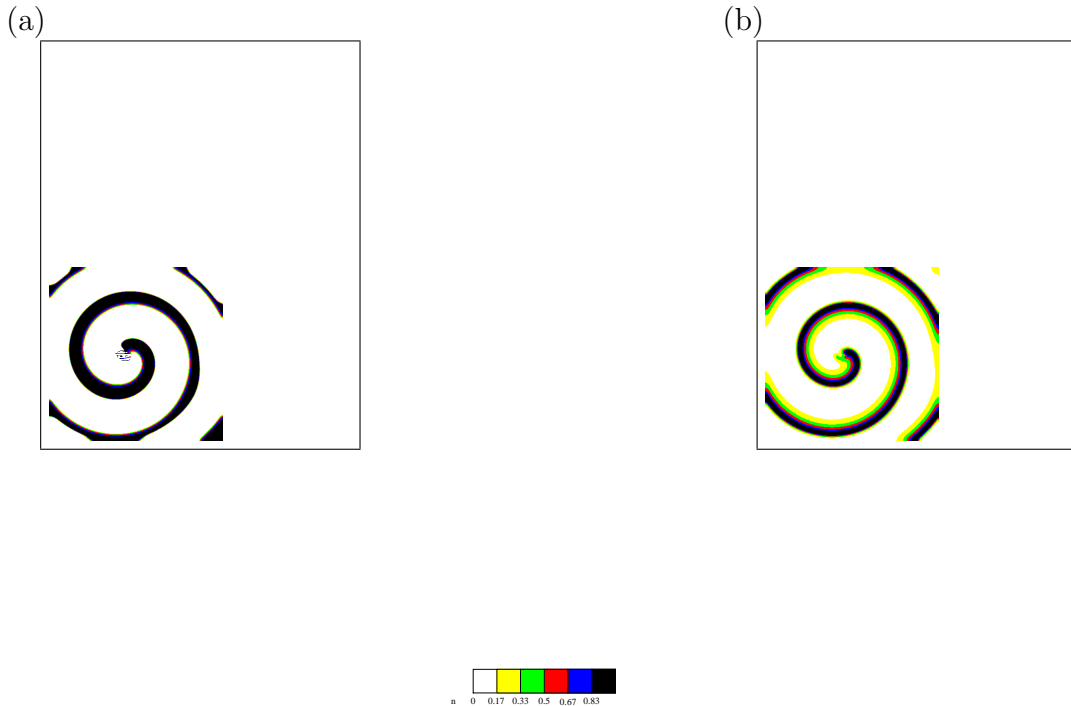
126

Figure 9.12: *The discrete predator-prey model with an Allee effect in a 350×350 arena. $u_m = 0.2$, $c_P = 0.3$, $k = 10$, $d = 0.05$, $\Delta t = 0.5$ and $\Delta x = 1$. (a) is a snapshot of the prey distribution and (b) is a snapshot of the predator distribution at $t = 720$. There is a pattern formation at the tip of the spiral of a smaller scale than is of interest.*

9.3.2 The Predator-Prey Model

In the predator-prey model the spiral wave (see figure 9.12) was initiated from an assymetric half line condition as described for the 2 stage epidemic model (Gurney et al. 1998).

The wave characteristics observed from the spiral waves are compared with predictions made by the Shooting method in table 9.3. The Shooting method predicts the spiral expansion velocity and peak height well, and the observed width of the front is about 10% larger than the predictions. So the Shooting method

can be used to make predictions about the characteristics of a spiral wave front in this model.

k	c_T	Predicted Values			Observations from Spiral		
		v	w_f	c_m	v	w_f	c_m
10	0.3	0.6114	9.388	22.34	0.6006	10.45	23.01
10	1	0.5463	8.384	21.67	0.5487	9.420	22.12

Table 9.3: *Comparisons between wave characteristics of spiral waves observed from simulations of the 2 dimensional discrete predator-prey model and predicted values made by the Shooting method.* $\Delta x = 2$, $\Delta t = 0.5$, $u_m = 0.2$ *and* $\delta = 0.05$. *v is the velocity of the wavefront, c_m is the maximum density of predators at the peak of the wavefront and w_f is the width of the wave front, measured from 5% to 95% of c_m.*

9.3.3   The Three Stage Epidemic Model

Again the spiral wave was initiated by the assymetric half line initial condition. In the case of the 3 stage epidemic model, when the condition is created, the incubating stage is treated as the infective stage. The spiral formed is shown by figure 9.13.

The wave front characteristics of the spiral waves are compared with those predicted by the Shooting method. Table 9.4 shows that the Shooting method predicts the wave front characteristics to around 10%, so the Shooting method can be used to make predictions about the wave front characteristics of the spiral waves formed by the 3 stage epidemic model.

b	r_T	Predicted Values			Observations from Spirals		
		v	w_f	r_m	v	w_f	r_m
2	0.001	0.2514	5.759	0.02229	0.2242	5.686	0.01845
2	0.002	0.2075	4.968	0.02091	0.1900	5.306	0.01882

Table 9.4: *Comparisons of observed wave front characteristics from simulations of the discrete 3 stage epidemic model of spiral waves and predictions made by the Shooting method.* $\Delta x = 2$, $\Delta t = 0.5$, $l = 0.2$, $q = 0.006$ *and* $m = 0.006$. *v is the velocity of the wavefront, r_m is the maximum density of predators at the peak of the wavefront and w_f is the width of the wave front, measured from 5% to 95% of r_m.*
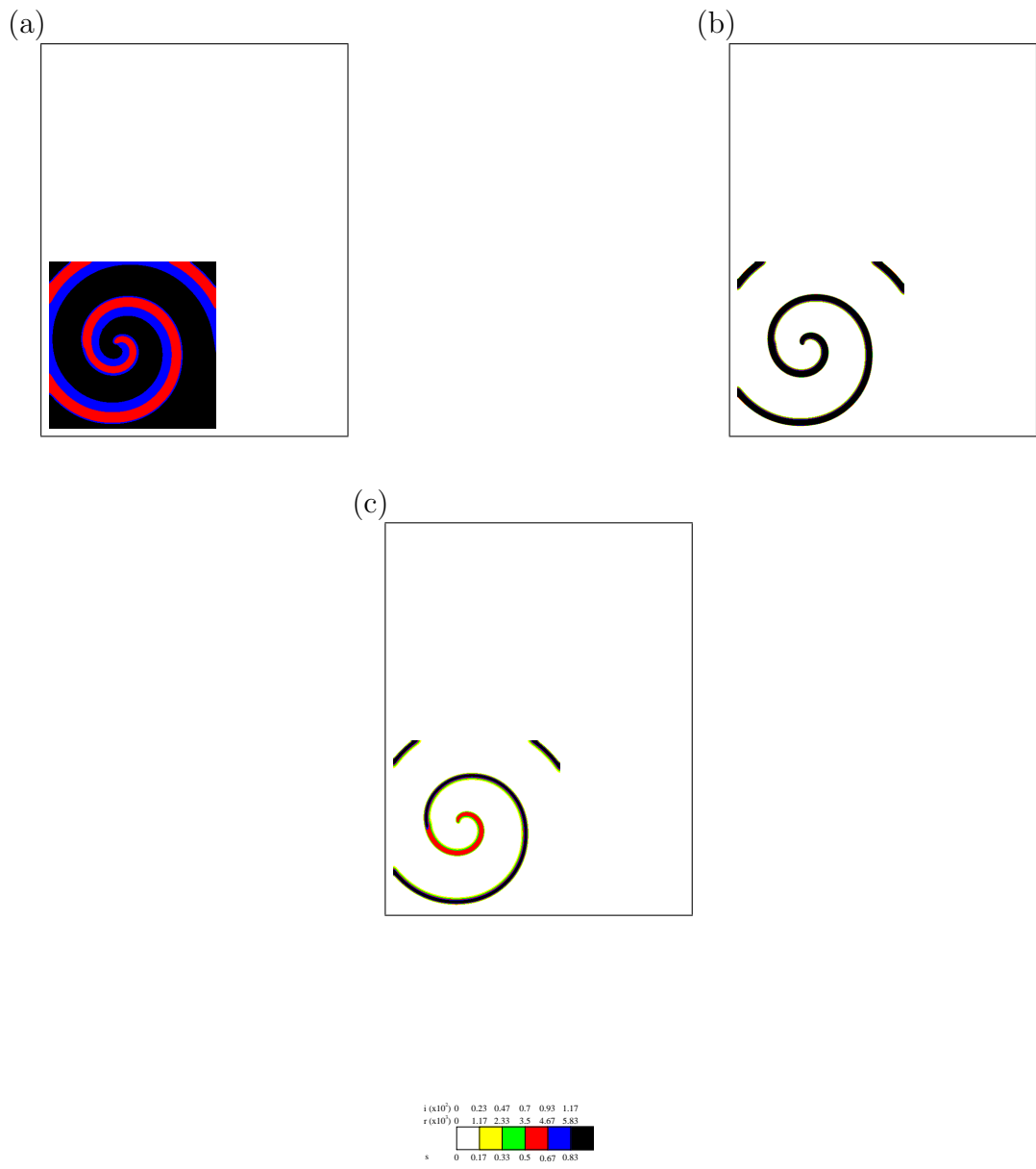
Figure 9.13: *Spiral wave formed by the discrete 3 stage epidemic model in a 350×350 arena. $l = 0.2$, $r_P = 0.001$, $m = 0.006$, $q = 0.006$, $b_0 = 1.5$, $\Delta t = 0.5$ and $\Delta x = 1$. (a), (b) and (c) are snapshots of the susceptible, incubating and infective distributions respectively at $t = 2740$.*

9.4 Discussion

Circular waves can be formed from any point initialisation large enough to form a wave in the presence of the given threshold. In cross section, the circular waves are similar in profile to the 1 dimensional waves for all the models. In the Fisher model the invading population spreads out to fill whole arena. In multi component models where the wave is a soliton, when the wave reaches the reflective boundary, the organisms reflect back into the area of resource depletion and the invasion or epidemic dies out. So there is still a problem of persistence of the epidemic or invasion behind the wave front in the 2 dimensional spatial models where the wave propagated is a circular wave. The Shooting method can be used to make predictions about the velocity, peak height and width of the wave fronts in all 4 of the models considered.

Spiral waves are self organised patterns which are formed by using an "asymmetric half line" initial condition. The spiral wave has characteristics of the same scale as the circular wave, so the Shooting method can be used to predict the scale but not exact magnitudes of the characteristics. The spiral may to be too large to fit into the given arena. The self organisation of spirals may be a mechanism which allows persistence of an epidemic or an invasion behind the wave front; this is investigated in the next part of the thesis.

There can be difficulties forming spiral waves. The space steps have to be large enough to allow the arena to fit the spiral in. It has been shown that the point of transition between soliton and wave trains is affected by space step size. So the spiral may go through phases when it is not a soliton at all points, causing the spiral to buckle and eventually break up. This generally happens in the core of the wave.

Models have been formulated which are computationally efficient. They are good discrete analogues of the continuous models. The arena has been expanded into 2 dimensions. The Shooting method can be used to make predictions about the velocity, wave front width and peak height of both spiral and circular waves.

The procedures carried out in this part have created the tools which permit a thorough investigation into mechanisms which allow persistence of epidemics and the establishment of invading species.

Part III

Persistence Mechanisms

Chapter 10

Persistence Mechanisms

10.1 Introduction

In the multi-component models used in this thesis, altering the formulation of the models, so that there is no growth or infection from low density populations, creates soliton waves where no endemic or established state is reached behind the wave front. In both epidemics and invasions of exotic species, frequently the epidemic or species continues to survive in the area that the wave front has passed over.

A number of biological mechanisms, which have been omitted from the models as they stand, are considered as mechanisms for allowing the epidemic to become endemic or the invading species to become established. They shall be described in this chapter and then applied to the multi-component models in the following chapters of this part.

The modified Fisher model is not considered in this part of the work; its role in this thesis was as a well understood model to be used as a vehicle for devising a method of predicting the characteristics of wave fronts with no regrowth at the toe. Its job is now complete. In the Fisher model, the invading population does not die out behind the wave front. The mechanisms described here are chosen to promote the growth of populations behind the wave front and are not going to have much impact on the dynamics of the Fisher model.

10.2 Environmental Heterogeneity

10.2.1 Spatial Heterogeneity: Patches

Frequently, work on spatial heterogeneity looks to understand the effects of habitat fragmentation on the stability of populations of endangered species (Fahrig 1992) or on epidemic control regimes (Lloyd and May 1996). Such studies consider patches of suitable habitat in a matrix of unsuitable habitat. These systems are well described by meta-population models (Hanski 1994) and diffusion models (Seno 1991). The results of these studies show that the presence of very suitable patches encourages settlement of less suitable or unsuitable matrix.

Scheffer and de Boer (1995) consider a predator-prey model with the same growth functions as the unmodified predator-prey model, as described in chapter 3, but the predators are immobile and the prey disperse diffusively. They found that when the predators are restricted to a patch, and the prey diffuse freely in and out of the patch, the oscillatory dynamics of the system are reduced.

In this thesis, the oscillatory dynamics of the systems, which result in the formation of soliton wave fronts, are caused by the richness of the habitat. So, to investigate the effects of spatial heterogeneity on the persistence of epidemics or invasions behind the wave front, spatial heterogeneity is in the form of patches of less suitable habitat within a matrix of suitable habitat. Inequality (3.1.14) shows that in the predator-prey model, if the carrying capacity is low, the dynamics are stable. The amplitude of the oscillations in the unstable case increases with carrying capacity. Also, at high thresholds, the system can become non-oscillatory with a steady state dictated by the threshold (equation (3.3.9)), as shown by figure 3.3. The effect of spatial heterogeneity in the form of a patchwork of different carrying capacities throughout the arena on a the predator-prey model with a threshold was investigated by Gurney et al. (1998). They showed that new invasions appeared in low carrying capacity patches if the threshold density was low. The wake of the 2 stage epidemic model becomes more oscillatory as the carrying capacity is increased, as shown by inequality (4.1.9). This means that at low car-

rying capacities, the first trough of the wake is less likely to fall below threshold density so the wave does not become a soliton. Also, at high thresholds and low carrying capacities the model becomes non-oscillatory (equation (4.1.9))and the steady state depends on the threshold (equation (4.3.5)), as shown by figure 4.3. The oscillatory nature of the 3 stage epidemic model also decreases with carrying capacity and this effects the dynamics of the system in the same way as in the 2 stage epidemic model. So decreasing the carrying capacity in a patch may create an area of stable dynamics in the arena.

10.2.2   Seasonal Variation

White and Harris (1994) showed that contacts between foxes from neighbouring territories increased during winter in Bristol foxes as foraging took male foxes farther afield and into the territories of others. Varying the contact rate throughout the year may reduce the oscillatory nature of the wake behind the epidemic front in the epidemic models, so for part of the year the dynamics may be stable.

10.3   Long Range Dispersal

Continuous immigration from outside the arena would allow the invasion or epidemic to persist (Gurney et al. 1998), but the assumption in these models is that there is only a finite initial innoculum in the given arena, so this persistence mechanism is not investigated.

Kot et al. (1996) discuss how many organisms disperse leptokurtically. The description of dispersal by diffusion does not successfully describe the dispersal of these organisms. To compensate for this, they used integrodifference equations with long tailed dispersal kernels to represent long range dispersal, so that some individuals migrate further than is described by diffusion. In chapter 12, the predator-prey model is modified so that occasionally a predator will disperse much further than most others. In the 2 stage epidemic case, the occasional infective individual travels a longer distance than that described by diffusion.

At the end of the journey the infective starts infecting susceptibles locally. This process cannot be applied to a rabies epidemic, but it may be possible in other epidemics.

In the 3 stage epidemic model, it is unlikely that rabid fox will live long enough to travel further than the distances described by the diffusive term in the model, so the rabid population is not chosen to migrate long distances. The model assumes that once recruited into the adult population the susceptibles and incubating individuals remain within their territories. However, young foxes may embark on long journeys to find empty territories to inhabit as adults. A young fox may be incubating the rabies virus when it embarks on such a journey (Murray 1989). The fox then becomes rabid, stops travelling, and infects the local susceptibles. Although Macdonald (1980) has shown that young foxes are less likely to be infected, this process may still happen occasionally.

10.4   Self Organised Patterns

10.4.1   Spiral Waves

It has already been shown, in chapter 9, that spiral waves form in these models. Now the issue is whether or not spirals can be formed by environmental processes. Much work has been carried out on host-parasitoid models which form spiral waves, e.g. (Hassell et al. 1991)(Comins et al. 1992) (Hassell et al. 1994), but the relevance of such pattern formation to ecology is not obvious. No spiral waves have been witnessed in ecological systems (Rohani et al. 1997).

Can a natural process be found to create the half line initial condition? Rohani et al. (1997) discuss the possibilities for the formation of spirals due to an asymmetry , stochasticity or inhomogeneities in the medium. G. Ruxton (pers. comm.) suggested that a river, too wide, deep or fast flowing to be crossed, going through a period of drought may be a possible ecological system which could form a half line initial condition. This idea is tested in chapter 13.

If a spiral were to form in an ecological system, would it be robust to environmental and individual heterogeneities as described in the previous sections? Ruxton and Rohani (1996) modified the (Hassell et al. 1991) host-parasitoid model so that there were temporal and spatial heterogeneity. They found that spiral waves formed in this system were robust to variations in the host's fecundity but not to random local extinctions. Gurney et al. (1998) found that spiral waves in a predator-prey model with a threshold are robust to random immigration used as an approximation to long range dispersal, and robust to spatial heterogeneity provided that the soliton is not compromised in any patches.

The long range dispersal algorithm used in these models moves individuals. This would create gaps in the spiral wave, similar to the local extinctions in Ruxton and Rohani's work, so the robustness of spiral waves to long range dispersal is investigated in chapter 13. Spatial heterogeneity in the form of patches that are known to compromise the soliton wave form will also be added to arenas which contain spirals to monitor the effects. The interference pattern formed by multiple spiral waves may break the spirals up. The interactions of two spirals turning in the same direction and the opposite directions are investigated.

10.4.2   Small Scale Patterns

Another form of self-organised pattern arises in this investigation. Self-organised patterns on a very small scale are formed when space is heterogeneous (McLaughlin and Roughgarden 1991) (McLaughlin and Roughgarden 1992) (Gurney and Veitch 1998) and, in the case of the predator-prey model, when a spiral is formed. These patterns have already been described fully by Gurney and Veitch (1998) for the predator-prey model used in this thesis, and shall not be investigated further.

Chapter 11

Environmental Heterogeneity

11.1 Introduction

Environmental heterogeneity has not so far been included in any of the three models. Two forms of heterogeneity are considered in this chapter - temporal and spatial. The affects of the inclusion of seasonal variation and patches of reduced carrying capacity in the models are investigated in this chapter.

11.2 Seasonality

It was observed by White and Harris (1994) that contacts between foxes from different territories increase in winter. This seasonal factor was included in the model in the form of a contact rate varying sinusoidally throughout the year.

Figure 11.1 shows that varying the contact rate creates persistence of the epidemic behind the front in the 3 stage epidemic model in 1 dimension. When the contact rate is reduced the dynamics of the system become less oscillatory, so the trough does not dip to low densities which are affected by the threshold.

The break up of the soliton wave front in a model due to a seasonal factor was only observed in the 1 dimensional 3 stage epidemic model. The observed change in dynamics was sensitive to the time and space steps chosen. In the other models the only observed effect was the periodic decrease in velocity, peak height and
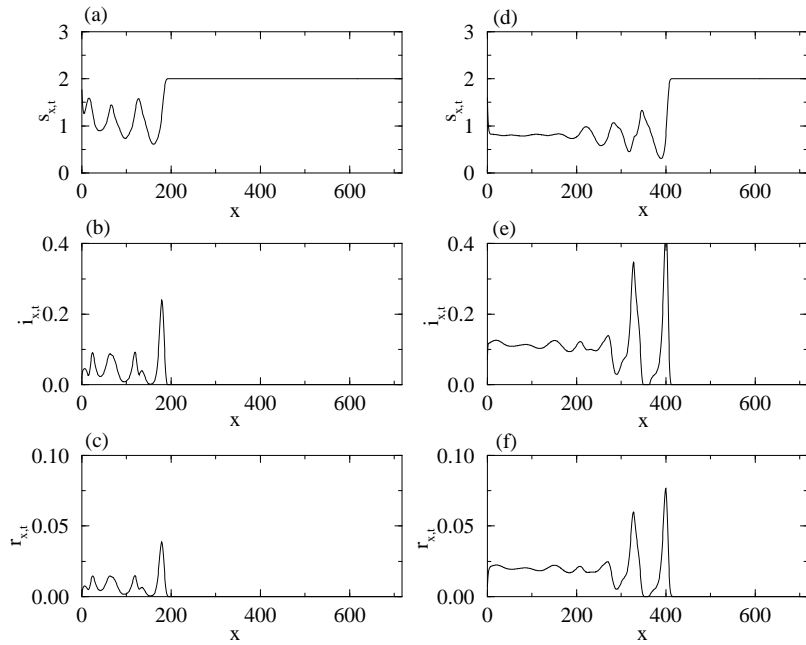
Figure 11.1: *3 stage epidemic model with seasonal contact rate.* $K = 2$, $M = 0.5$, $L = 13$, $Q = 0.5$, $D = 73$, $\Psi = 150$, $B_0 = 80 \rightarrow 100$, $R_P = 0.001$, $\Delta t = 0.1$ *and* $\Delta x = 0.5$. *(a), (b) and (c) show the spatial distribution of the susceptibles, incubating and infective individuals respectively after 5.5 years and (d), (e) and (f) at 11 years.*

front width. In 2 dimensional models, a larger innoculum is needed to start an epidemic because the epidemic spreads in many directions instead of only 2 in the 1 dimensional model. Therefore a larger population is needed to establish behind the wave front in the 2 dimensional model to allow the epidemic to persist

behind the wave front. The incubating stage may have acted as a buffer which allowed the effects of if the decreased contact rate to persist when the contact rate increased. The predator-prey model was altered so that conversion efficiency was seasonal. The predator-prey model will always be unstable for periods of the year.

11.3   Spatial Heterogeneity

In this section spatial heterogeneity in the form of patches where the carrying capacity of the susceptibles or prey is reduced is investigated as a persistence mechanism.

11.3.1   The Three Stage Epidemic Model

A patch of low carrying capacity is placed in the centre of a 1 dimensional arena. The patch is parabolic in shape to reduce edge effects. Figure 11.2 (c) and (d) shows that when the original soliton first reaches the patch, the rabies epidemic survives in the patch as the dynamics are less oscillatory. Wave trains start to emanate from either side of the patch. Eventually, as shown by figure 11.2 (e) and (f) the coexistence steady state begins to form around the patch. After a long time, as shown by figure 11.2 (i) and (j), the entire arena is at the coexistence steady state.

This was then repeated in a 2 dimensional arena, as shown by figure 11.3. The patch in 2 dimensions is the shape of an inverted Gaussian distribution. Again a wave train emanates out from the patch, but instead of the whole arena eventually reaching the epidemic steady state, a small scale pattern forms. The pattern forms around the patch and then spreads outwards. The simulation was run over 2 millenia, and the patterns continued to appear (but reduced in intensity). The pattern may be a very long lived transitional behaviour, it may be caused by interference from waves reflected by the boundaries, or it may be that the equilibrium properties of the system are different in 2 dimensions from the 1
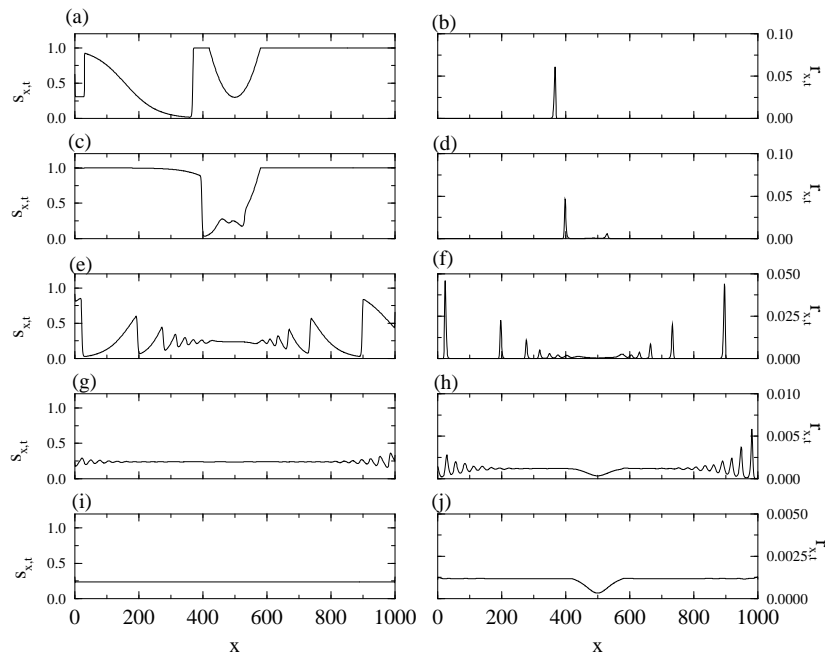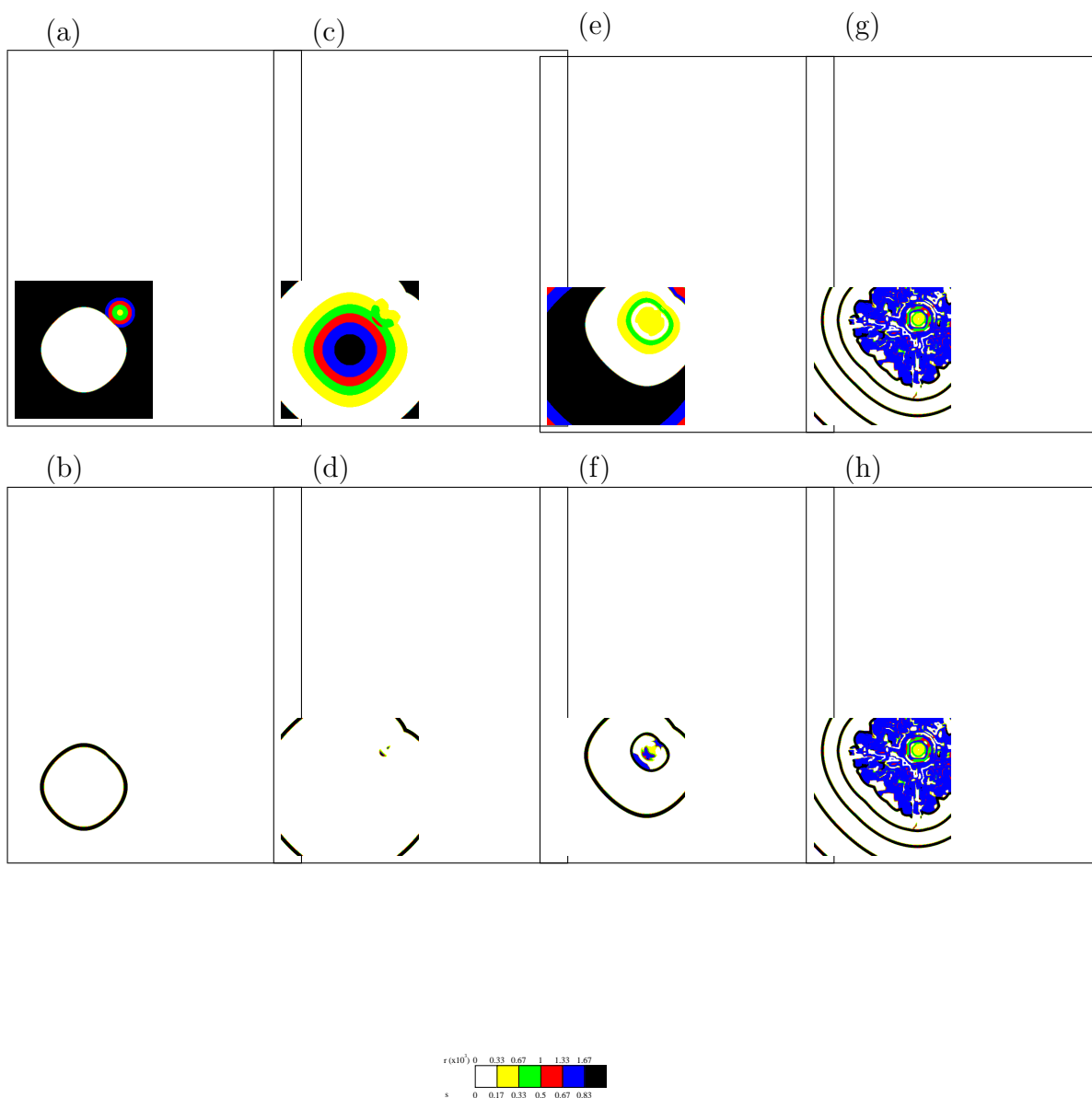
Figure 11.2: *3 stage epidemic model with a patch of low carrying capacity in 1 dimension.* $B_0 = 80$, $D = 73$, $L = 13$, $M = 0.5$, $Q = 0.5$, $\Delta t = 0.5$, $\Delta x = 2$, $R_P = 4 \times 10^{-6}$ *and* $K = 4$ *and the minimum value of* K *in the patch of low density is* 1.2. *(a) and (b) are snapshots of the susceptible and infective populations at time 14 years. (c) and (d) are snapshots of the susceptible and infective populations at time 27 years. (e) and (f) are snapshots of the susceptible and infective populations at time 54 years. (g) and (h) are snapshots of the susceptible and infective populations at time 109 years. (i) and (j) are snapshots of the susceptible and infective populations at time 164 years.*

dimensional model.

Figure 11.3: *3 stage epidemic model with one patch of low carrying capacity in a 301 × 301 arena.* $B_0 = 80$, $D = 73$, $L = 13$, $M = 0.5$, $Q = 0.5$, $\Delta t = 0.5$, $\Delta x = 2$, $R_P = 4 \times 10^{-6}$ *and* $K = 4$ *and the minimum value of* K *in the patch of low density is* 1.2. *(a) and (b) are snapshots of the susceptible and infective populations at time 5 years. (c) and (d) are snapshots of the susceptible and infective populations at time 12 years. (e) and (f) are snapshots of the susceptible and infective populations at time 23 years. (g) and (h) are snapshots of the susceptible and infective populations at time 68 years. The infectives are spreading out from the patch of low carrying capacity.*

The interaction of 2 patches of low carrying capacity is now investigated. The rabies epidemic survives in the patches as before. When the wave trains form, there is interference where they meet and figure 8 shaped waves are formed. When the unexplained pattern spreads out from the patches, they form a filled in figure 8, and then spreads throughout the whole arena as before. This also demonstrates that above a minimum size, the dynamics are not sensitive to the patch size.

11.3.2   The Two Stage Epidemic Model

A patch of low carrying capacity is created in the 1 dimensional 2 stage epidemic model in the same manner as in the 3 stage epidemic model. Figure 11.5 shows that, like the one dimensional 3 stage epidemic model, eventually the whole arena reaches the coexistence steady state.

The experiment is then repeated in a 2 dimensional arena (figure 11.6). Again the sequence of events is the same as those involved in the whole arena reaching its coexistence steady state as in the 1 dimensional, 2 stage epidemic model.

11.3.3   The Predator-Prey Model

It is known (see chapter 3) that if inequality (3.1.14) is not satisfied then there is no coexistence steady state in the predator-prey model. This poses the question of what will happen if a patch of non oscillatory dynamics (where inequality (3.1.14)) is satisfied.

Figure 11.7 shows that in the 1 dimensional arena, where again the patch is parabolic in shape, again the invading organisms establish themselves in the patch. Repeated solitons then emanate out from the patch. A complex pattern is formed in the patch, a feature of the model described in detail in Gurney and Veitch (1998).

The experiment was then repeated in a 2 dimensional arena (figure 11.8). Again the resultant pattern was repeated solitons emanating from the patch.
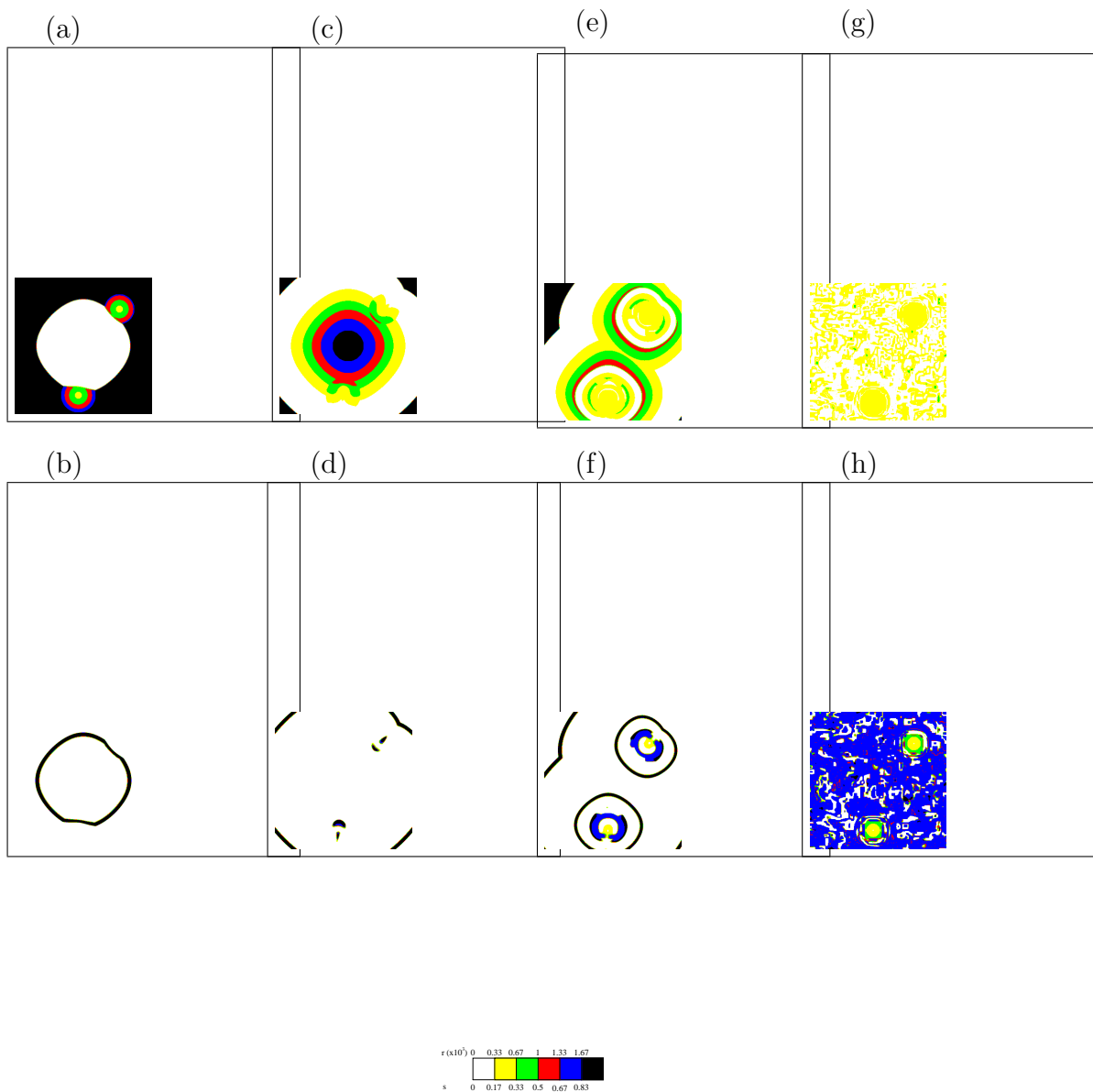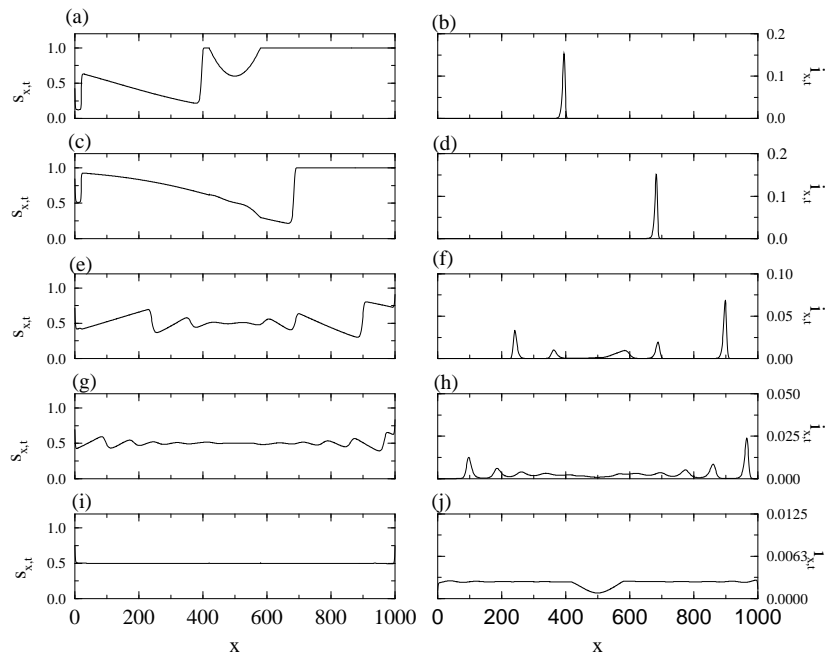
Figure 11.4: *3 stage epidemic model with two patches of low carrying capacity. Parameters are the same as in figure 11.3. (a) and (b) are snapshots of the susceptible and infective populations at time 5 years. (c) and (d) are snapshots of the susceptible and infective populations at time 12 years. (e) and (f) are snapshots of the susceptible and infective populations at time 27 years. (g) and (h) are snapshots of the susceptible and infective populations at time 137 years. The infectives spread out from the low carrying capacity patches.*

Figure 11.5: *2 stage epidemic model with patch of low carrying capacity in 1 dimension. $r = 0.01$, $b_0 = 2$, $i_P = 10^{-6}$, $\Delta t = 0.1$, $\Delta x = 1$, the unscaled carrying capacity is 2 and the minimum carrying capacity in the patch is 1.2. (a) and (b) are snapshots of the distribution of susceptibles and infectives respectively at time $t = 300$. (c) and (d) are snapshots of the distribution of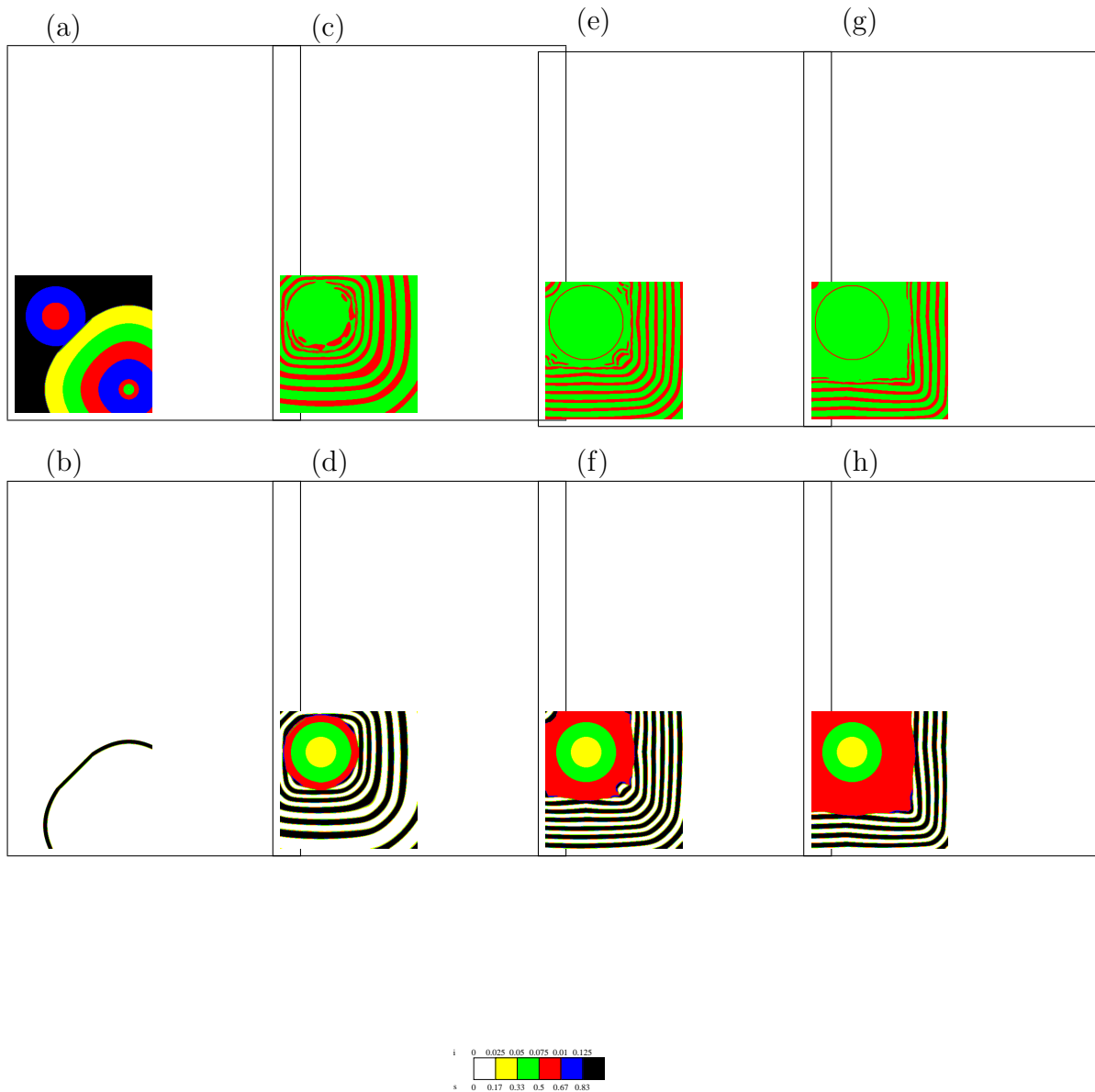 susceptibles and infectives respectively at time $t = 600$. (e) and (f) are snapshots of the distribution of susceptibles and infectives respectively at time $t = 900$. (g) and (h) are snapshots of the distribution of susceptibles and infectives respectively at time $t = 1200$. (i) and (j) are snapshots of the distribution of susceptibles and infectives respectively at time $t = 2000$.*

145

Figure 11.6: *2 stage epidemic with one patch of low carrying capacity in a 301×301 arena. The infectives are spreading out from the patch of low carrying capacity. $r = 0.01$, $b_0 = 2$, $i_P = 10^{-6}$, $\Delta t = 0.2$, $\Delta x = 4$, the unscaled carrying capacity is 2 and the minimum carrying capacity in the patch is 1.2. (a) and (b) are snapshots of the distribution of susceptibles and infectives respectively at time $t = 280$. (c) and (d) are snapshots of the distribution of susceptibles and infectives respectively at time $t = 4000$. (e) and (f) are snapshots of the distribution of susceptibles and infectives respectively at time $t = 7360$. (g) and (h) are snapshots of the distribution of susceptibles and infectives respectively at time $t = 12000$.*
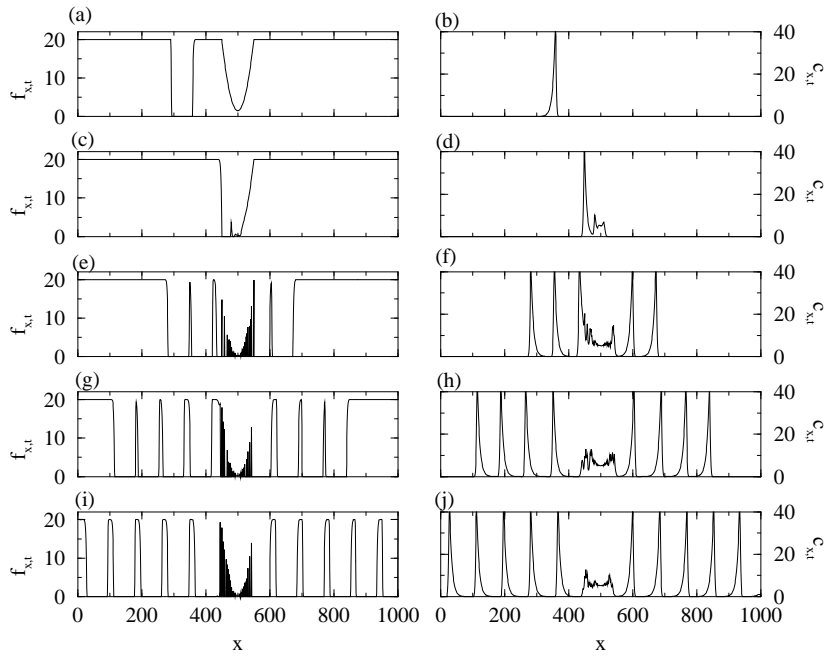
Figure 11.7: *Predator-prey model with patch of low carrying capacity in 1 dimension. $u_m = 0.2$, $d = 0.05$, $c_P = 0.1$, $\Delta t = 0.5$, $\Delta x = 2$, $k = 20$ and the minimum carrying capacity of the patch is 1.5. (a) and (b) are the snapshots of the prey and predators respectively at time $t = 1000$. (c) and (d) are the snapshots of the prey and predators respectively at time $t = 1500$. (e) and (f) are the snapshots of the prey and predators respectively at time $t = 2000$. (g) and (h) are the snapshots of the prey and predators respectively at time $t = 2500$. (i) and (j) are the snapshots of the prey and predators respectively at time $t = 4000$. Repeated solitons are produced from the patch of low carrying capacity.*

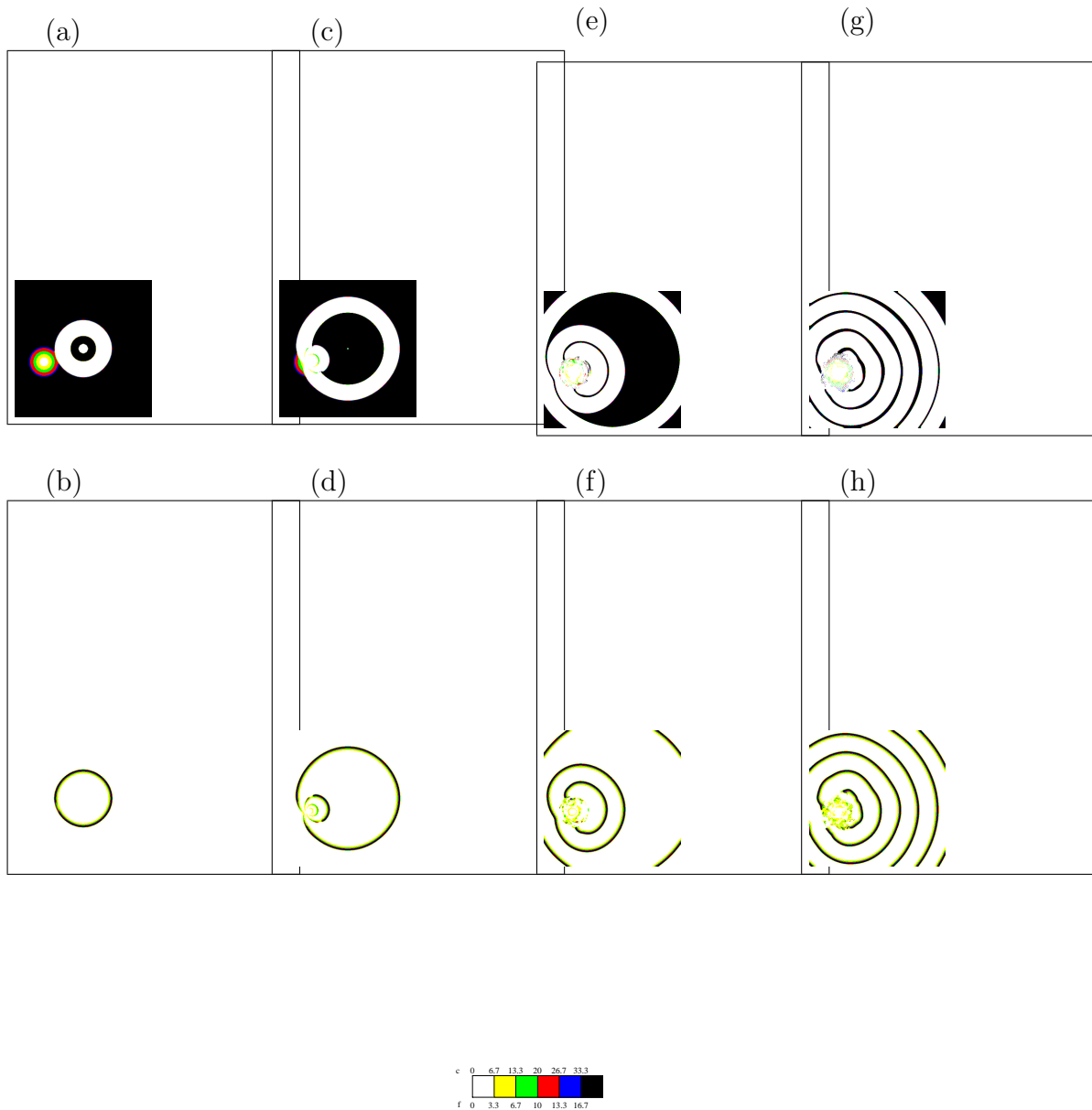Then a second patch of low carrying capacity to look at the interactions of the

Figure 11.8: *Predator-prey model with one patch of low carrying capacity in a 301 × 301 arena.* $u_m = 0.2$, $d = 0.05$, $c_P = 0.1$, $\Delta t = 0.5$, $\Delta x = 4$, $k = 20$ *and the minimum carrying capacity of the patch is* 1.5. *(a) and (b) are the snapshots of the prey and predators respectively at time* $t = 300$. *(c) and (d) are the snapshots of the prey and predators respectively at time* $t = 600$. *(e) and (f) are the snapshots of the prey and predators respectively at time* $t = 1000$. *(g) and (h) are the snapshots of the prey and predators respectively at time* $t = 1850$. *Repeated solitons are produced from the patch of low carrying capacity.*

repeating solitons (figure 11.9). When the solitons meet, there is interference and the solitons form figure 8s. As the patches are different sizes this also demonstrates that the effect is not sensitive to the size of the patch providing that the patch is over a critical size.

11.4   Discussion

Temporal heterogeneity , i.e. seasonality in a given parameter value only, created persistence of an epidemic behind the wave front in the case of the 3 stage rabies epidemic in 1 dimension. This result was sensitive to the space and time steps chosen for the simulation. This sensitivity is probably what caused the non-occurrence of the effect in the 2 dimensional model. To clarify the effect of seasonality, real parameter sets should be obtained for the 2 stage epidemic and predator prey models.

In the epidemic models a persistent, endemic state of the infection spreads out from patches of low carrying capacity. In the predator- prey model repeated solitons radiate out from the patches. The patches act as sources of infection/invasion. This result may have implications for epidemic and wildlife management.

The effects are not affected by the size of the patch, provided the patches are larger than a critical size. Multiple patches do not have any great affect either. So spatial heterogeneity acts as a robust mechanism which allows reinfection or reinvasion behind the original wave front.

In the predator-prey model, small scale patterns are formed. These small scale self-organised patterns have been investigated for predator-prey models by McLaughlin and Roughgarden (1991) McLaughlin and Roughgarden (1992) and more specifically for the predator-prey model used in this thesis by Gurney and Veitch (1998).
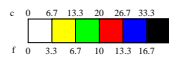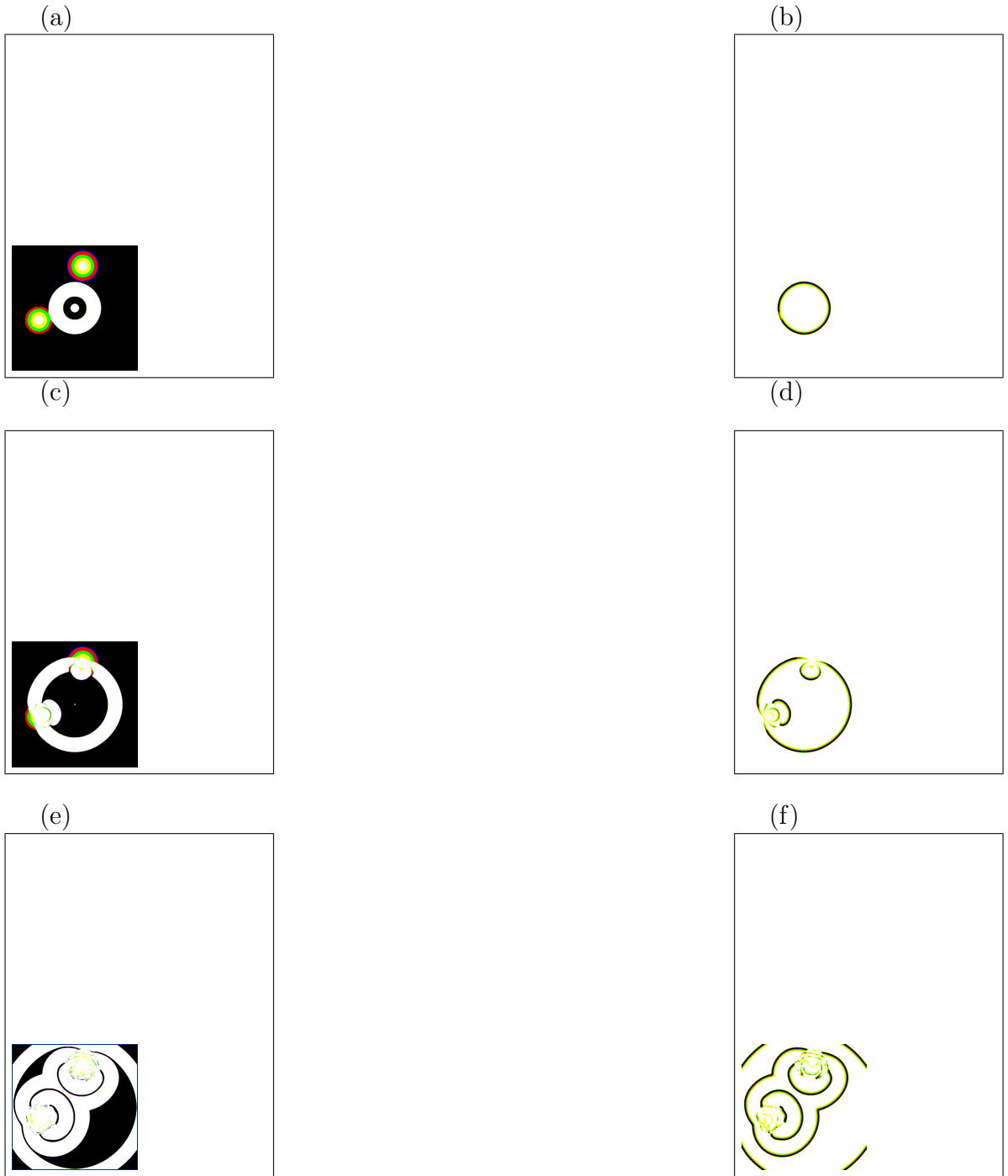
(a)

(b)

(c)

(d)

(e)

(f)

| c | 0 | 6.7 | 13.3 | 20 | 26.7 | 33.3 |
| f | 0 | 3.3 | 6.7 | 10 | 13.3 | 16.7 |

150

Figure 11.9: *Predator-prey with two patches of low carrying capacity in a* 301×301

Chapter 12

Long Range Dispersal

12.1   Introduction

In this chapter the long range dispersal of mobile individuals is investigated as a mechanism for allowing the establishment of an invading species or an epidemic to become endemic in systems where the initial wave front is a soliton (Gurney et al. 1998). This process involves a single individual moving a long distance with a higher probability than is suggested by diffusion. In the predator-prey model this may involve a pregnant or asexually reproducing organism settling away from the wave front. In the 2 stage epidemic model long range dispersal involves in infective individual travelling and after a period becoming too ill to move on and proceeding to infect susceptibles in the area it has settled in. In the 3 stage epidemic model, an incubating individual moves, becomes infective and starts to infect susceptibles locally.

In models with 1 spatial dimension the arena is infinitely thin. To identify an individual in an spatial model where density is the dependent variable, an area has to be found where

$$\text{area} \times \text{density} = 1 \ . \tag{12.1.1}$$

Area is not a property of a 1 dimensional arena, so to identify an individual, an arbitrary width would have to be attributed to the arena. If the migrating individual moves ahead of the front in a 1 dimensional arena, the new innoculum

will send a soliton both forwards and backwards (in relation to the movement of the initial wave front). The backwards moving soliton will collide with the original wave front and the mobile component of the system dies out locally. The wavefront immediately moves to the position of the forwards moving soliton created by the outlier. This greatly increases the velocity of the wave front. Because of these consequences of long range dispersal in 1 dimension, long range dispersal has only been investigated in 2 dimensional arenas in this chapter.

12.2   The Three Stage Epidemic Model

In this model, it is assumed that the susceptible and incubating populations are immobile in the sense that once adult, they have fixed territories. In the long range dispersal formulation, it is assumed that a proportion of young foxes, setting out to find a territory away from their families, are incubating rabies. If a fox is rabid, it is assumed that it sets off in a random direction, and after a short time it becomes infective and starts to infect the susceptibles foxes around it.

In the model, an incubating fox is chosen at random. This is done by picking an address in the arena by means of a random number generator. An edge of the arena (top, bottom, left or right) was then chosen randomly, then the transect between the address and the edge of the arena specified is scanned for a maximum density of incubating foxes. The direction of the scan (starting either at the edge of the arena or at the address) was also chosen at random. If a sizable (10^{-4}) incubating fox density is found, the immediate surroundings are searched for a fox; the nearest neighbour of highest density is the next looked at, then it's nearest neighbour of highest density, until a whole fox is found. Another random address is generated in the locality of the original position of the fox, and the incubating fox is removed from its original position to the new address, turning rabid during its journey. If a whole incubating fox is not found during the search, nothing happens.
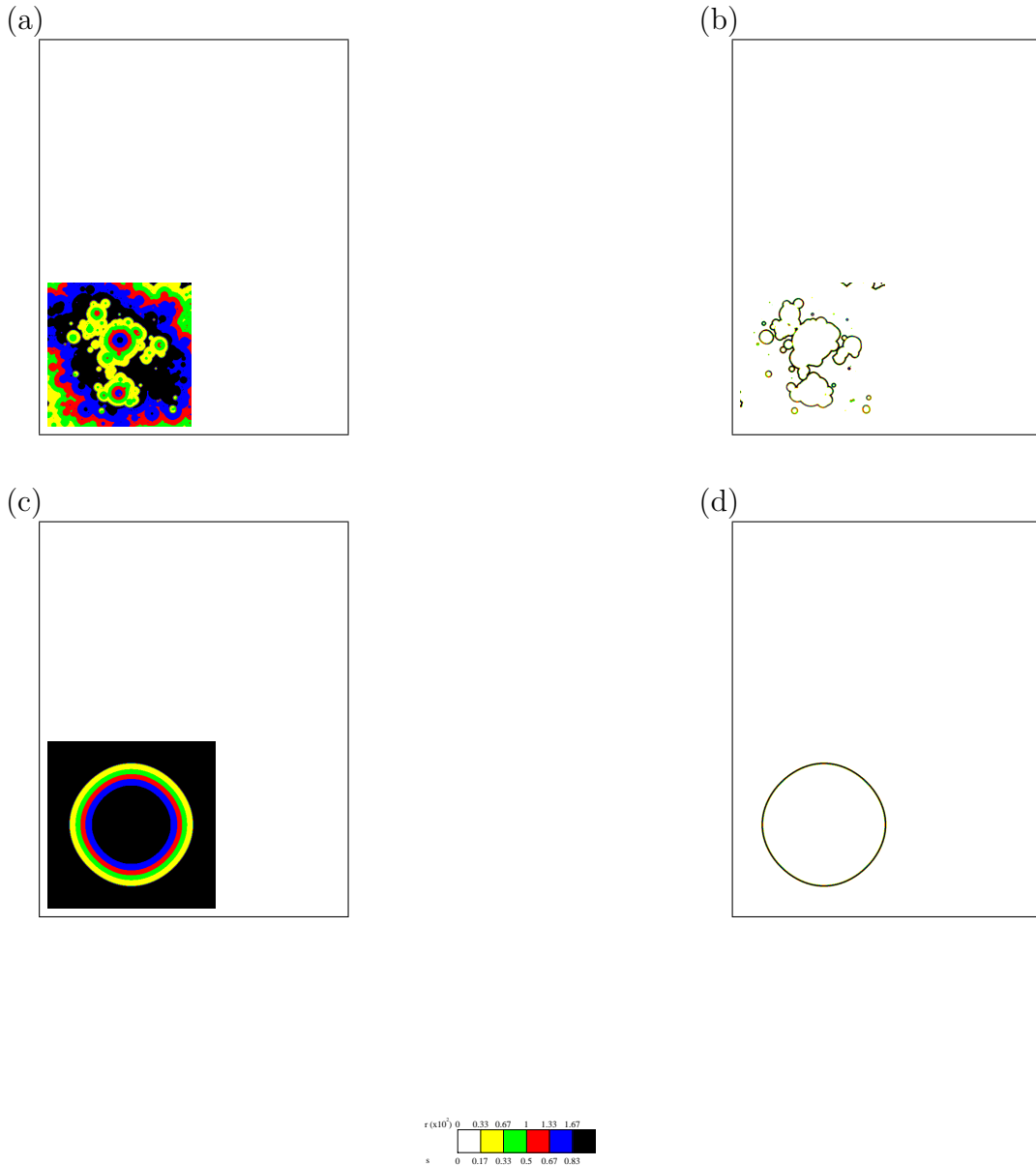
Figure 12.1: *(a) and (b) show the distribution of susceptibles and infectives respectively of the 3 stage epidemic model with long range dispersal, and (c) and (d) show the distribution of susceptibles and infectives respectively, of the 3 stage epidemic model with no long range dispersal, both at time 15 years in a 301×301 arena. $b_0 = 2.1$, $q = 0.006$, $l = 0.2$, $m = 0.006$, $r_P = 0.0001$, $\Psi = 150km^2yr^{-1}$, $\Delta t = 0.5$ and $\Delta x = 4$ in both models. In the model with long range dispersal, the maximum dispersal distance is 170km.*

Figure 12.1 (a) and (b) shows the distribution of the rabies epidemic after 15 years when long range dispersal of incubating foxes occurs.

If the fox moves ahead of the front, it starts a new circular wave. The section of the wave moving towards the original front causes interference with the section of front it meets, and the section of the new front moving in the same direction as the original becomes part of the original front. This only causes an increase in spatial distribution locally, so does not affect the front velocity greatly. The velocity of the front when there is no long range dispersal, as shown by figure 12.1 (c) and (d). The velocity of the circular wave is 36 km yr^{-1} and the velocity of the new wave is approximately 60 km yr^{-1}, so it is still within the observed range of $30 \rightarrow 60$ km yr^{-1}.

If the fox migrates behind the front 2 things can happen. The rabid fox can land in the region of susceptible depletion and the localised epidemic will die out. The fox can land on the region of susceptible regeneration and a new epidemic starts in the centre of the original epidemic. This repeats itself up to and over 100 years, shown by figure 12.2. Figure 12.3 shows that with no long range dispersal, the epidemic would die out within the arena after 20 years and the susceptibes return to carrying capacity within 25 years.

Obviously for the repeating epidemics to happen ,it is necessary for incubating foxes to migrate long enough distances that they can reach the area of susceptible recovery within the circle. Other than that there is a question of whether persistence of the rabies epidemic is sensitive to the maximum distance the foxes travel. Figure 12.4 (a) and (b) shows the same long range dispersal algorithm as describes above, but the distance the foxes can travel is greater. The result is still qualitatively the same as with the shorter maximum migration distance.

The algorithm as described above may have a bias as to the positions of foxes found. The the use of long range dispersal as a persistence mechanism may be dependent on the frequency of finding a whole incubating fox. To test the robustness of the mechanism to the algorithm and frequency of finding a fox, a slightly different algorithm is used to find the incubating fox. A line in either the

154

(a)

(b)

(c)

(d)

r (x10²) 0   0.33 0.67   1   1.33 1.67

s   0   0.17 0.33 0.5 0.67 0.83

Figure 12.2: *(a) and (b) show the distribution of susceptibles and infectives respectively of the 3 stage epidemic model with long range dispersal at time 50 years, and (c) and (d) show the distribution of susceptibles and infectives respectively of the same model at time 100 years. The parameters are the same as those in figure 12.1.*
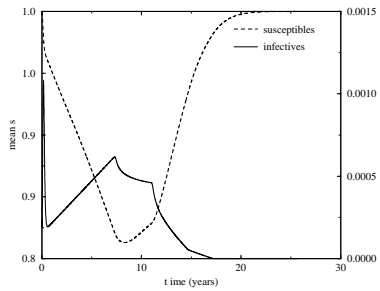
Figure 12.3: *Time series of the mean density of susceptibles and infectives in the arena. By time 20 years infectives no longer exist within the arena and by time 25 years the susceptibles have all reached their carrying capacity. The parameters are the same as those in figure 12.1.*

vertical or horizontal directions is chosen randomly. A start point and end point for a search along the line is then generated. The maximum density of incubating foxes is sought along the line, and if it is greater than 10^{-4}, a whole incubating fox is sought in the same manner as above. This alteration to the search algorithm reduces the frequency of finding an incubating fox as less of the chosen line is searched. Figure 12.4 (c) and (d) shows that this change in algorithm does not change the success of the persistence mechanism.

12.3   The Two Stage Epidemic Model

When thinking about using this model for rabies, having infective foxes dispersing long distances does not make biological sense. The 2 stage epidemic model is bloody useless as a rabies model; it does not account for the latent period before rabies is developed or that some foxes develop the paralytic form of the disease. In this chapter it is considered as a more general epidemic model. An infective is assumed to be healthy enough to travel long distances when it first contracts
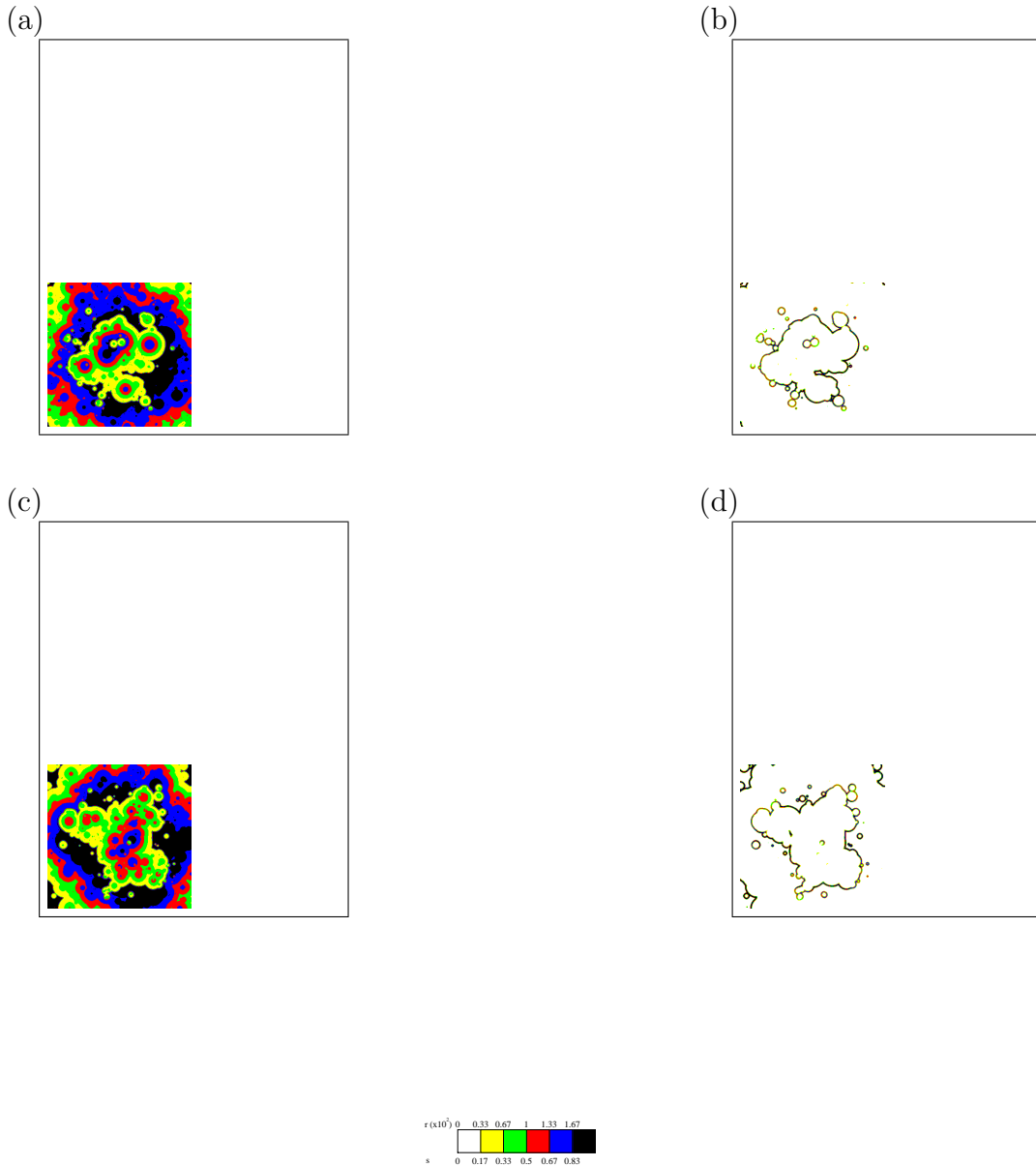
156

Figure 12.4: *(a) and (b) show the susceptible and infective distributions respectively of the 3 stage epidemic model with long range dispersal. Parameter values are as in figure 12.1 but the maximum dispersal distance is 200km. (c) and (d) show the susceptible and infective distributions respectively of the 3 stage epidemic model with long range dispersal in a 301×301 arena. Parameter values are as in figure 12.1 but the algorithm used to choose an incubating fox has been modified so that they disperse less frequently. All snapshots are taken at time 15 years.*
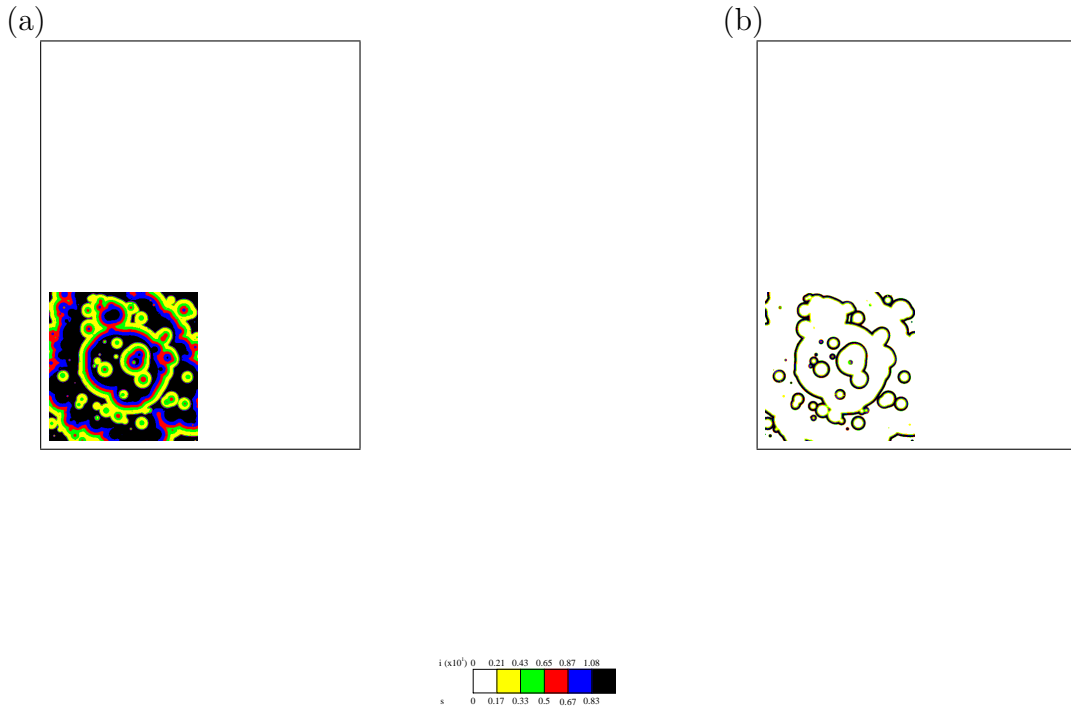
(a) (b)

Figure 12.5: *The 2 stage epidemic model with long range dispersal. (a) is a snapshot of the susceptible distribution and (b) is a snapshot of infective distribution at $t = 137$ in a 301×301 arena. $r = 0.1$, $i_P = 0.005$, $b_0 = 2.1$, $\Psi = 10$, $D = 10$, $\Delta t = 0.125$, $\Delta x = 2$ and the maximum dispersal distance is 30 space steps.*

the disease. After it has travelled a long distance, the infective stops and begins to infect susceptibles around it.

A whole infective is found in the same manner as the first algorithm described in the previous section. A random address within a certain distance of the infective's original position is generated, and the infective is moved to the new address.

Figure 12.5 shows that long range dispersal works as a mechanism for allowing an endemic state to be created behind the initial wave front.
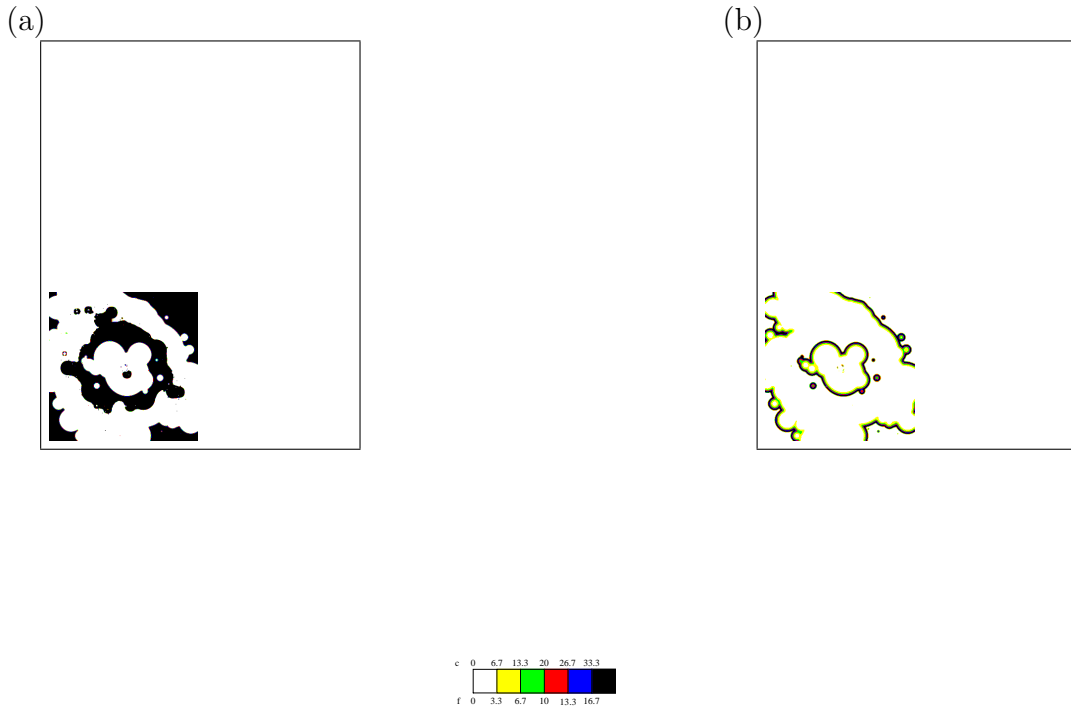
158

Figure 12.6: *Predator-prey model with long range dispersal. (a) is the prey distribution and (b) is the predator distribution at time $t = 548$ in a 301×301 arena. $k = 20$, $u_m = 0.2$, $d = 0.05$, $c_P = 0.1$, $R = 1$, $\Psi = 0.1$, $\Delta t = 0.5$, $\Delta x = 4$ and the maximum dispersal distance is 30 space steps.*

12.4 The Predator-Prey Model

In the predator prey model a predator migrates a distance longer than that associated with diffusion. A predator is chosen in the same manner as described for the incubating foxes in the 3 stage epidemic model. A random address within a finite distance is then generated and the predator is moved to the chosen address, where it establishes itself and starts to feed on the local prey.

Figure 12.6 shows that the predator prey model has the same pattern of new waves behind the front as the 3 stage epidemic model.

This has already been done (Gurney et al. 1998) for a very similar model with random immigration approximating long range dispersal. The pattern produced by random immigration is more broken than that due to long range dispersal. This is due to the limitation to the number of migrating predators to the number that exist within the arena.

12.5   Discussion

Long range dispersal of incubating or infective individuals permits repeated epidemic waves to form behind the initial epidemic front in the 2 and 3 stage epidemic models. Long range dispersal of predators in the predator prey model allows predators to establish behind the initial invasion front and create repeating invasion waves. The mechanism is robust to the maximum distance the given individual can disperse, the algorithm used to find the individual which disperses and the frequency of long range dispersal events. The resulting pattern is independent of new individuals immigrating into the arena.

The choice of parameters in the 2 stage epidemic and the predator-prey models was arbitrary, and the experiments should be repeated with real parameter sets.

Chapter 13

Spiral Waves

13.1   Introduction

It has already been demonstrated that the 3 models considered are able to form spiral waves. It has also been shown that spiral waves are a mechanism for continuing an epidemic or invasion behind the epidemic or invasion front. No spirals have been observed in ecological systems, so this chapter will consider a likely ecological mechanism for initiating a spiral wave. Gurney et al. (1998) showed that spirals propagated by the predator-prey model with a threshold were robust to random immigration and a very fine heterogeneous spatial patchwork, so this chapter will also investigate the robustness of spirals to the forms of long range dispersal and spatial heterogeneity as described in the previous 2 chapters and to interactions with other spirals.

13.2   Creating the "Assymetric Half Line" Initial Condition with an Environmental Process

A naturally occurring initial condition for a spiral is needed. If an invasion or epidemic wave is travelling at one side of the barrier, then the barrier disappears, allowing the wave to spread to new virgin territory, an assymetric half line initial
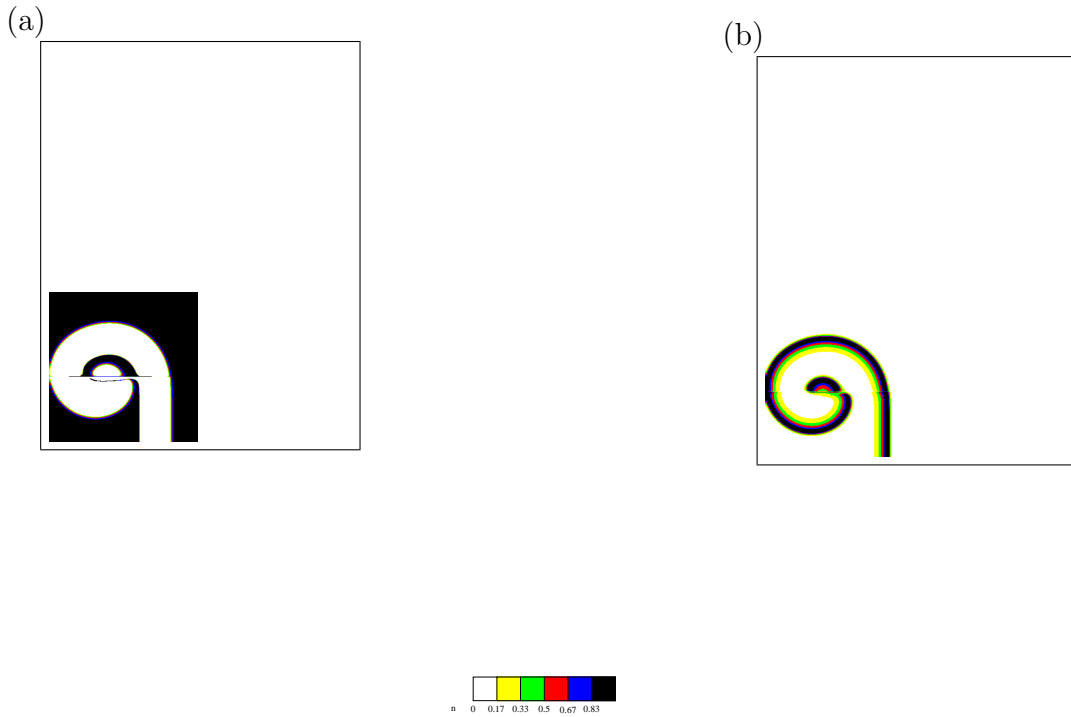
Figure 13.1: *Spiral waves formed from a periodic river initial condition. (a) and (b) are snapshots of the prey and predator distributions respectively of the predator-prey model at $t = 420$. $k = 10$, $u_m = 0.2$, $d = 0.05$, $c_P = 0.3$, $\Delta t = 0.5$ and $\Delta x = 1$ in a 301×301 arena.*

condition would be created. A likely candidate for this barrier is a river (G. Ruxton, pers. comm.). A river may be too wide and deep for the given organism to cross. A change in rainfall or temperature may reduce the flow of the river and it becomes traversable. Rivers can have seasonal cycles of flow. In this model it is assumed that the river is a barrier at the start of the run with the invasion or epidemic wave running along one bank, then when the environmental change occurs the river becomes periodic, so the river becomes traversable for part of each year. In the case of the simulations shown in figures 13.1, 13.2 and 13.3 the river becomes periodic when the wave front reaches the centre of the arena.
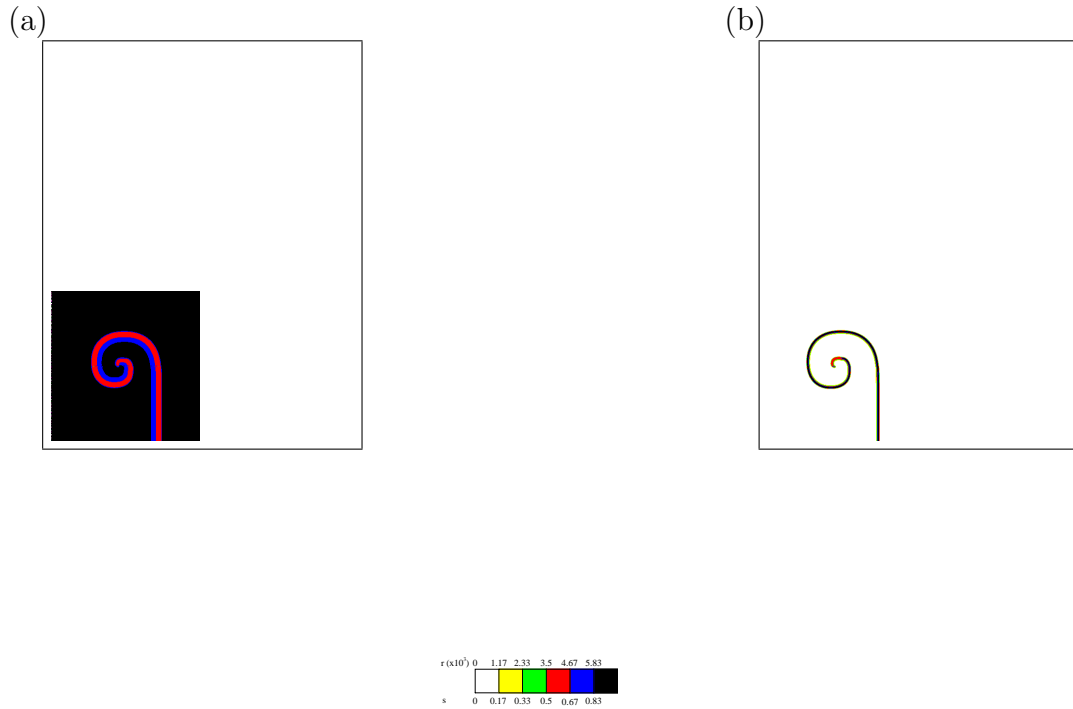
Figure 13.2: *Spiral waves formed from a periodic river initial condition. (a) and (b) are snapshots of susceptibles and infectives of the 3 stage epidemic model at time 43 years in a* $301 times 301$ *arena.* $b_0 = 1.5$, $q = 0.006$, $l = 0.2$, $m = 0.006$, $r_P = 0.001$, $\Delta t = 0.5$ *and* $\Delta x = 2$.

(a)

(b)

i (x10⁵) 0   0.21 0.43 0.65 0.87 1.08

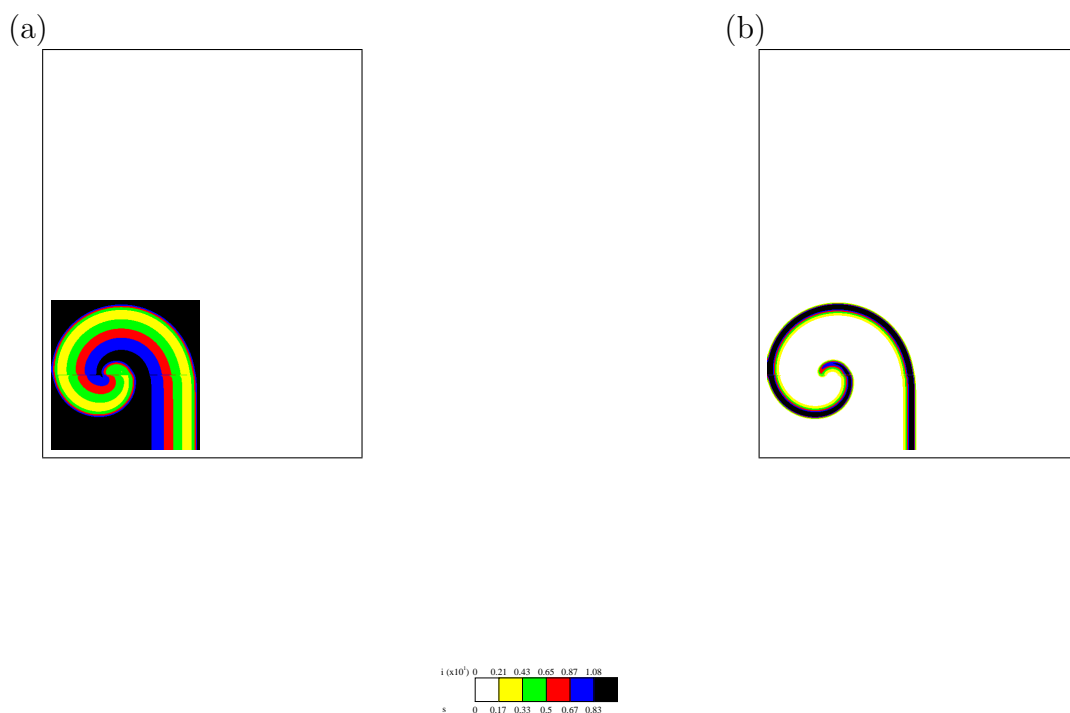s   0   0.17 0.33   0.5 0.67 0.83

Figure 13.3: *Spiral waves formed from a periodic river initial condition in a 301 × 301 arena. (a) and (b) are snapshots of susceptibles and infectives of the 2 stage epidemic model at $t = 100$. $b_0 = 2$, $r = 0.1$, $i_P = 0.01$, $\Delta t = 0.125$ and $\Delta x = 0.5$.*

Figures 13.1, 13.2 and 13.3 show that all 3 of the models form spirals with the assymetric half line initial condition created by a river acting as a barrier initially then altering so that there is less flow for a period each year. The spirals are slightly square in shape due to the periodicity of the river.

13.3 Robustness of Spirals to the Environment

Now that a plausible natural mechanism for forming a spiral is known, the robustness of spiral waves to intrinsic and environmental factors is examined. The river has not been included in the models tested for robustness; it is assumed that once formed the spirals are not different from artificially formed spirals.

13.3.1 Multiple Spirals

If it is possible for one spiral to form, it should be possible for more than one spiral to form. Two solitons meeting cancel each other out as there are regions of resource depletion behind both waves. This raises the question of whether 2 (or more) spirals cancel each other out. There are two situations to be considered; one where the spirals are turning in the same direction, and one where the spirals are turning in different directions.

Figure 13.4 (a) and (b) shows that when the spirals are turning in the same direction, as long as the cores of the spirals to not meet, the outer waves of the spirals combine to figure 8 shapes, with the cores continuing in the centre.

Figure 13.4 (a) and (b) shows that when the spirals are turning in different directions, the top of the spirals form half of the 8 shape, and the bottom of the left spiral becomes the bottom of the right spiral.

More than one spiral forming in a small arena does not compromise the integrity of the spiral waves.

(a)

(b)

(c)

(d)
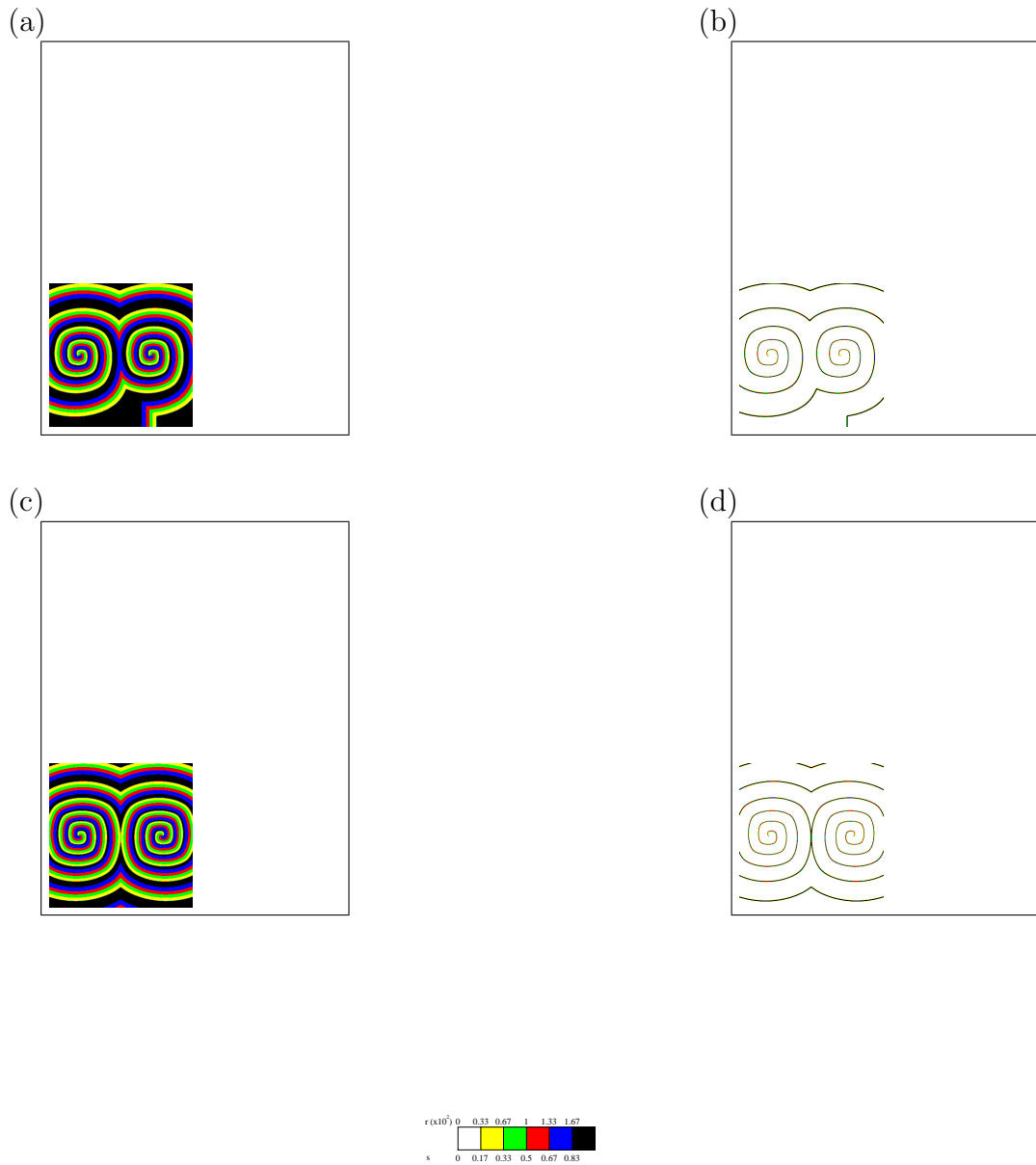
Figure 13.4: *Interactions between spirals in* 301×301 *arenas. The 3 stage epidemic model with* $q = 0.006$, $b_0 = 2.1$, $l = 0.2$, $m = 0.006$, $r_P = 0.001$, $\Delta t = 0.5$ *and* $\Delta x = 4$. *(a) and (b) show the susceptible and infective distributions at time 44 years with 2 spirals spinning in the same direction. (a) and (b) show the susceptible and infective distributions at time 58 years with 2 spirals spinning in opposite directions.*

13.3.2　Spatial Heterogeneity

In chapter 11, a patch of low carrying capacity acts as a source for reinvasion of the region behind a soliton wave front. If a spiral form in a spatially heterogeneous arena, do these reinvasions break the spiral up? This question is investigated for both the 3 stage epidemic model and the predator-prey model.

In the 3 stage epidemic model, a patch of low carrying capacity causes an area of the epidemic steady state to spread out from the patch, as shown by figure 13.5 (a) and (b). The spiral wave is broken up by this because there is not a region of susceptible depletion behind the secondary epidemic. In the predator-prey model, when the soliton waves radiating from the patch meet the spiral, there are regions of prey depletion behind the reinvasion wave and immediately behind the section of the spiral wave. Both waves die out. As long as the core is unaffected by this, the spiral continues with a diffraction pattern around the low carrying capacity patch.

13.3.3　Long Range Dispersal

The robustness of a spiral wave to the long range dispersal of incubating individuals in the 3 stage epidemic model as described in chapter 12 is tested. This has already been carried out for a predator-prey model by Gurney et al. (1998) with random immigration acting as an approximation of long rage dispersal. The spiral is allowed to form a core before the long range dispersal algorithm is applied.

Figure 13.6 shows that the spiral is robust to the long range dispersal of incubating foxes. In a spiral wave, if a fox lands on another part of the wave, the wave returns to its original shape. If it lands in a trough the susceptible population is too low to sustain a new invasion wave. Therefore long range dispersal does not break the spiral up.
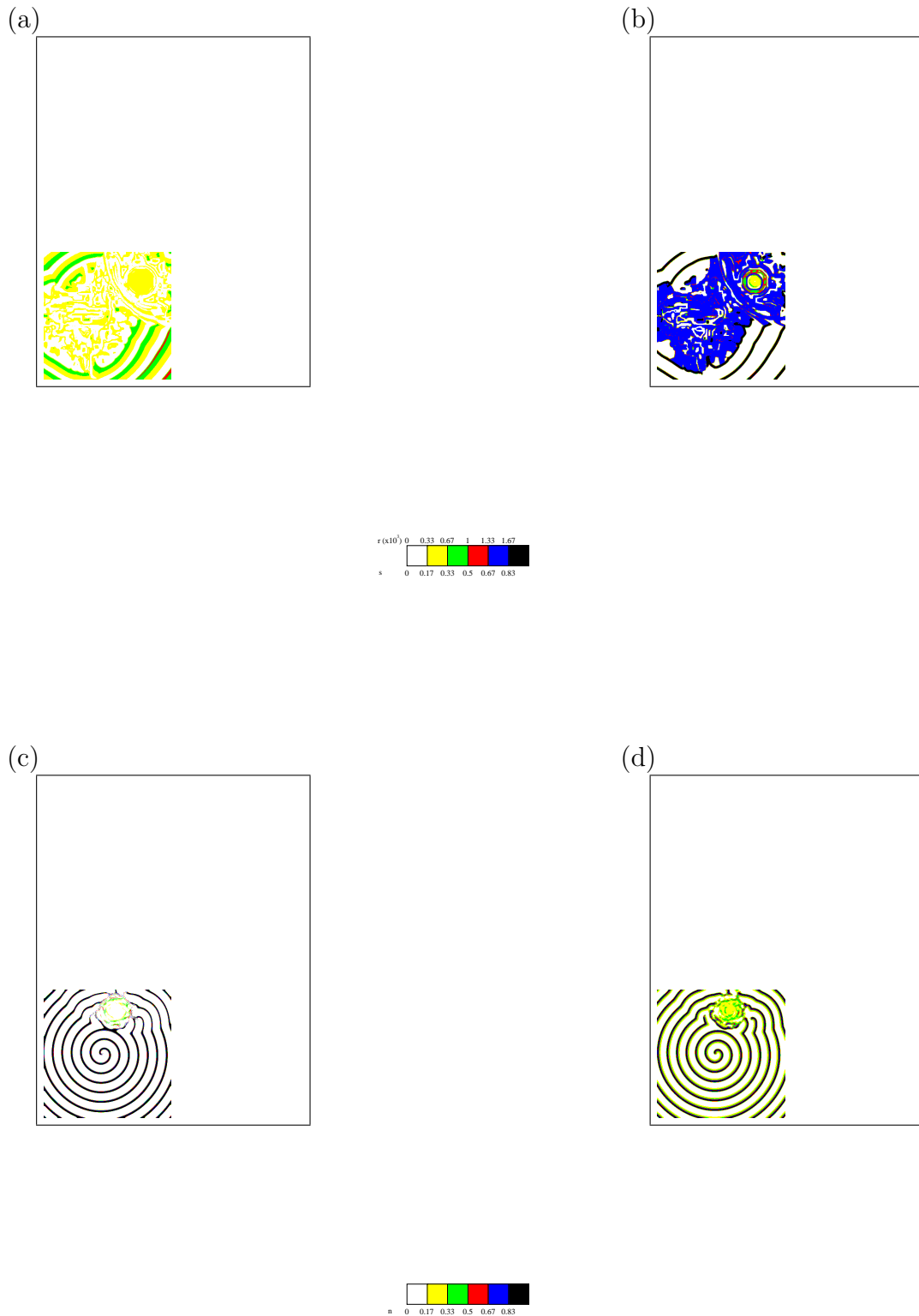
Figure 13.5: *Spiral waves in heterogeneous* 301×301 *arenas. (a) and (b) are the susceptible and infective distributions of the 3 stage epidemic model at time 68 years.* $B_0 = 80$, $Q = 0.5$, $D = 73$, $L = 13$, $M = 0.5$, $\Delta t = 0.5$, $\Delta x = 2$, $K = 4$ *and the lowest carrying capacity in the patch is* 1.2. *(c) and (d) are the prey and predator distributions of the predator-prey model at* $t = 4100$. $u_m = 0.2$,
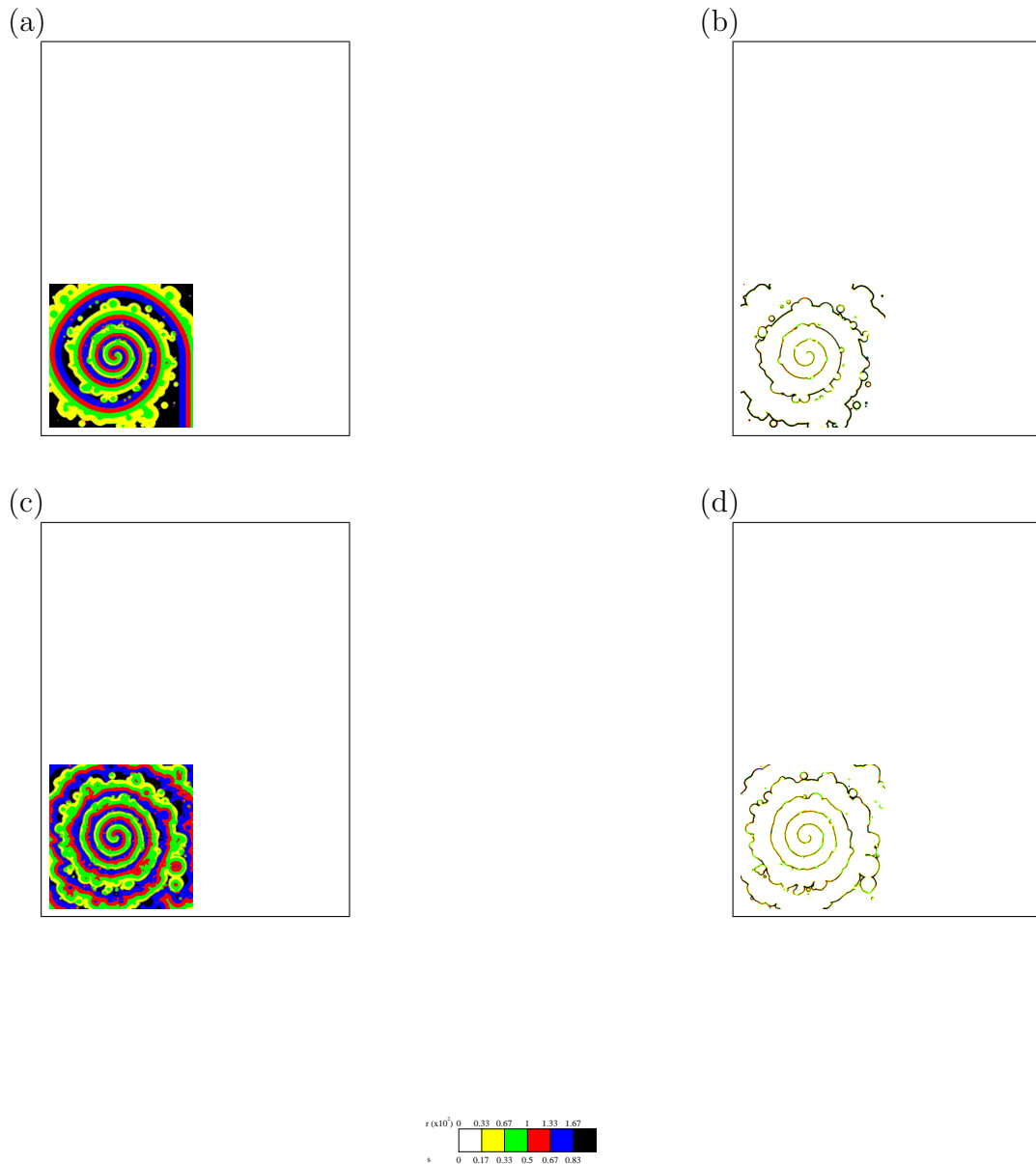
Figure 13.6: *Spiral wave formed by the 3 stage epidemic model with long range dispersal starting at time 41 years. (a) and (b) are the distributions of susceptibles and infectives at time 45 years and (c) and (d) are the distributions of susceptibles and infectives at time 61 years in a 301×301 arena. $b_0 = 2.1$, $q = 0.006$, $l = 0.2$, $m = 0.006$, $r_P = 0.0001$, $\Delta t = 0.5$, $\Delta x = 4$, and the maximum dispersal distance is 170km.*

13.4   Discussion

There are plausible natural phenomena that might give rise to spirals, in this case a river which fluctuates periodically. The length of a year in the 2 stage epidemic and predator prey models was chosen arbitrarily and these simulations should be run again with parameters observed from nature.

The spiral waves produced by the 3 stage epidemic model are robust to interactions with other spiral waves and long range dispersal. The predator prey spiral wave is robust to the presence of a patch of low carrying capacity as long as the core is unaffected. The epidemic spiral wave is not robust to the presence of a patch of low carrying capacity because the steady state manages to spread out through the spiral.

All that remains is for a spiral to be observed in a population other than a laboratory culture (Rohani et al. 1997).

Part IV

Discussion

Chapter 14

Discussion

14.1 Thresholds and Allee Effects

Mollison's atto-individual effect has been effectively removed from the original reaction-diffusion models by adding thresholds and Allee effects. At low densities deterministic models do not act as an average of stochastic realizations, since at low densities stochastic effects are much more important to population dynamics that at high densities (Rand and Wilson 1991). At high densities deterministic models act as approximations of stochastic models. So, if the dynamics of unrealistically low density populations are altered so that they can no longer increase in reaction-diffusion models, but the dynamics of the high density populations are preserved, the deterministic model should become an approximation of the stochastic model.

A demonstration of the importance of atto-individuals in reaction-diffusion models is the formation of soliton waves in the multi component models. In the unstable case of the predator prey model, a wave train forms behind the wave front. In the oscillatory case of the 2 and 3 stage epidemic models, there is a series of damped oscillations behind the wave front. If the growth of populations at low densities is the same as that of high density populations, the growth of the small populations in the first trough behind the wave front creates the wake behind the front. Remove the regrowth of these low density populations, and

there is no wake - the wave front becomes a soliton and the invasion or epidemic dies out behind the front. This behaviour has important consequences for the spreading population and needs careful investigation.

14.2   Analysis of Wavefronts

The wave fronts of the original, unmodified reaction-diffusion models with no threshold or Allee effect can be analysed (Fisher 1937) (Kolmogorov et al. 1937) (Dunbar 1983) (Dunbar 1984) (Murray et al. 1986) (Murray 1989). The threshold or Allee effect slows the wave down, and makes the front narrower, so a new method must be found to analyse these wave fronts.

Brunet and Derrida (1997) devised a calculation for the velocity of the Fisher model with a cutoff. The calculation correctly predicted the velocities of Fisher wave fronts with low thresholds, but the calculation does not work at high thresholds. The below threshold per capita mortality rate is not included in the calculation. The cutoff formulation used by Brunet and Derrida cannot be simulated by a continuous time model. Therefore this calculation was not considered useful in this context.

In the predator-prey model with a threshold, it is assumed that a soliton wave front velocity is only minimally effected by the threshold due to a careful choice of parameters (Gurney et al. 1998). The velocity calculation of Dunbar can then be used to predict the width of the wave front and the velocity. It is then assumed that the prey nearly die out behind the wave front. This assumption allows the prediction of the width of the soliton, the height of the soliton and the width of the region of prey depletion. This method cannot be extended to the epidemic models as in epidemics, the susceptible population rarely falls to near zero.

A single component model - the Fisher model - was chosen to develop a method of predicting the characteristics of wave fronts which don't have regrowth from low densities. This model does not form solitons when a threshold or Allee effect is applied, but is used as an easily understandable vehicle.

The method devised, termed the Shooting method (Cruickshank et al. 1998), involves transforming the model into a moving frame of reference, reducing the number of variables the population depends on from 2 to 1. This simplifies the model further. A bisection search was developed to find the correct velocity of the wave front by searching for the frame of reference velocity which was equal to it. This was possible due to the behaviour of the transformed model; if the frame of reference velocity is greater than the wave front velocity the trajectory of the solution eventually reaches infinity and if the frame of reference velocity is less than the wave front velocity the trajectory dips below zero before increasing to ∞. The closer the frame of reference velocity is to the wave front velocity the further the trajectory of the solution follows the shape of the wave front in the untransformed model (Brunet and Derrida 1997) (Kessler and Levine 1989). The wave front velocity is never found exactly, but can be found to arbitrarily high accuracy. If the velocity is known, the shape of the wave front can be traced and characteristics such as the wave front width can be estimated.

The Shooting method was applied to 3 formulations of the Fisher model with no regrowth at low densities. When the growth function of the model was completely continuous, with an Allee effect achieved by Michaelis-Menten like growth, the Shooting method estimates were correct to arbitrary accuracy. Unfortunately, this model did not have the same dynamics as the Fisher model at high densities. When the growth function was discontinuous, either by the addition of a threshold to the model or by making mortality linearly dependent on density at low densities, there were errors created in the simulations by the numerical integration process. Once it was confirmed that a working method of estimating wave front characteristics of a model with no regrowth from low densities had been developed, it was investigated whether it could be applied to the multi-component models.

The Shooting method was then applied to 2 formulations of the predator-prey model with no regrowth of the predator at low population densities. In the threshold formulation, the Shooting method worked well. In the multi component models the height of the peak of the wave front can also be predicted by the

Shooting method. The velocity, peak height and front width can all be substituted into the calculations for estimating the width of the peak and the region of prey regeneration developed by Gurney et al. (1998). The Shooting method also worked well for the Allee effect formulation.

Next, the Shooting method was adapted to 2 formulations of the 2 stage epidemic model with no reinfection at low densities. It worked well at making predictions about the threshold formulation; as in the single component model the transformed model was solved with the initial population density at the threshold, so the only error occurred in the simulations. The Shooting method also worked for the formulations which were continuous in value but not in slope.

The Shooting method was then applied to 2 formulations of the 3 stage epidemic model with no reinfection at low densities. The method worked well for both formulations.

In these models, it was decided that the formulations which are continuous in slope and not in value, which were simulated more accurately by the adaptive timestep RK4 numerical integration algorithm, should become our formulations of choice for the remainder of the thesis.

14.3   Discrete Models

Now that predictions can be made about the wave front characteristics of 1 dimensional continuous models, the next step in investigating the systems where solitons formed was finding formulations of the models which were faster and easier to run simulations. The forms chosen were discrete analogues of the reaction-diffusion models.

It was important that the discrete models did not show behaviours which were not observed in the continuous models and that the models were predictable in some way.

A distribution kernel, based on capture-mark-recapture experiments, where dis-

persal probability fell linearly with distance from point of origin, was chosen.

At first a model which was a piecewise-constant approximation of the Fisher model with an Allee effect was investigated. A calculation, adapted from Kot et al. (1996)'s work, was developed to predict the velocity of the wave front.

This method was then applied to the discrete Fisher model with an Allee effect. The method only worked well when the Fisher model was forced to behave like the piecewise-constant approximation. It did not make any prediction about the shape of the wave. The calculation produced 2 roots, and it was not always obvious which should be chosen.

It was shown that for a range of smallish time and space steps the Shooting method made good predictions about the Fisher wave front characteristics. The Shooting method worked well for a range of parameter values. This was also shown to be true for discrete formulations of the multi-component models. One problem occurred as the value of threshold which creates a soliton wave in the predator prey model increases at large time and space steps.

These discrete analogues of the reaction-diffusion models were extended into 2 dimensional arenas. Circular waves were initiated from a compact point innoculum in all 4 models. In the Fisher model with an Allee effect the wave front spread outwards from the innoculum at then same rate in all directions. Behind the wave front the populations were at carrying capacity. When the wave front reached the edge of the arena, the arena remained at carrying capacity. In the multi-component models, when the wave was a soliton, the wavefront spread outwards at the same velocity from the innoculum. Behind the front the resource component was exhausted by the mobile component, but eventually regrew to the carrying capacity and the spreading component died out. When the wave front reached the edge of the arena the spreading components were reflected back into the region of resource depletion and died out. Eventually the arena reached a state when all the resource component was at carrying capacity and the spreading component had died out.

Circular wave characteristics are similar to the characteristics of the 1 dimensional

176

models and can be estimated by the Shooting method to around 10%.

Spiral waves were then considered. These only occur in systems where there are soliton waves. The spirals were initiated from an assymetric half line initial condition; a plane wave travelling from left to right across the arena is halved so the top half of the arena is reinitialised with the resource component at carrying capacity and no spreading component. The space step had to be increased in some cases to allow a complete spiral to form. The Shooting method also managed to predict the shape and velocity of the spiral waves to within 10%.

Discrete models in 1 and 2 dimensions have been formulated as approximations of the continuous models. These models have been shown to be predictable by the Shooting method, either exactly, or, as in the case of spiral waves, the scale can be predicted. Now these models can be used to investigate mechanisms which would allow the persistence of the spreading species behind soliton wave fronts.

14.4   Persistence behind the Front

14.4.1   Environmental Heterogeneity

Spatial heterogeneity worked as a method of allowing epidemics and invasions to persist behind soliton wave fronts. The populations within the low carrying capacity patches had less oscillatory dynamics than in the rest of the arena and allow the invading species or epidemic to established. These patches then acted as sources of the epidemic or invading species within the arena. In the case of the predator prey model persistence was in the form of repeating solitons radiating out from the patches. In the epidemic models a persistent endemic state of the spread out from the patches (the coexistence steady state in the case of the 2 stage model and a complex, so far unexplained in the 3 stage model). These effects happened as long as the patches were larger than a critical size. The ability of patches of low carrying capacity to act as local sources of an epidemic or invading species has implications for management.

The presence of patches produces small scale self organised patterns within a reasonable arena size; this is described in detail by Gurney and Veitch (1998).

A seasonal variation in contact rate is known to alter the dynamics of measles models (London and Yorke 1973). European foxes have seasonal contact rates. In the epidemic models in this thesis a seasonal contact rate added to the models to try and create a time each year when the dynamics are less oscillatory. In the predator prey model the conversion rate is made oscillatory. The only model in which the inclusion of seasonal effects created the persistence of the epidemic or invasion behind the wave front is the 1 dimensional 3 stage epidemic model. The effect was dependent on time and space steps chosen but not on the amplitude of the seasonal variation. This sensitivity to size and time steps is thought to be the reason the same effect was not repeated in the 2 dimensional model. The waves of the other models slowed down and widened in response to the seasonal term, but persistence was not produced.

14.4.2   Long Range Dispersal

Long range dispersal, dispersal of longer distances than are associated with diffusion, allows the epidemic or invasion to persist behind the initial wave front. In the 3 stage epidemic model long range dispersal was of the form of young incubating individuals dispersing to find a territory as an adult, and then becoming infective. In the 2 stage epidemic it was of the form of an infective individual travelling while still relatively healthy. In the predator prey model a predator travelled a long distance. The frequency of the long distance dispersal events was dictated by the success of the individual finding algorithm, so increased with arena population. If , by dispersal, predators or infectives become established in the region of resource recovery behind the wave front, new wave fronts form behind the original, so repeating waves pulse through the arena. This effect is robust to changing the distance the individual moves (as long as it can jump over the region of resource depletion behind the wave front), the frequency of event and changing the algorithm for finding whole individuals.

14.4.3 Spiral Waves

It is already known that spiral waves form in the threshold or Allee effect formulations of epidemic and predator prey model. The interest of spiral waves in an ecological context is whether spirals can be formed by a natural process and whether they can withstand the rigours of environmental and individual variability. A river which cannot be crossed, acting as a barrier while a wave front travelled along one side of it, becoming periodically crossable (G. Ruxton, pers. comm.), is a possible mechanism for forming a spiral in an ecological context. It formed spirals in all three models. Spiral formation is not sensitive to the length of the yearly cycle the river is periodic (over a critical length). The spirals are robust to spatial heterogeneity if solitons are emitted by the patch, as in the predator-prey model, but not if a wave front with a wake is spreading out from the patch, as in the 3 stage epidemic model. Spirals maintain their integrity while interacting provided the cores are not affected. Long range dispersal does not affect spiral waves as the dispersing individual either lands on the wave itself or in a trough, neither outcome altering the spiral dynamics.

14.5   Conclusions

The aim of this thesis was to remove a biological inaccuracy from some reaction-diffusion models which represent ecological epidemics and invasions. The feature to remove from the reaction-diffusion models is the ability for tiny populations to grow as large populations do. This was removed from the models by the addition of a threshold or an Allee effect, allowing no growth below a certain density. It was important that there was some way to predict the dynamics of the systems of the models. A semi-numerical method, the Shooting method, was then devised to make these predictions. The success of the Shooting method was only compromised by the limitations of the numerical integration method used to deal with discontinuities in the growth function.

This initial success threw up another problem to be solved; in models that had

oscillatory dynamics in the wake behind the wave front or limit cycles, if the trough behind the wave front dipped to densities near those of the threshold, the wave died pit behind the front, leaving a soliton wave. Although this may occasionally occur in ecological systems, it is far from usual. So mechanisms which would allow establishment of the invasion or epidemic behind the front were looked for.

Both intrinsic and extrinsic factors were considered. Mobile individuals may occasionally travel distances longer than those associated with diffusion. Spatial inhomogeneities may cause formation of persisting patterns or local sources for the invasion or epidemic. There may be seasonality in the contact or reproductive rates of the species concerned. All these ideas had some success at helping establishment of the invasion or epidemic behind the wave front.

So the result of this work is that the models have been modified to be more biologically realistic in two ways; by removing regrowth from low densities and adding individual and environmental heterogeneities.

14.6 Further Work

Time has not permitted certain questions raised by this work to have been fully investigated.

The reaction-diffusion models with no regrowth from low densities are hopefully good approximations of stochastic models. The next step is to formulate stochastic models to allow a direct comparison.

The initial innoculum in every simulation had to be large enough to spread out without falling beneath the threshold. The relationship between the initial conditions and the thresholds should be worked out, as this has implications both for releasing locally extinct species and controlling pest species and epidemics. Knowing the minimum size and shape the innoculum has to be to be successful would also save computer time as some simulations of high threshold systems have to be repeated to find the minimum innoculum.

Inaccuracies in the Shooting method are laid at the door of the numerical integration package used to simulate the models. A program should be found or developed which restricts the length of time steps so that the discontinuity is not over stepped in either the simulations of the original or the transformed models. Such a program would be very computationally intensive and would take a very long time to run simulations, but is necessary to simulate models with discontinuities in value or slope.

In all the models considered in this thesis, only one component is mobile. This is unrealistic in many systems. The properties of wave fronts in systems where more than one component is mobile should be considered in a similar way to those in the thesis.

Predicting the threshold value which turns a wave train or wave front with a wake into a soliton has not been investigated in this thesis. An attempt was made for the predator-prey model by (Gurney et al. 1998), but this was based on many assumptions which do not always hold, even for the model it was devised for. A bisection search could be written but would not be insightful into the processes dictating this change in behaviour.

The critical patch size and shape has not fully been investigated in the models with spatial heterogeneity. The critical period of time the river has to be crossable to allow a spiral should also be investigated.

The spatially heterogeneous 3 stage epidemic model shows that patches of reduced carrying capacity of susceptibles help the epidemic to persist behind the wave front. If a 4 stage epidemic model were used, would vaccination in patches create the same pattern?

One problem encountered while investigating the affects of long range dispersal, spiral formation and seasonality on the predator-prey an 2 stage epidemic models was that the choice of spatial and temporal scales was arbitrary. This may mean that observed effects are artifacts of unrealistic parameterisation. The work investigating persistence mechanisms for the 2 stage epidemic and predator-prey models should be repeated with real parameter sets.

In the last part, patterns were formed which were claimed to be possible results of individual and environmental heterogeneities. If these patterns are to be looked for in the environment, methods should be found to identify these patterns.

Bibliography

Allee, W. (1938). *The Social Life of Animals.* W.W. Norton and Co, New York.

Anderson, R., H. Jackson, R. May, and A. Smith (1981). Population dynamics of fox rabies in europe. *Nature 289*, 765–771.

Brunet, A. and B. Derrida (1997). Shift in the velocity of a front due to a cutoff. *Physical Review E 56*(3), 2597–2604.

Bryant, H. (1915). Sea otters nea point sur. *Calif. Fish Game 1*(3), 134–135.

Comins, H., M. Hassell, and R. May (1992). The spatial dynamics of host-parasitoid systems. *J. Anim. Ecol. 61*, 735–748.

Cruickshank, I., W. Gurney, and A. Veitch (1998). The characteristics of epidemics and invasions with thresholds. *submitted to theor. pop. Biol.*.

Dunbar, S. (1983). Travelling wave solutions of diffusive lotka-volterra equations. *Journal of Mathematical Biology 17*, 11–32.

Dunbar, S. (1984). Travelling wave solutions of diffusive lotka-volterra equations: a heteroclinic connection in $\mathbf{r}^4$. *Transactions of the American Mathematical Society 286*(2), 557–594.

Fahrig, L. (1992). Relative importance of spatial and temporal scales in a patchy environment. *Theor. Pop. Biol. 41*, 300–314.

Fisher, R. (1937). The wave of advance of advantageous genes. *Ann. Eugenics. 7*, 353–369.

Gilpin, M. (1972). Enriched predator-prey systems: Theroetical stability. *Science 177*, 902–904.

Gurney, W. and R. Nisbet (1998). *Ecological Dynamics.* Oxford University Press.

Gurney, W. and A. Veitch (1998). Self-organisation, scale and stability in a spatial predator-prey interaction. *submitted to Ecology.*

Gurney, W., A. Veitch, I. Cruickshank, and G. McGeachin (1998). Circles and spirals: Population persistence in a spatially explicit predator-prey model. *Ecology, in press.*

Hadeler, K. and F. Rothe (1975). Travelling fronts in nonlinear diffusion equations. *J. Math. Biol. 2*, 251–263.

Hanski, I. (1994). Spatial scale, patchiness and population dynamics on land. *Phil. Trans. R. Soc. Lond. B 343*, 19–25.

Hassell, M., H. Comins, and R. May (1991). Spatial structure and chaos in insect population dynamics. *Nature 353*, 255–258.

Hassell, M., H. Comins, and R. May (1994). Species coexistence and self-organizing spatial dynamics. *Nature 370*, 290–292.

Källén, A., P. Arcuri, and J. Murray (1985). A simple model for the spatial spread and control of rabies. *J. Theor. Biol. 116*, 377–393.

Keener, J. and J. Tyson (1986). Spiral waves in the belousov-zhabotinski reaction. *Physica D 21*, 307–324.

Kessler, D. and H. Levine (1989). Effect of diffusion on patterns in excitable belousov-zhabotinskii systems. *Physica D 39*(1), 1–14.

Kessler, D. and H. Levine (1998). Fluctuation-induced diffusive instabilities. *Nature 394*, 556–558.

Kolmogorov, A., I. Petrovsky, and N. Piscounov (1937). Etude de l'equation de la diffusion avec croissance de la quantite de matiere et son application a un probleme biologique. *Moscow Universitat Bull. Math. 1*, 1–25.

Kot, M., M. Lewis, and P. van den Dreissche (1996). Dispersal data and the spread of invading organisms. *Ecology 77*(7), 2027–2042.

Levin, S. (1974). Dispersion and population interactions. *Amer. Nat. 108*(960), 207–228.

Lewis, M. and P. Karieva (1993). Allee dynamics and the spread of invading organsims. *Theor. Pop. Biol. 43*, 141–158.

Lloyd, A. and R. May (1996). Spatial heterogeneity in epidemic models. *J. theor. Biol 179*, 1–11.

London, W. and J. Yorke (1973). Recurrent outbreaks of measles, chickenpox and mumps. i. seasonal variation in contact rates. *Am. J.Epidemiol. 98*, 453–468.

Lubina, J. and S. Levin (1988). The spread of reinvading species: range expansion in the california sea otter. *Am. Nat. 131*, 526–543.

Macdonald, D. (1980). *Rabies and Wildlife: a biologist's perspective.* OUP, Oxford.

McLaughlin, J. and J. Roughgarden (1991). Pattern and stability in predator-prey communities:how diffusion in spatially variable environments affects the lotka-volterra model. *Theor. Pop. Biol. 40*, 148–172.

McLaughlin, J. and J. Roughgarden (1992). Predation across spatial scales in heterogeneous environments. *Theor. Pop. Biol. 41*, 277–299.

Mollison, D. (1977). Spatial contact models for ecological and epidemic spread. *R. Statist. Soc. B. 39*(3), 283–326.

Mollison, D. (1991). Dependence of epidemic and population velocities on basic parameters. *Mathematical Biosciences 107*, 255–287.

Murray, J. (1987). Modeling the spread of rabies. *Sci. Am. 75*, 280–285.

Murray, J. (1989). *Mathematical Biology*, Chapter 11, pp. 274–310. Springer-Verlag.

Murray, J., E. Stanley, and D. Brown (1986). On the spatial spread of rabies among foxes. *Proc. R. Soc. Lond. B 229*, 111–150.

Nisbet, R. and W. Gurney (1982). *Modelling Fluctuating Populations*, Chapter 2, pp. 19–61. John Wiley and Sons.

Peterson, R. and M. Odemar (1969). Population growth of the sea otter in california: results of serial cencuses abd behavioral studies. In *Proc. Annu. Conf. Biol. Sonar Diving Mamm.*, Number 6, pp. 69–72.

Rand, D. and H. Wilson (1991). Chaotic stochasticity: a ubiquitous source of unpredictability in epidemics. *Proc. R. Soc. Lond. B 246*, 179–184.

Renshaw, E. (1991). *Modelling Biological Populations in Space and Time*. Cambridge University Press.

Rohani, P., T. Lewis, D. Grünbaum, and G. Ruxton (1997). Spatial self-organisation in ecology: pretty patterns or robust reality? *TREE 12*(2), 70–74.

Rosenzweig, M. (1971). Paradox of enrichment: Destabilization of exploitation ecosystems in ecological time. *Science 171*, 385–387.

Rosenzweig, M. and R. MacArthur (1963). Graphical representation and stability conditions of predator-prey interactions. *Amer. Natur. 97*, 209–223.

Ruxton, G. and P. Rohani (1996). The consequenses of stochasticity for self-organised spatial dynamics, persistence and coexistence in spatially extended host-parasitoid communitites. *Proc. R. Soc. Lond. B 263*(1370), 625–631.

Scheffer, M. and R. de Boer (1995). Implications of spatial heterogeneity for the paradox of enrichment. *Ecology 76*(7), 2270–2277.

Seno, H. (1991). Predator's invasion into an isolated patch with spatially heterogeneous prey distribution. *Bulletin of Mathematical Biology 53*(4), 557–577.

Skellam, J. (1951). Random dispersal in theoretical populations. *Biometrika 38*, 196–218.

van den Bosch, F., R. Hengeveld, and J. Metz (1992). Analysing the velocity of animal range expansion. *Journal of Biogeography 19*, 135–150.

van den Bosch, F., J. Metz, and O. Diekmann (1990). The velocity of spatial population expansion. *J. Math. Biol. 28*, 529–565.

White, P. and S. Harris (1994). Encounters between red foxes *vulpes vulpes*: implications for territory maintainence, social cohesion adn dispersal. *J. Anim. Ecol. 63*, 315–327.

White, P. and S. Harris (1995a). Bovine tuberculosis in badger (*meles meles*) populations in southwest england: an assessment of past, present and possible future control strategies using simulation modelling. *Phil. Trans. R. Soc. Lond. B 349*, 415–432.

White, P. and S. Harris (1995b). Bovine tuberculosis in badger (*meles meles*) populations in southwest england: the use of a spatial stochastic simulation model to understand the dynamics of the disease. *Phil. Trans. R. Soc. Lond. B 349*, 391–413.

Winfree, A. (1972). Spiral waves of chemical activity. *Science 175*, 634–636.

Appendix A

Solutions of

$$\frac{dn}{dz} = \phi \qquad\qquad n(0) = n_0 , \qquad\qquad (0.0.1)$$

$$\frac{d/\phi}{dz} = v_R\phi - g(n) \qquad\qquad \phi(0) = \phi_0 \qquad\qquad (0.0.2)$$

are sought. This is equivalent to

$$\frac{d/\phi}{dn} = \gamma(n, v_R, \phi) \qquad\qquad \phi(n_0) = \phi_0 \qquad\qquad (0.0.3)$$

where

$$\gamma(n, v_R, \phi) \equiv v_R - \frac{g(n)}{\phi} . \qquad\qquad (0.0.4)$$

The solution of this system is represented by $\phi(n, v_R, \phi_0)$ and $\phi_c(v)$ is defined such that $\phi(n, v, \phi_c(v)) \to 0$ as $n \to 1^-$.

Equation (0.0.4) implies that

$$v_1 > v_2 \quad\Rightarrow\quad \gamma(n, v_1, \phi) > \gamma(n, v_2, \phi) , \qquad\qquad (0.0.5)$$

which in turn implies that, so long as $\phi(n, v_1, \phi_0) > 0$,

$$v_1 > v_2 \quad\Rightarrow\quad \phi(n, v_1, \phi_0) \geq \phi(n, v_2, \phi_0) . \qquad\qquad (0.0.6)$$

Now 2 trajectories are considered, the first calculated with $phi(n_0) = \phi_c(v_1)$ and $v_R = v_1$, and the second calculated from the same initial condition but with $v_R = v_2 < v_1$. The first trajectory hits (1,0). Inequality (0.0.6) shows that while the first trajectory is above the N-axis, the second trajectory thus crosses the n axis ($\phi = 0$) at or to the left of (1,0). If it hits (1,0) then we know that $\phi_c(v_1) = \phi_c(v_2)$. If it crosses to the left of (1,0) then the phase plane analysis shown in Figure 2.1c implies that to cause it to hit (1,0) we must use an increased value of $\phi(n_0)$, so $\phi_c(v_1) < \phi_c(v_2)$. Hence, we know that

$$v_1 > v_2 \quad\Rightarrow\quad \phi_c(v_1) \leq \phi_c(v_2) . \qquad\qquad (0.0.7)$$